Effects of Defects and Other Field Interactions on Channeling Radiation

Thesis submitted for the award of the Degree of

Doctor of Philosophy

By

JUBY GEORGE

School of Physics

University of Hyderabad

Hyderabad - 500 046

India

May 2009

To my Parents

DECLARATION

I hereby declare that the research work embodied in this thesis entitled **"Effects of Defects and Other Field Interactions on Channeling Radiation"** carried out by me under the supervision of **Prof. A. P. Pathak**, School of Physics, University of Hyderabad, has not been submitted for any other degree or diploma either in part or full to this or any other university or institution.

Place: Hyderabad

Date: **Juby George**

CERTIFICATE

This is to certify that the research work embodied in this thesis entitled **"Effects of Defects and Other Field Interactions on Channeling Radiation"** has been carried out by **Juby George** under my supervision and the same has not been submitted for any other degree or diploma either in part or full to this or any other university or institution.

Place: Hyderabad

Date: **Prof. A. P. Pathak,**

(Thesis supervisor)

Dean
School of Physics
University of Hyderabad

ACKNOWLEDGEMENTS

"Some people come into our lives and quickly go. Some stay for awhile and leave footprints on our hearts. And we are never, ever the same"
— Anonymous.

I would like to avail this opportunity to express my deep sense of gratitude and indebtedness to **Prof. A. P. Pathak** for giving me the opportunity to work with him and introducing me to the field of Channeling. His inspiring guidance and constant encouragement, throughout my PhD enabled me to finish my thesis in a reasonable time. He was not just a teacher to me, but also a friend and philosopher. I also thank his family for their kindness.

I am thankful to **Prof. Vipin Srivastava**, Dean, School of Physics for providing the necessary facilities.

I express my sincere thanks and gratefulness to **Prof. Ashok Chatterjee**, my doctoral committee member for his valuable suggestions and **Prof. V. S. S. Sastry**, who acted as my incharge guide for many occasions. I am extremely thankful to **Prof. A. K. Kapoor**, who included me in his website development programme in my initial years of PhD that enabled me to learn Latex along with problem solving. That project with him have supported me financially.

Discussions with Prof. A. V. Solv'yov and Prof. A. Korol on many occasions were really helpful and I acknowledge Prof. Solovyov's hospitality in FIAS during my stay there in 2006. I also thank Maneesh for his company in FIAS.

When it comes to the research, 'group' comes first. Srinivas, Deva and Sai Kiran provided me a lot of help in finalizing my thesis. I appreciate the way they have taken time off from their works for my thesis correction. I wish them all the best for their thesis as well. I thank my seniors Sathish and Dr. Dhamodaran for their help in the initial years of my PhD. I also acknowledge the help of Dr. S. V. S Nageshwara Rao during my MPhil days.

I thank my colleagues and my best friends in SoP, Saravanan, Joji, Shinto, Abhilash, Chaitanya, Brahma and (Dr.)Ajith for their support and above all their firendship. I also thank Yugander, Ramudu, Sandhya, Kalyan, Hongray, Regina, SaiPriya, Ratnam, Jayasri, SaiPreethi, Thejal, Manoj, Kiran, Prasanth, Vikram, Sanjeev, Ashuthosh, Basheed, Sudha, Mahendra, Arun, Chari, Sitalakshmi, Sultan, Vijayan, Venkaiah, Swaroop, Devendra, Bhaskar and all the other scholars in the school for helping me directly or indirectly.

I also thank my good friends in campus Kerri, Queenie, Dame, Naveen, the DSP and Misfit gang and the whole of mallu community in the campus especially Shalu and Santhosh, Azher, Biju, Rohit, Dinesh, Muneer, Rajesh for making my campus life pleasant. I also appreciate their patience in handling a 'difficult' person like me.

I thank Gin, Sushil and Sampy for their support and encouragement. There were a wonderful company to me from their MTech days in HCU. I also mention my room mate during my MPhil, Sari for her words of wisdom and encouragement. Cannot miss acknowledging Gireesh, Anoopettan and Sankarettan for their words of encouragement 'online'.

My life in LH was really a pleasant one and it provided a perfect atmosphere for my research work thanks to my wonderful friends there. I mention Sowmia, Madhu,

Anitha and Nabs and all my hostel-mates in my MPhil and PhD days for the hell lot of fun we had in the hostel.

I thank Mr. Abraham for his help on every occasion. I also acknowledge all other staff members in the school for helping me in one way or other. I am thankful to the whole of CAS staff (past and present); Narasimha, Ramesh, Shailaja and Sujatha for their helping hands in matters regarding our group.

I thank center for Advanced Studies in Physics, University of Hyderabad and CSIR for fellowships in the form of JRF and SRF respectively.

I thank all my teachers from school to college till university for making me what I am today.

Words are not enough to express to thanks my parents and my siblings. Their love and support through my PhD time are not expressible by any words. The immense confidence and patience they have on me is my strength. I won't forget to specially mention my brother Jacob who gave me the biggest moral boost. My best friend and companion from childhood, his mental support kept me going through many difficult times during my stay in Hyderabad. Million thanks to my cousin Mable who encouraged me and made sure that my spirits are never down through her phone calls.

Above all, I thank the God Almighty for EVERYTHING and making me cross the bridge even when it seemed a rough path.

SYNOPSIS

Channeling and Channeling Radiation

When a charged particle is incident upon a solid target, several physical phenomena occur like elastic scattering, inelastic energy-loss processes, secondary-electron emission, bremmsstrahlung, nuclear reactions, etc. Channeling is the process which confines the path of a particle in a crystalline solid. It can take place when the particle is aligned along one of the major symmetry directions in the solid. These are the open directions (channels) between rows or planes of atoms [1, 2].

Since the steering of the particles involves collisions with many atoms, one may consider a continuum model in which the nuclear charge of the atomic row or plane is uniformly averaged along the row or plane. The moving particles will not be able to feel the interaction due to individual atoms sitting at various lattice sites but rather experience a collective effect of all the atoms sitting along a particular axial or planar direction. Lindhard's continuum model [3] gives a complete initial description of this phenomena. According to this model, channeling can takes place when the time of flight to cross one lattice spacing is less than the collision time with any individual target atom. This means that by the time the particle can feel itself to be in the field of one atom, it is already in the field of next atom along the string or plane and it will see only continuum potentials [4] instead of individual atom field.

The charged particles penetrating through matter experience electromagnetic force due to atoms. As a result, these particles undergo acceleration or retardation and may be deflected due to collisions along their trajectory. This causes the emission of bremmsstrahlung. In the case of normal bremmsstrahlung, these deflections are highly uncorrelated (random). Correlated deflections give rise to coherent bremmsstrahlung

where the particles move *almost* in a straight line along various channels of SAME symmetry (family). But at very small angle of incidence, below the critical angle, the motion is influenced by the continuum axial or planar potential of the SAME channel and the particles are channeled. The corresponding radiation is called channeling radiation. In the quantum picture channeling radiation is associated with jumps between the quantum states of the transverse motion in the planar or axial continuum potential. But the observation of this radiation is difficult because the transverse oscillation frequencies and the corresponding energies are very low (of the order of eV). However, the relativistic effects shift the energies to keV or even MeV for MeV or GeV positrons and electrons. All the results presented here pertain to these relativistically fast channeled particles [5].

Channeling has a variety of applications. One of the first applications in conjunction with the RBS, has been for the lattice location of point defects in crystals. Subsequently, more complex defects and damages have been studied over the last four decades with RBS/Channeling. More recently, channeling radiation is being used as a radiation source and applied to study of various kinds of defects and strain.

Outline of the Thesis

The thesis consists of 6 chapters;

1. Introduction
2. Effects of hypersonic field and anharmonic interactions on channeling radiation
3. Quantum calculations for the effects of dislocations on channeling
4. Dechanneling of positrons by dislocations: Effects of anharmonic interactions

5. Effects of Dislocations on Channeling Radiation from a Periodically Bent Crystal

6. Summary and Concluding remarks

In the introduction chapter, a brief summary of channeling and channeling radiation with relativistic effects are given. Also the importance of quantum mechanical effects and applications of channeling are mentioned.

Chapter 2 is the study of the effects of hypersonic field on channeling radiation. These external fields, both longitudinal and transverse, modify the wavefunction of the positrons propagating along a planar channel. The transverse potential becomes both x and z (directions of transverse oscillation of the channelon and propagation of the hypersonic field waves respectively) dependent and changes the observable parameters like frequency and intensity. The effects of anharmonicity of the positron planar potential is studied. The quartic term makes the transverse potential more complicated and influences the spectral distribution. In the longitudinal case, the anharmonicity increases the spectral distribution of radiation intensity by a considerable percentage. The study of the effects of transverse perturbation is important in the realization of crystalline undulators [6] (where acoustic waves with sufficiently high amplitudes are used). In the present study, waves of lower amplitudes are considered, whose dependencies make weaker interactions on the spectral distribution when compared to the longitudinal case.

In chapter 3, a quantum mechanical treatment of the effects of dislocation on channeling is given. Using the Schrodinger equation, the longitudinal and transverse motion is separated out and the effects of dislocations are incorporated by a centrifugal energy term. Around the dislocation core, we can divide a particular channel into four regions; two curved parts with curvatures in opposite directions

together bounded by two perfect and undistorted regions. The change in the transverse potential and frequency of oscillation in the perfect channels and two regions of dislocation affected channel are calculated. Using the corresponding wavefunctions and the boundary conditions across these four regions, we find the reflections and transmission co-efficients. These co-efficients give the dechanneling and channeling probabilities respectively. Both positron and electron channeling are considered. The difference in the positron and electron channeling in a dislocation affected channel is studied by these probability co-efficients. In the case of electron channeling, the variation of the spectral distribution due to dislocation is also found.

In chapter 4, the effects of anharmonic interactions on positron channeling in a dislocation affected channel is studied in a quantum mechanical framework. The wavefunctions in the perfect and the dislocation affected regions of the channel are found and compared with that for the harmonic case. The anharmonicity affects the number of bound states as well as the distortion parameters. The variation in the frequency of oscillations is expected with the inclusion of the anharmonic terms. The above factors influence the transition among various states. The transition probabilities and the resulting dechanneling probabilities are found for initially well-channeled particles in states $|0\rangle$ and $|1\rangle$. It is found that, anharmonic effects tend to increase the radius of curvature of the dechanneling cylinder. The change in these observable parameters are in good agreement with the previous calculations with anharmonic interactions (chapter 2).

Chapter 5 deals with the effects of dislocations on the positrons channeling in a periodically bent crystal (crystalline undulator [6]). Two cases of high and low dislocation densities are considered. Both the dislocation affected region and the periodically bent channel are represented by their radii of curvature and wavelengths and we consider the modulation of these effects of dislocation over the periodicity

of the channel. The varying dislocation densities change these modulation effects. Correspondingly, the dependencies of the channeling radiation on the periodicity of the channel are also varied; at higher dislocation densities the influence of this channel periodicity is less. Both dislocation effects and periodicity of the channel are complimentary to each other's effects on channeling and is studied in detail in this chapter.

Finally in chapter 6 the summary of the thesis is given with some concluding remarks and the future directions of works in this field.

Thesis Summary

The basic motivation of the work presented in this thesis has been to study the interactions of internal and external perturbations on the channeling process. The internal perturbations are defects like dislocations and the external ones are mechanical periodic perturbations like hypersonic/acoustic waves (both longitudinal and transverse). The presentation is divided into three parts:

(i) Effects of hypersonic field on channeling radiation

The effects of both transverse and longitudinal hypersonic waves on channeling radiation are considered. Also the influence of anharmonicity of the planar transverse continuum potential on the wavefunction of the positron and the fractional change in frequency due to these anharmonic effects are calculated. The transverse perturbation effects are given special mention, which is a first step in the study of undulator radiation.

(ii) Effects of dislocations on channeling radiation

Effects of dislocations on channeling are studied for both positron and electron channeling. A quantum mechanical model, where the affected region is divided into four parts separated by 3 boundaries, has been developed. Continuity of wave functions

and their derivatives across these boundaries gave channeling and dechanneling co-efficients. The effects of anharmonic term in the positron planar potential on the distortion co-efficient and number of bound states and other channeling parameters like frequency of radiation, are studied in detail and compared with those obtained in the harmonic case.

(iii) Effects of dislocations on channeling in a periodically bent crystal

The effects of dislocations on channeling phenomena in a periodically bent crystal are studied for the first time. The distortion effects of both the dislocation affected regions and the periodically bent channels are represented in terms of waves with comparable amplitudes and wavelengths. Therefore, the distortion effects due to dislocations can be modulated on the periodic distortions (resulting for example due to undulators). In this analysis, we consider both the situations namely; $\lambda_d > \lambda_u$ (low dislocation density) and $\lambda_d < \lambda_u$ (high dislocation density). It is found that for low dislocation density, the crystalline undulator parameters play a major role where as in the case of high dislocation density, undulator parameters have minimal effects on the radiation.

In summary, no crystal is perfect and study of channeling/channeling radiation and crystalline undulators are incomplete without the consideration of defects and other field interactions. The present work is a broad study of these effects of distortions and field interactions on channeling of both positive and negative particles through crystals.

References

1. D. S. Gemmell, *Rev. Mod Phys.* **46**, 129 (1974).

2. A. P. Pathak, *J. Phys. C.* **8**, L 439 (1975);
   A. P. Pathak, *Rad. Eff.***61**, 1 (1982).

3. J. Lindhard, *Phys. Lett.* **12**, 124 (1964);
C. Erginsoy, *Phys. Rev. Lett.* **15**, 360 (1965);
J. Lindhard, *K. Dan. Vidensk. Selsk. Mat. Fys. Medd.* **34**, No.14 (1965).

4. J. Lindhard, V. Nielsen and M. Scharff, *K. Dan. Vidensk. Selsk. Mat. Fys. Medd.* **36**, 10 (1968).

5. J. U. Andersen, E. Bonderup and E. Laegsgaard, *Topics in Current Physics* **38**, 127 (1985).

6. A. V. Korol, A. V. Solov'yov and W Greiner, *J. Phys. G: Nucl. Part. Phys.* **24**, L45 (1998).

Contents

CHAPTER 1

Introduction

1.1 Channeling

When a beam of energetic charged particles is incident on a solid target, a variety of phenomena take place like scattering, nuclear reactions, x-ray production etc. The scattering studies give information about the microscopic as well as the macroscopic properties of matter. The interaction between the incident beam and the target is orientation-dependent. The arrangement of atoms in a solid determines the crystallographic properties of the material in general, particularly in single crystals it determines the directional effects on incident ion - target atom interactions. The influence of the crystal lattice on the trajectories of ions penetrating into the crystal gives rise to phenomena known as channeling - a term that visualizes the atomic rows and planes as guides that steer energetic ions along the "channels" between rows and planes. Channeling of energetic ions occurs when the beam is carefully aligned with

a major symmetry direction of a single crystal. By a major symmetry direction we mean one of the open directions as viewed down a row or plane of atoms in a single crystal. Figure 1.1 shows a view of this process in diamond structure along the $< 110 >$ axial direction where most of the ion beam is steered (channeled) through the channels formed by the strings of atoms.

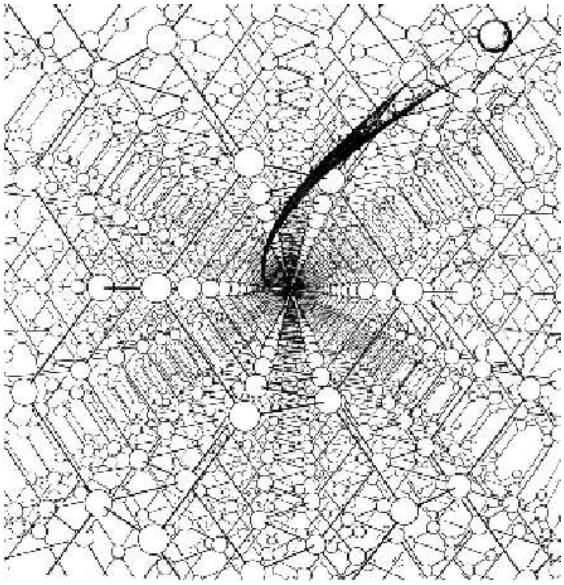

Figure 1.1: Particle along the $< 110 >$ axial channel in a diamond structure.

1.1.1 Continuum Model

The trajectory of channeled particles is such that the ion makes a glancing angle impact with the axes (axial channeling) or planes (planar channeling) of the crystal and is steered by small angle scattering collisions at distances greater than $0.1\mathring{A}$ from the atomic cores. Since the steering of the channeled particle involves collisions with many atoms, one may consider a continuum model in which the nuclear charge of the atoms in a row (or plane) is uniformly averaged along the row (or plane).

A charged particle, when steered along the axial or planar channels, will not feel the interaction due to individual atoms sitting at various lattice sites but rather experience a collective effect of all the atoms sitting along a particular axial or planar direction so that the moving particle will experience only continuum strings or planes. The conditions for this to happen have been derived by Lindhard [1] and Erginsoy [2] in an analysis based on the idea that the particle velocity component parallel to the axial or planar direction is such that the time of flight to cross one lattice spacing is less than the collision time with any individual target atom. This means that by the time the particle can feel itself to be in the field of one atom, it is already in the field of next atom along the string or plane. Hence the particle will see only continuum potential instead of individual atomic potentials and we can assume an oscillatory motion of the channeled particles during its passage through the crystal. Figure 1.2 illustrates the condition of channeling.

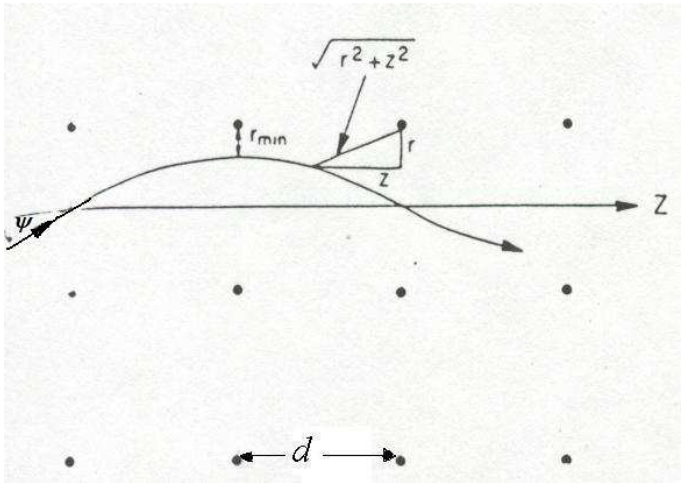

Figure 1.2: Channeling condition.

The continuum condition as discussed above may be is written mathematically as [3],

$$\frac{r_{min}}{v \sin \psi} > \frac{d}{v \cos \psi} \tag{1.1}$$

where 'r_{min}' is the distance of minimum approach to the string, 'd' is the interatomic spacing, 'ψ' is the angle at which the particle enters the channel and 'v' is the velocity of the particle.

We can obtain the continuum potential which describes the interaction of the channeled particle with the atomic rows or planes by averaging the atomic potential along the rows or planes. For the axial case

$$U_a(r) = \frac{1}{d} \int_{-\infty}^{\infty} V(\sqrt{z^2 + r^2})\, dz \tag{1.2}$$

where $V(\sqrt{z^2 + r^2}) = V(R)$ is the interatomic potential and may be written as,

$$V(R) = \frac{Z_1 Z_2 e^2}{R}\, \varphi(R) \tag{1.3}$$

where $\varphi(R)$ is the screening function and Z_1 and Z_2 are the atomic numbers of the incident ion and target atom respectively. The screening function $\varphi(R)$ may be expressed either as power law or exponential form. For simplicity Lindhard chose a power law form given by [4],

$$\varphi(R) = 1 - \frac{R}{\sqrt{R^2 + C^2 a_{TF}^2}} \tag{1.4}$$

where C is the Lindhard constant($=\sqrt{3}$) and a_{TF} is the Thomas-Fermi screening distance given by,

$$a_{TF} = \frac{0.8853}{\sqrt{Z_1^{2/3} + Z_2^{2/3}}}\, a_0$$

where a_0 is the Bohr radius.

Several other forms of screening function are discussed in the next section 1.1.2. Using the Lindhard power law screening function we get the axial continuum potential as,

$$U_a(r) = \frac{Z_1 Z_2 e^2}{d} \ln\left[\left(\frac{Ca_{TF}}{r}\right)^2 + 1\right] \tag{1.5}$$

For small values of 'r' (high energies), the above equation reduces to,

$$U_a(r) = \frac{2Z_1 Z_2 e^2}{d} \ln\left(\frac{Ca_{TF}}{r}\right) \tag{1.6}$$

At the point r_{min}, the transverse kinetic energy is equal to the repulsive continuum potential $U(r_{min})$. i.e.,

$$E\psi^2 = U(r_{min}) \tag{1.7}$$

Using equations (1.6) and (1.7), we can obtain the value of r_{min} as,

$$r_{min} = Ca_{TF} \exp\left[-\frac{Ed\psi^2}{2Z_1 Z_2 e^2}\right] \tag{1.8}$$

From the above equations we can find the critical angle for channeling. The continuum condition (Eqn.(1.1)) may be rewritten as,

$$r_{min} > d\ \psi \tag{1.9}$$

which becomes using equation (1.8),

$$\frac{Ca_{TF}}{d\ \psi} \exp\left[-\frac{Ed\psi^2}{2Z_1 Z_2 e^2}\right] > 1 \tag{1.10}$$

This condition is obviously satisfied for extremely small values of ψ. As ψ increases from zero, the condition is violated with the exponential function decreasing rapidly, provided $Ca_{TF}/d\psi$ remains large. The condition (1.10) will remain fulfilled for

$$\psi < \psi_1 = \left(\frac{2Z_1 Z_2 e^2}{Ed}\right)^{1/2} \tag{1.11}$$

provided $Ca_{TF}/d\psi_1 > 1$. ψ_1 in the above equation gives the critical angle for channeling at higher energies. i.e., this equation is valid only for energies $E > E' = \frac{2Z_1 Z_2 e^2 d}{a_{TF}^2}$.

For low energies $E < \frac{2Z_1Z_2e^2d}{a_{TF}^2}$, one should use the full continuum potential (1.5) and we obtain the condition

$$\psi < \psi_2 = \left(\frac{Ca_{TF}}{d\sqrt{2}}\psi_1\right)^{1/2} \tag{1.12}$$

ψ_2 is the critical angle for channeling at lower energies when the value of 'r' is large.

In the planar case, two-dimensional averaging of the interatomic potential results in a sheet of charge. The corresponding planar continuum potential is given by,

$$U_p(y) = Nd_p \int_0^\infty V(\sqrt{y^2 + r^2})\ 2\pi r\ dr \tag{1.13}$$

where 'y' is the distance from the plane, Nd_p is the number of atoms per unit area in the plane and 'd_p' is the interplanar spacing. The planar continuum potential can be written as,

$$U_p(y) = 2\pi Z_1 Z_2 e^2 Nd_p \left[\sqrt{y^2 + C^2a_{TF}^2} - y\right] \tag{1.14}$$

Similar to the axial case, we find the characteristic angle for planar channeling from the continuum condition as

$$\psi_p = \left(\frac{2\pi Z_1 Z_2 e^2 a_{TF} Nd_p}{E}\right)^{1/2} \tag{1.15}$$

The critical angle in the planar case is found to be smaller than that in the axial case.

1.1.2 Interatomic Potential

The interatomic potential (Eqn. (1.3)) mentioned in the last section is most crucial and basic quantity needed to understand any phenomena in condensed matter physics in general and ion channeling in particular. The screening function $\varphi(R)$ basically represents the effects of electrons, which tend to screen the Coulomb interaction between projectile nucleus Z_1e and the target nucleus Z_2e. In principle, one has to incorporate the effects of electrons attached to the nuclei as well as the conduction

electrons moving in the solid. This is best done via Thomas Fermi equation for screening function which can be solved only numerically [5]. However, several accurate analytical approximations to this screening function have been used. Lindhard used a power law form shown in Eqn. (1.4). This gives reasonable approximation for distance of interest in the crystallographic channels. However for larger distances, power law decrease is too slow and exponential form of Thomas Fermi screening have been used. The most frequently used one is the Moliere approximation and is given by,

$$V_M(R) = \frac{Z_1 Z_2 e^2}{R}(0.35e^{-bR} + 0.55e^{-4bR} + 0.1e^{-20bR}) \tag{1.16}$$

where $b = 0.3/a_{TF}$. Here the screening function is given by,

$$\varphi\left(\frac{R}{a_{TF}}\right) = \sum_{i=1}^{3} \alpha_i \ \exp(-\beta_i R/a_{TF}) \tag{1.17}$$

where $\{\alpha_i\} = \{0.1, 0.55, 0.35\}$ and $\{\beta_i\} = \{6.0, 1.2, 0.3\}$.

Lindhard and Moliere expressions for the screening function are the ones most widely used to describe ion-atom interactions in channeling. Other forms of interatomic potentials used in channeling calculations include Born-Mayer potential [6] given by,

$$V_{BM}(R) = A_{BM} \exp(-R/a_{BM}) \tag{1.18}$$

where a_{BM} is the Born-Mayer screening radius and Bohr potential [7] given by,

$$V_{BO}(R) = \frac{Z_1 Z_2 e^2}{R} \exp(-R/a_b) \tag{1.19}$$

where a_b is written as,

$$a_b = \frac{a_0}{\sqrt{Z_1^{2/3} + Z_2^{2/3}}} \tag{1.20}$$

This screening function has the disadvantage at large distances ($R > a_b$) where it provides excessive screening and the potential decreases too rapidly to fit actual ion-atom interactions.

It is seen that there is no single potential which can be used for the analytical calculations for entire range of interatomic distances. Alternative mathematical approximations have been made for both planar [8] and axial potentials [9] in problems involving the effects of defects like dislocations, stacking faults etc on channeling. In the planar case, a simpler approximation has been proposed by Pathak [10, 11] which is essentially a mathematical approximation to the Lindahard's standard potential. This has been used extensively in the study of the defects and the dechanneling of the particles and is given by,

$$V_{PM}(R) = \frac{Z_1 Z_2 e^2}{R} \frac{C a_{TF}^2}{(R + a_{TF})^2} \tag{1.21}$$

Using Eqn. (1.21) in (1.13), one gets the planar potential,

$$U_{PM}(y) = \frac{2\pi Z_1 Z_2 e^2 N d_p C a_{TF}^2}{y + a_{TF}} \tag{1.22}$$

The potential experienced by the particle in a planar channel is the superposition of potentials due to both the planes. This can be obtained by substituting $y = l \pm x$, where $l = d_p/2$, x is distance measured in the transverse direction from the mid-plane between the two planes. Hence the total planar potential is given by,

$$U_{PM}(x) = 2\pi Z_1 Z_2 e^2 N d_p C a_{TF}^2 \left(\frac{1}{l + a_{TF} - x} + \frac{1}{l + a_{TF} + x} \right) \tag{1.23}$$

which can be written in a simplified form given by,

$$U(x) = \frac{4 V_0 L a_{TF}}{L^2 - x^2} \tag{1.24}$$

where $L = l + a_{TF}$ and $V_0 = \pi Z_1 Z_2 e^2 C a_{TF} N d_p$.

1.2 Channeling Radiation

When charged particles penetrate through matter, they experience electromagnetic force due to atoms. As a result acceleration or deceleration of the particles occurs.

The particles may be deflected due to collisions along their trajectory. This results in the emission of bremsstrahlung. In a crystal, we may distinguish between normal (incoherent) bremsstrahlung, coherent bremsstrahlung and channeling radiation. This distinction is related to the correlation of deflections in time and space. Normal bremsstrahlung occurs when the incident particles are deflected randomly by individual atoms. These deflections due to close collisions with atoms are highly uncorrelated. However, deflections in more distant collisions are highly correlated when they are due to the interaction with one or two-dimensional continuum potential over planes or axes respectively. The projectile motion is only slightly deflected by the potential and the trajectory of the particle is almost straight along various channels of same symmetry (family), as shown by 'a' in Figure 1.3.

For particles incident at very small angles (within the critical angles) to a plane or axis, the projectile motion is governed by continuum planar or axial potential of the same channel. The particles are channeled and the radiation associated with the transverse motion perpendicular to the plane or axis is called channeling radiation. 'b' in Figure 1.3 shows the trajectory of a channeled particle. Quantum mechanically, channeling radiation is associated with jumps among quantum states of transverse motion.

However, the observation of this radiation was difficult because the transverse oscillation frequencies and the corresponding energies are very low (of the order of eV). The breakthrough came with the relativistic effects shifting the energies to keV or even MeV for MeV or GeV positrons and electrons. Therefore we consider a relativistic particle moving along a channel. For the present explanation of the effect we consider a relativistic positron incident with a velocity 'v' channeling along the z-direction with transverse oscillation in the x-direction as shown in Figure 1.4.

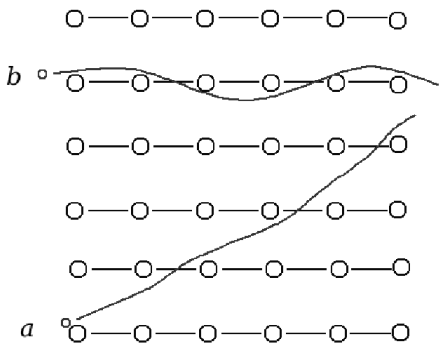

Figure 1.3: The electron motion along or close to crystallographic planes/axes. 'a' represents the trajectory of the particle in the coherent bremsstrahlung and 'b', in channeling.

The emission process takes place in the rest frame of the particle due to the transition among the discrete energy levels. Since in the particle rest frame, the crystal is moving back at a speed -v, it appears Lorentz contracted. Therefore the interatomic spacing is reduced in the rest frame, $d_R = d/\gamma$. Correspondingly, we expect the transverse force and hence the continuum potential governing the motion to increase by a factor γ. This results in increase of separation among the transverse energy levels to increase by γ [12]. i.e.,

$$\Delta E_R = \gamma \Delta E \tag{1.25}$$

These Lorentz transformations are illustrated in Figure 1.4. The characteristic frequency of oscillations ω_0, changes accordingly with the change in ΔE and is given by,

$$\omega_R = \gamma \omega_0 \tag{1.26}$$

where ω_0 is the characteristic oscillation frequency of the particle.

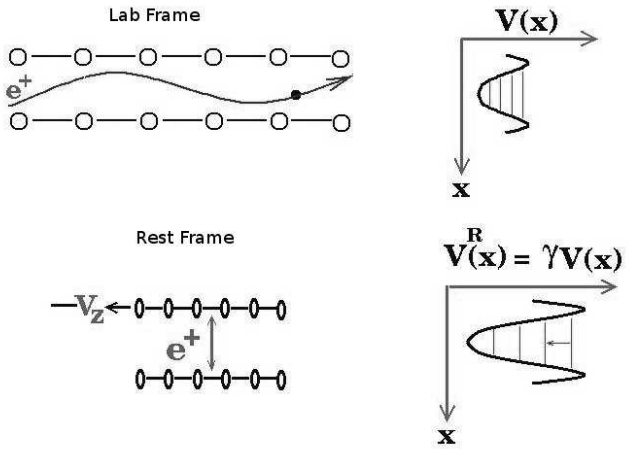

Figure 1.4: Lorentz transformations between the Laboratory and Rest Frames.

Now the emission taking place in the rest frame has to be observed in the lab frame. We use Doppler equation and the observed frequency in the lab frame is given by,

$$\omega_L = \frac{\omega_R}{\gamma(1 - \beta\cos\theta)} \tag{1.27}$$

In the forward direction, at $\theta = 0$, emission is maximum. The corresponding frequency of radiation is,

$$\omega_L = 2\gamma^2\omega_0 \tag{1.28}$$

The intensity distribution of the radiation by positron is characteristic of a dipole as shown in Figure 1.5.

Channeling radiation was observed for the first time for positrons [13] about 30 years ago and has been studied by various groups [14-18] Theory was formulated [16] and experimental confirmation was made for positrons [13] and electrons [19, 20] as well.

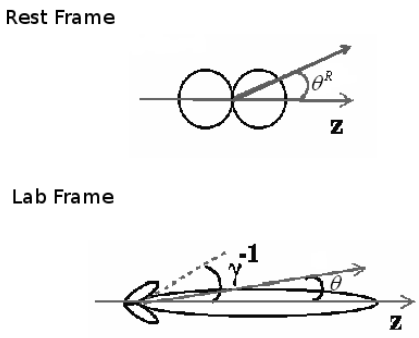

Figure 1.5: The intensity distribution in the rest frame and lab frame.

1.3 Quantum Mechanical Effects

Most of the early experimental works after the publication of Lindhard's classical theory of channeling were related to the determination of critical angles, minimum yield and stopping power for protons and heavier ions channeled in single crystals. The classical theory provided a complete description of channeling phenomena for these relatively heavy ions. But the works on electron microscopy, especially transmission electron microscopy (TEM) with crystalline materials, was being extended to channeling situations and there were clear indications of quantum and diffraction effects dominating the patterns.

In quantum mechanical approach, the confinement of transverse motion of channeled particles between two planes or in an axial channel surrounded by several strings, leads to discrete energy levels as mentioned in Section 1.2. Based on the number of allowed quantum states for transverse motion in the potential well of channel, it has been shown that positrons and electrons do not behave exactly similarly, as one might expect purely on the basis of their opposite charge. The number of quantum states for positron case is smaller than for electron case. This happens because transverse motion of positively and negatively charged particles is qualitatively different in chan-

neling situations. For electrons the potential minima are at the center of atomic string and channeled electrons have an increased probability for bound motion with respect to axial string. This implies that channeling states for electrons are more stable than for positrons.

We use in our calculations, both Dirac and Schrodinger equations for the motion of these charged particles through the crystallographic axis. The relativistic effects are included by introducing the γ factor. The spin effects are neglected. The quantum mechanical concept in the channeling can be extended to explain the theory of classical effects like undulator radiation.

1.4 Applications of Channeling

A variety of practical uses have been found for channeling effects. Channeling effects can be used as tools to investigate the properties of the crystal lattice as well as the perturbations (like defects and doping) in the bulk region that may not be accessible to X-rays.

One of the main applications of channeling is the study of defects. It involves location of the defects and their density measurements in the solids. We can pin-point the exact position of the foreign impurity by doing the channeling experiments along various crystallographic directions [21, 22]. Similarly the extended defects like dislocations and stacking faults can be studied both qualitatively and quantitatively.

Surface studies are of general interest to material scientists [23-26]. These studies give the information on the structure of a few surface layers, and for defective and damaged surfaces where the knowledge and control of damage can be of enormous value in technological applications.

At very high energies (tens of GeV), the applications include the channeling radiation for enhanced production of high energy gamma photon. Channeling in bent crystals has been used to bend ion beams [27, 28] and also focus it [29].

1.5 Outline of the Thesis

The motivation behind the work presented in this thesis has been to study the interactions of internal and external perturbations on the channeling process. Quantum mechanical formulations have been developed based on the existing theoretical assumptions for internal perturbations in the form of defects like dislocations and external ones like hypersonic/acoustic wave (both longitudinal and transverse) propagations.

Chapter 2 is the study of the effects of hypersonic field on channeling radiation. These external fields, both longitudinal and transverse, modify the wavefunction of the positrons propagating along a planar channel. The transverse continuum potential becomes dependent on both x (direction of transverse oscillation of the channelon) and z (propagation of the hypersonic field waves) and changes the observable parameters like frequency and intensity. The effects of anharmonicity of the positron planar potential is studied. The study of the effects of transverse perturbation is important in the realization of crystalline undulators (where acoustic waves with sufficiently high amplitudes are used). Here the waves of lower amplitudes are considered.

In chapter 3, a quantum mechanical treatment of the effects of dislocations on channeling is given. We consider both positron and electron channeling. Using the Schrodinger equation, the longitudinal and transverse motion is separated out and the effects of dislocations are incorporated by a centrifugal energy term. Around the dislocation core, we can divide a particular channel into four regions; two curved parts

with curvatures in opposite directions together bounded by two perfect and undistorted regions on either side. The change in the transverse potential and frequency of oscillation in the perfect channels and two regions of dislocation affected channels are calculated. Using the corresponding wavefunctions and the boundary conditions across these four regions, we find the reflections and transmission co-efficients. These co-efficients give the dechanneling and channeling probabilities respectively.

In chapter 4, the effects of anharmonic interactions on positron channeling in a dislocation affected channel is studied in a quantum mechanical framework. The wavefunctions in the perfect and the dislocation affected regions of the channel are found and compared with that for the harmonic case. The anharmonicity affects the number of bound states as well as the distortion parameters. The variation in the frequency of oscillations is expected with the inclusion of the anharmonic terms. The above factors influence the transition among various states. The transition probabilities and the resulting dechanneling probabilities are found for initially well-channeled particles in states $|0\rangle$ and $|1\rangle$. It is found that, anharmonic effects tend to increase the radius of curvature of the dechanneling cylinder. The change in these observable parameters are in good agreement with the previous calculations with anharmonic interactions (chapter 2).

Chapter 5 deals with the effects of dislocations on the positrons channeling in a periodically bent crystal (crystalline undulator). Two cases of high and low dislocation densities are considered. Both the dislocation affected region and the periodically bent channel are represented by their radii of curvature and wavelengths and we consider the modulation of the effects of dislocations over the periodicity of the channel. The varying dislocation densities change these modulation effects. Correspondingly, the dependencies of the channeling radiation on the periodicity of the channel are also varied. At higher dislocation densities the influence of this channel periodicity

is less. Both dislocation effects and periodicity of the channel are complimentary to each other's effects on channeling and is studied in detail in this chapter.

Finally in chapter 6 the summary of the thesis is given with some concluding remarks and outlook and the future directions of works in this field.

CHAPTER 2

Effects of Hypersonic Field and Anharmonic Interactions on Channeling Radiation

2.1 Introduction

The subject of interactions of radiation with matter is of great interest in several branches of science. It is well known that electromagnetic processes are influenced by the medium. Some of the important examples are Cherenkov radiation, transition radiation, channeling radiation and synchrotron radiation where the medium plays a crucial role. In most of these processes, the motivation is to extract the maximum intensity with tunable frequencies of the emitted radiation by optimization and proper understanding of the underlying mechanisms. An enhancement of radiation intensity can also be achieved by the use of resonance effects between an external field (quite often an electromagnetic field) and the stimulated radiation process. In the context of channeling radiation, the Dirac equation with a quasi-static transverse potential,

followed by an analysis parallel to that of Kumakhov [16] using spinor components, resulted in the broadening of the radiation band width. Hypersonic/ultrasonic excitations of the medium by an external probe also have the ability to produce such resonance effects. The problem of radiation by ultra-relativistic particles channeling in the crystal in the presence of hypersonic wave fields has been discussed by several authors [30-39]. In this chapter, we investigate the influence of hypersonic vibrations excited in a single crystal on the channeling radiation from positrons.

The hypersonic field results in compressions and rarefactions along the direction of propagation. The crystal potential in the transverse direction follows these compressions and rarefactions and the particles feel a periodic potential along its direction of propagation. Grigorian *et. al.* [34, 35] treated this process in a harmonic approximation for the transverse planar potential. However, a more accurate description is required to include the actual influence of these acoustic fields on the already existing parabolic transverse potential. As a result, the shape of this transverse potential becomes more complex, and hence the resulting anharmonicity effects should also be included.

In the present investigation, the influence of such anharmonicity effects due to hypersonic waves are studied. Section 2.2 deals with the mathematical formulation of the process where the effects due to longitudinal hypersonic field is considered. Section 2.2.1 gives harmonic model of the effects of the hypersonic field on channeling radiation. Section 2.2.2 discusses the effects of anharmonicity.

In section 2.3 we investigate the effects of transverse hypersonic periodic perturbations on the channeling radiation. When a transverse acoustic wave of sufficient amplitude is incident on a crystal, the crystal channels bend periodically. Channeling of energetic ions through this periodically bent crystal gives rise to undulator radia-

tion [40-46], produced due to the curvature of the trajectory; in addition to channeling radiation. As the amplitude of bending of the channels increases, undulator radiation dominates over channeling radiation. Transverse acoustic wave propagation is one of the many methods to produce undulation in a crystal. We will discuss this in detail in chapter 5. In this section, we consider the lower regime of the amplitudes of transverse wave. Therefore the undulator radiation produced is very weak and we need to consider only the effects on the channeling radiation.

2.2 Effects of Longitudinal Hypersonic Field

2.2.1 Harmonic Model

The planar potential based on the Lindhard standard potential with slight modification [10, 11] has been shown to be reasonable for both dechanneling calculations [47] and channeling radiation characteristics [48]. We continue to use this potential so that in harmonic approximation, the planar potential due to both the planes surrounding a channel can be written as

$$V(x) = V_0 x^2 \tag{2.1}$$

where

$$V_0 = \frac{4\pi Z_1 Z_2 e^2 C a^2 N_p}{(l+a)^3} \tag{2.2}$$

The coefficient V_0 is obtained by incorporating the appropriate crystal parameters. 'x' is the position coordinate in the transverse space, measured from the mid-plane.

The effects of the external hypersonic field on the planar potential 'seen' by the relativistic positron are incorporated as [32, 33].

$$U(x,z) = U_0 \cos(k_s z) + V(x)[1 + \mu \cos(k_s z)] \tag{2.3}$$

where $k_s = 2\pi/\lambda_s$, λ_s is the wavelength of the hypersonic wave, and U_0 and μ are the modulation parameters of the potential. The z-dependence of the potential arises since the hypersonic field is propagating in the z-direction, and reflects the periodic compression and rarefaction in the medium. Hence the equation of motion of the relativistic positron in this external field is given by the modified Dirac equation:

$$[(E-U)^2 - m_0^2c^4 + \hbar^2c^2\bigtriangledown^2]\ \psi_E(r) = 0 \tag{2.4}$$

The above equation assumes that the spin effects are negligible; at high energies (>10 MeV). The derivation of the above equation from the Dirac equation is given in detail in the Appendix.

Without the acoustic field, the above Dirac equation is satisfied by the wavefunction,

$$\psi^{(0)}_{np_yE}(r) = \frac{1}{\sqrt{l_y l_z}} S_{nE}(x)\ \exp\left[\frac{i}{\hbar}(p_y y + p_z z)\right] \tag{2.5}$$

where p_y and p_z are the projections of the momentum of the positron on the y-axis and z-axis respectively, and l_y and l_z denote the thickness of the crystal along the y and z coordinates. S_{nE} are the oscillator wavefunctions, defined by

$$S_{nE} = \frac{\exp\left(-\frac{x^2}{2\alpha^2}\right)}{\sqrt{2^n n!\alpha\sqrt{\pi}}}\ H_n\left(\frac{x}{\alpha}\right) \tag{2.6}$$

which satisfy the Schrodinger equation,

$$\left(-\frac{\hbar^2}{2M}\frac{d^2}{dx^2} + V(x)\right)S_{nE} = \varepsilon_{nE}S_{nE} \tag{2.7}$$

where $M = \frac{E}{c^2}$ and,

$$\begin{aligned} \varepsilon_{nE} &= \hbar\omega_E\left(n + \frac{1}{2}\right) \\ \omega_E &= \sqrt{\frac{2V_0}{E}} \\ \alpha &= \sqrt{\frac{\hbar}{m\omega_E}} \end{aligned} \tag{2.8}$$

To find the positron wavefunction in the presence of a hypersonic field, we make the series expansion,

$$\psi_{np_yE}(r) = \exp\left(\frac{i}{\hbar}p_y y\right)\sum_{k=0}^{\infty} C_{knE}(z)S_{kE}(x). \tag{2.9}$$

Substituting Eqn. (2.9) in (2.4) and using the condition $|U| \ll E$, we get

$$\begin{aligned} - & \left(\frac{E^2 - m_0^2c^4 - p_y^2c^2}{2E}\right)\psi_{np_yE}(r) + U\psi_{np_yE} - \frac{\hbar^2c^2}{2E}\frac{\partial^2}{\partial x^2}\exp\left(\frac{i}{\hbar}p_y y\right)\sum_{k=0}^{\infty} C_{knE}(z)S_{kE}(x) \\ - & \frac{\hbar^2c^2}{2E}\frac{\partial^2}{\partial z^2}\exp\left(\frac{i}{\hbar}p_y y\right)\sum_{k=0}^{\infty} C_{knE}(z)S_{kE}(x) = 0 \end{aligned} \tag{2.10}$$

To further simplify, we use the creation and annihilation operator representation for x as $(a + a^\dagger)\frac{\alpha}{\sqrt{2}}$. Here a (annihilation operator) and $a^\dagger$ (creation operator) satisfy the well-known general relations,

$$\begin{aligned} a\psi_n &= \sqrt{n}\psi_{n-1} \\ a^\dagger\psi_n &= \sqrt{n+1}\psi_{n+1} \end{aligned}$$

After some detailed algebra and simplifications, this leads to a system of recursive relation for the coefficients C_{knE} appearing in Eqn. (2.9) as follows:

$$\begin{aligned} -\frac{\hbar^2c^2}{2E}\frac{\partial^2}{\partial z^2}C_k &+ \left[U_0\cos(k_s z) + \varepsilon_{nE}\left(1 + \frac{\mu}{2}\cos(k_s z)\right) - \frac{E^2 - m_0^2c^4 - p_y^2c^2}{2E}\right]C_k \\ &+ \frac{1}{4}\mu\hbar\omega_E\cos(k_s z)\left[\sqrt{k(k-1)}\,C_{k-2} + \sqrt{(k+1)(k+2)}\,C_{k+2}\right] \\ &= 0 \end{aligned} \tag{2.11}$$

The evaluation of the unknown coefficients, C_k , is carried out by expanding them in terms of plane waves along the direction of motion of the positron (i.e., the z-axis),

$$C_k(z) = A_k(z)\exp(iB_k(z)) \tag{2.12}$$

$$\hbar B_k(z) = p_{kE}z + \int \sigma_k(z)dz. \tag{2.13}$$

The values of σ_k are the solutions of the equation

$$i\hbar\frac{d\sigma_k}{dz} = \sigma_k(\sigma_k + 2p_{kE}) + \frac{E}{c^2}(2U_0 + \mu\varepsilon_{nE})\cos(k_s z) \tag{2.14}$$

and

$$p_{kE}c = \sqrt{E^2 - m_0^2c^4 - p_y^2c^2 - 2E\varepsilon_{nE}} \tag{2.15}$$

Since $|U| \ll E$ and $k_s \leq \omega_E$, we can use the approximation $|\frac{dF_k}{dz}| \approx k_s|F_k| \leq \omega_E F_k$ where $F_k = \sigma_k, A_k$, and using $\frac{\sigma_k}{p_{kE}} \ll 1$ we have

$$\sigma_k = -\zeta_h\left(U_0 + \frac{\mu}{2}\varepsilon_{nE}\right)\cos(k_s z) \tag{2.16}$$

where

$$\zeta_h = \frac{E}{p_{kE}c^2}$$

Substituting the above equations in Eqn. (2.11) and rearranging, we get

$$\begin{aligned} i\frac{dA_k}{dz} &= \frac{1}{4}\mu\zeta_h\omega_E\cos(k_s z).\exp(-iB_k)\Big[\sqrt{k(k-1)}\ A_{k-2}\exp(-iB_{k-2}) \\ &+ \sqrt{(k+1)(k+2)}\ A_{k+2}\exp(-iB_{k+2})\Big] \end{aligned} \tag{2.17}$$

Also we can rewrite Eqn. (2.13) as

$$\hbar B_k = p_{kE}z - \zeta_h\left(1 + \frac{\mu}{2}\cos(k_s z)\right)\frac{\sin(k_s z)}{k_s} \tag{2.18}$$

Introducing the column matrix,

$$\hat{A} = \begin{pmatrix} A_1 \\ A_2 \\ ... \\ ... \end{pmatrix} \tag{2.19}$$

Eqn. (2.17) can be written in a compact form

$$i\frac{d\hat{A}}{dz} = \mu\hat{H}\hat{A} \tag{2.20}$$

with

$$\hat{H} = \begin{pmatrix} 0 & 0 & u^*\sqrt{2} & 0 & ... \\ 0 & 0 & 0 & u^*\sqrt{6} & ... \\ u\sqrt{2} & 0 & 0 & 0... & \\ 0 & u\sqrt{6} & 0 & 0 & ... \\ ... & ... & ... & ... & ... \end{pmatrix} \tag{2.21}$$

where

$$u = \frac{1}{4}\zeta_h \cos(k_s z) \exp\left\{ i\zeta_h \omega_E \left[2z + \mu \frac{\sin(k_s z)}{k_s} \right] \right\} \tag{2.22}$$

The solution of Eqn. (2.20) can be written as

$$\hat{A}(z) = \hat{Q}(z).\hat{R} \tag{2.23}$$

where $\hat{Q}(z) = \exp\left[-i\mu \int \hat{H}(z)\ dz \right] = 1 - i\mu \int \hat{H}(z)\ dz$ to the first order in μ. The column matrix $\hat{R}$ is composed of integration constants R_k, normalized by the condition,

$$\sum_k |R_k| = \frac{1}{\sqrt{l_y l_z}}$$

The solution corresponding to different transverse states can be found by setting

$$R_k = \frac{\delta_{kn}}{\sqrt{l_y l_z}} \qquad n, k = 0, 1, 2...$$

The wavefunction of the positron is then written as

$$\psi_{np_yE}(r) = \frac{1}{\sqrt{l_y l_z}} \exp\left(\frac{i}{\hbar} p_y y \right) \sum_{k=0}^{\infty} S_{kE}(x) Q_{kn}(z). \tag{2.24}$$

Resonant influence of hypersound

Due to the external hypersonic wave momentum $\hbar k_s$, the positron momentum p_z takes three possible values as

$$p_z = \begin{cases} p_{nE} - \hbar k_s \\ p_{nE} \\ p_{nE} + \hbar k_s \end{cases} \tag{2.25}$$

Correspondingly, Eqn. (2.24) can now be written in the form of a superposed wave-function and is given by,

$$\psi_{np_yE} = \psi^{(-1)}_{np_yE} + \psi^{(0)}_{np_yE} + \psi^{(+1)}_{np_yE} \tag{2.26}$$

where

$$\psi^{(0)}_{np_yE} = \frac{1}{\sqrt{l_y l_z}}\ S_{nE}(x)\ \ \exp\left\{\frac{i}{\hbar}[p_y y + p_{nE} z]\right\} \tag{2.27}$$

$$\begin{aligned} \psi^{(\pm1)}_{np_yE} = \frac{1}{\sqrt{l_y l_z}} \quad & \left[\ \ b^{(\pm1)}_{n-2} S_{n-2,E}(x) + b^{(\pm1)}_{n} S_{n,E}(x) + b^{(\pm1)}_{n+2} S_{n+2,E}(x)\right] \\ \times \quad & \exp\left\{\frac{i}{\hbar}[p_y y + (p_{nE} \pm \hbar k_s) z]\right\} \end{aligned} \tag{2.28}$$

During the above simplification, the amplitudes are found to be,

$$\begin{aligned} b^{(\pm1)}_{n-2} &= \frac{\mu\xi\sqrt{n(n-1)}}{16(\xi \mp 1)} \\ b^{(\pm1)}_{n} &= \mp\frac{\zeta_h}{2\hbar k_s}\left(U_0 + \frac{1}{2}\mu\varepsilon_{nE}\right) \\ b^{(\pm1)}_{n+2} &= -\frac{\mu\xi\sqrt{(n+1)(n+2)}}{16(\xi \pm 1)} \end{aligned} \tag{2.29}$$

where $\xi = \frac{2\zeta_h\omega_E}{k_s}$.

From the above Eqn. (2.29), it follows that $b^{(+1)}_{n-2} \to b^{(-1)}_{n+2} \to \infty$ when $\xi = \frac{2\zeta_h\omega_E}{k_s} \to 1$. Thus the absolute values of the amplitudes of the states with $p_z = p_{nE} \pm \hbar k_s$ show a

sudden (resonance) increase when the wavelength $\lambda_s = 2\pi/k_s$ decreases and reaches the critical value

$$\lambda_h^c = \frac{\pi}{\zeta_h \omega_E} \tag{2.30}$$

The radiation frequency obtained by the Doppler formula is given by,

$$\omega_h = \frac{\Omega_{fi} - \nu k_s \zeta_h^{-1}}{1 - \beta_{\parallel} \cos\theta} \tag{2.31}$$

where

$$\Omega_{fi} = \frac{E_{ni} - E_{nf}}{\hbar}$$

Radiative transitions induced by hypersound

Let us consider the radiative transitions of the channeled positrons that are stimulated by the hypersound.

The probability of transitions from an initial state i to a final state f is given by the formula [50],

$$W_{fi} = \frac{4\pi^2 e^2}{\hbar V} \sum_{\vec{q}} |\vec{q}|^{-1} |\vec{\alpha}_{fi}.\vec{e_k}|^2 \ \delta(\omega_{fi} - \omega) \tag{2.32}$$

where V is the volume of the system and $\vec{q}$ and $\vec{e_k}$ are the wavevector and polarization vector of the photon and the matrix elements $\vec{\alpha}_{fi}$ are given by,

$$\vec{\alpha}_{fi} = \frac{1}{E} \delta_{\sigma_{iz},\sigma_{fz}} \int e^{-i\vec{q}\vec{r}} \psi_f^*(\vec{r}) \ \hat{\vec{p}} \ \psi_i(\vec{r}) \ d\vec{r} \tag{2.33}$$

After integration over y and z, we have the following expression for the matrix elements

$$\begin{aligned} \vec{\alpha}_{fi} = \delta_{\sigma_{iz}\sigma_{fz}} \delta_{p_{iy},p_{fy}+\hbar q_y} \quad \Big[& \quad \vec{D}_{fi}^{(-2)} \delta_{p_{n_i E_i - 2\hbar k_s}, p_{n_f E_f + \hbar q_z}} + \vec{D}_{fi}^{(-1)} \delta_{p_{n_i E_i - \hbar k_s}, p_{n_f E_f + \hbar q_z}} \\ & + \quad \vec{D}_{fi}^{(0)} \delta_{p_{n_i E_i}, p_{n_f E_f + \hbar q_z}} + \vec{D}_{fi}^{(+1)} \delta_{p_{n_i E_i + \hbar k_s}, p_{n_f E_f + \hbar q_z}} \\ & + \quad \vec{D}_{fi}^{(+2)} \delta_{p_{n_i E_i + 2\hbar k_s}, p_{n_f E_f + \hbar q_z}} \Big] \end{aligned} \tag{2.34}$$

where

$$\vec{D}_{fi}^{\nu} = \frac{1}{E}\sum_{\varepsilon_1,\varepsilon_2}\delta_{\nu,\varepsilon_2-\varepsilon_1}\int \exp(-iq_x x)\ F_f^{(\varepsilon_1)^*}\hat{\vec{p}}_{i\varepsilon_2}F_i^{(\varepsilon_2)}\ dx \tag{2.35}$$

where ν represents the transition between different states and

$$\hat{\vec{p}}_{i\varepsilon} = \hat{p}_x,\ p_{iy},\ p_{n_iE_i}+\varepsilon\hbar k_s \qquad\qquad \varepsilon = 0,\ \pm 1 \tag{2.36}$$

$$F_{nE}^{(\varepsilon)} = \begin{cases} S_{nE}(x) & \varepsilon = 0 \\ b_{n-2}^{(\varepsilon)}S_{n-2,E}(x) + b_n^{(\varepsilon)}S_{n,E}(x) + b_{n+2}^{(\varepsilon)}S_{n+2,E}(x) & \varepsilon = \pm 1 \end{cases} \tag{2.37}$$

From Eqn. (2.34), we can write the probability of transition as the sum of five terms given by,

$$W_{fi} = \sum_{\nu} W_{fi}^{(\nu)} \qquad\qquad \nu = 0,\ \pm 1\ \pm 2 \tag{2.38}$$

Angular and spectral distributions

(i) Matrix elements

To find the matrix elements we define the vector of polarization $\vec{e_1}$ in the plane having the wavevector $\vec{q}$ and the z-axis and a vector $\vec{e_2} \perp \vec{e_1}$ in the plane having the axes x and y [35].

$$\begin{aligned} \vec{e}_1 &= (\cos\theta\ \cos\varphi,\ \cos\theta\ \sin\varphi,\ -\sin\theta) \\ \vec{e}_2 &= (-\sin\varphi,\ \cos\varphi,\ 0) \end{aligned} \tag{2.39}$$

The summation in Eqn. (2.32) can be transferred into an integral form given by,

$$W_{fi}^{(\nu)} = \frac{e^2}{2\pi\hbar}\int (|\vec{\alpha}_{fi}^{(\nu)}.\vec{e_1}|^2 + |\vec{\alpha}_{fi}^{(\nu)}.\vec{e_2}|^2)\ |\vec{q}|^{-1}\delta(\omega_{fi}-\omega)\ d\vec{q} \tag{2.40}$$

where

$$\vec{\alpha}_{fi} = \delta_{\sigma_{iz},\sigma_{fz}}\delta_{p_{iy},p_{fy}+\hbar q_y}\delta_{p_{n_iE_i}+\nu\hbar k_s,p_{n_fE_f}+\hbar q_z}\vec{D}_{fi}^{(\nu)} \tag{2.41}$$

From the above equations, we can notice that a hypersonic field can induce five radiative transitions for the channeling radiation. Corresponding transition probabilities are given by $W_{fi}^{(\nu)}$. The case $\nu = 0$ is for channeling in the absence of a hypersonic field. Since $\nu = \pm 2$ are forbidden (see equations (2.25) and (2.34)) we are left with only three radiative transitions induced by the hypersound.

For $\nu = 0$, one obtains [16, 50]

$$\vec{D}_{fi}^{(0)} \approx -x_{fi}\left(\frac{\Omega_{fi}}{c},\ 0,\ q_x\beta\right) \tag{2.42}$$

with

$$q_x = \left(\frac{\omega\ \sin\theta\ \cos\varphi}{c}\right) \tag{2.43}$$

$$x_{fi} = \alpha\left(\sqrt{\frac{n_i+1}{2}}\delta_{n_f,n_i+1} + \sqrt{\frac{n_f+1}{2}}\delta_{n_i,n_f+1}\right) \tag{2.44}$$

It remains to calculate the matrix elements for $\nu = \pm 1$. It is found that only transitions with $n_i - n_f = \pm 1$ are allowed. Only direct transitions ($n_i - n_f = +1$) are possible for $\xi > 2$ and $\nu = \pm 1$. Direct as well as inverse transitions ($n_i - n_f = -1$) are possible for $\xi < 2$ and $\nu = -1$.

(ii) Transition Probabilities

The transition probabilities and the intensities for the case $\nu = 0$ (i.e., without the hypersonic field) are given by [16, 50]

$$\frac{dW_{fi}^{(0)}}{d\Omega} = \frac{e^2\omega_E^3 x_{fi}^2}{2\pi\hbar c^3(1-\beta\cos\theta)^4}[(1-\beta\cos\theta)^2 - (1-\beta^2)\sin^2\theta\cos^2\varphi] \tag{2.45}$$

$$\frac{dW_{fi}^{(0)}}{d\omega} = \frac{e^2\omega_E^2 x_{fi}^2}{\hbar c^3}\left[1 - 2\frac{\omega}{\omega_m} + 2\left(\frac{\omega}{\omega_m}\right)^2\right] \tag{2.46}$$

$$\frac{dI_{fi}^{(0)}}{d\Omega} = \frac{e^2\omega_E^4 x_{fi}^2}{2\pi c^3(1-\beta\cos\theta)^5}[(1-\beta\cos\theta)^2-(1-\beta^2)\sin^2\theta\cos^2\varphi] \quad (2.47)$$

$$\frac{dI_{fi}^{(0)}}{d\omega} = 3I_{fi}^{(0)}\ \frac{\omega}{\omega_m^2}\left[1-2\frac{\omega}{\omega_m}+2\left(\frac{\omega}{\omega_m}\right)^2\right] \quad (2.48)$$

where

$$I_{fi}^{(0)} = \frac{4}{3}\frac{e^2\omega_E^4\gamma^4 x_{fi}^2}{c^3} \quad (2.49)$$

We shall now analyze those transitions induced by hypersound.

Substituting q_x from Eqn (2.43) and using equations (2.29) and (2.37) we get,

$$\vec{D}_{fi}^{(\pm1)} \approx \pm\frac{ix_{fi}\omega_E\mu\xi}{8}\ \frac{(\xi\mp2)}{(\xi\mp1)} \quad (2.50)$$

for direct transitions, and

$$\vec{D}_{fi}^{(-1)} \approx \frac{ix_{fi}\omega_E\mu\xi}{8}\ \frac{(2-\xi)}{(\xi-1)} \quad (2.51)$$

for inverse transitions.

Performing integration over ω in Eqn. (2.40) and using equations (2.41), (2.50) and (2.51), we get,

$$\frac{dW_{fi}^{(\pm1)}}{d\Omega} = q_{3fi}^{(\pm1)}\ \frac{e^2\omega_E^3 x_{fi}^2}{2\pi\hbar c^3(1-\beta\cos\theta)^4}[(1-\beta\cos\theta)^2-(1-\beta^2)\sin^2\theta\cos^2\varphi] \quad (2.52)$$

where q_{sfi} are given by,

$$q_{sfi}^{(\pm1)} = \frac{\mu^2\xi^{(4-s)}(\xi\mp2)^s}{64(\xi\mp1)^2} \quad (2.53)$$

for direct transitions and

$$q_{sfi}^{(-1)} = \frac{\mu^2\xi^{(4-s)}(2-\xi)^s}{64(\xi-1)^2} \quad (2.54)$$

for inverse transitions.

Performing integration over the solid angle in Eqn. (2.40), we get

$$\frac{dW_{fi}^{(\pm1)}}{d\omega} = q_{2fi}^{(\pm1)} \frac{e^2\omega_E^2 x_{fi}^2}{\hbar c^3}\left[1 - 2\frac{\omega}{\omega_{\pm fi}} + 2\left(\frac{\omega}{\omega_{\pm fi}}\right)^2\right] \tag{2.55}$$

where

$$\omega_{\pm fi} = 2\gamma^2\omega_E \begin{cases} 1 - \frac{2}{\xi} & \nu = +1 \quad n_i - n_f = +1 \quad \xi > 2 \\ \frac{2}{\xi} + 1 & \nu = -1 \quad n_i - n_f = -1 \\ \frac{2}{\xi} - 1 & \nu = -1 \quad n_i - n_f = +1 \quad \xi < 2 \end{cases} \tag{2.56}$$

Multiplying equations (2.52) and (2.55) by $\hbar\omega$, we get the angular and spectral distribution of the radiation intensity as,

$$\frac{dI_{fi}^{(\pm1)}}{d\Omega} = q_{4fi}^{(\pm1)} \frac{e^2\omega_E^4 x_{fi}^2}{2\pi c^3(1-\beta\cos\theta)^5}[(1-\beta\cos\theta)^2 - (1-\beta^2)\sin^2\theta\cos^2\varphi] \tag{2.57}$$

$$\frac{dI_{fi}^{(\pm1)}}{d\omega} = 3I_{fi}^{(\pm1)} \frac{\omega}{\omega_{\pm fi}^2}\left[1 - 2\frac{\omega}{\omega_{\pm fi}} + 2\left(\frac{\omega}{\omega_{\pm fi}}\right)^2\right] \tag{2.58}$$

where

$$I_{fi}^{(\pm1)} = \frac{4}{3}\frac{e^2\omega_E^4\gamma^4 x_{fi}^2}{c^3}\, q_{4fi}^{(\pm1)} \tag{2.59}$$

The expression for total intensity is proportional to the power of hypersound ($\sim \mu^2$). $q_{4fi}^{(\pm1)} \ll 1$ for $n_i - n_f = +1$ (direct transitions). Hence we can say that the influence of hypersound on direct transitions in weak. But on the otherhand, for inverse transitions $q_{4fi}^{(-1)} > 1$ and $\xi \to 1$. We will discuss this inverse transition case in detail in section 2.2.3 where the influence of anharmonicity will also be included.

2.2.2 Effects of Anharmonicity

Including the anharmonic term for the transverse periodic potential of the positron, the potential equation can be written as,

$$V(x) = V_0x^2 + V_1x^4 \tag{2.60}$$

where

$$V_1 = \frac{4\pi Z_1 Z_2 e^2 C a^2 N_p}{(l+a)^5} \tag{2.61}$$

The initial investigations on channeling radiation [16] did not consider the anharmonic part of the potential shown in Eqn. (2.1). Later, the effects of anharmonicity were studied by some authors [49]. The total energy spectrum is the sum of harmonic and anharmonic contributions, which can be written to the first order as

$$\varepsilon'_{nE} = \varepsilon_{nE} + \frac{3}{4} V_1 \alpha^4 (2n^2 + 2n + 1) \tag{2.62}$$

To find the effects of anharmonicity on wavefunction we use the Dirac equation (2.4). Substituting Eqn. (2.60) in (2.3) and then in Eqn. (2.10) we get after substituting x^2 and x^4 by their operator forms,

$$\begin{aligned}
-\frac{\hbar^2 c^2}{2E}\frac{\partial^2}{\partial z^2} C_k \;&+\; \left[U_0 \cos(k_s z) + \varepsilon'_{nE}\left(1 + \frac{\mu}{2}\cos(k_s z)\right)\right. \\
&+\; \left.\frac{\mu}{2}\cos(k_s z)\frac{3}{4} V_1 \alpha^4 (2k^2 + 2k + 1) - \frac{E^2 - m_0^2 c^4 - p_y^2 c^2}{2E}\right] C_k \\
&+\; \frac{1}{4}\mu\hbar\omega_E \cos(k_s z)\left[\sqrt{k(k-1)}C_{k-2} + \sqrt{(k+1)(k+2)}C_{k+2}\right] \\
&+\; \frac{1}{4}\mu V_1 \alpha^4 \cos(k_s z)\left[\sqrt{k(k-1)(k-2)(k-3)}C_{k-4}\right. \\
&+\; \sqrt{(k+1)(k+2)(k+3)(k+4)}C_{k+4} + (4k-2)\sqrt{k(k-1)}C_{k-2} \\
&+\; \left.(4k+6)\sqrt{(k+1)(k+2)}C_{k+2}\right] = 0
\end{aligned} \tag{2.63}$$

The coefficients, C_k are given by Eqn. (2.12), which is a function of $\exp(iB_k(z))$ given by Eqn. (2.13). The σ_k values in Eqn. (2.16) change due to the anharmonic term and is given by,

$$\sigma'_k = -\zeta_{ah}\left(U_0 + \frac{\mu}{2}\varepsilon'_{nE}\right)\cos(k_s z)$$

where

$$\zeta_{ah} = \frac{E}{p_{kE} c^2} \tag{2.64}$$

with p'_{kE} given by,

$$p'_{kE}c = \sqrt{E^2 - m_0^2c^4 - p_y^2c^2 - 2E\varepsilon'_{nE}}$$

Substituting C_k and the above equations in Eqn. (2.63) and rearranging, we get

$$\begin{aligned}
i\frac{dA_k}{dz} &= \zeta_{ah}\Bigg\{ \exp(-iB_k)\Bigg[\frac{1}{4}\mu\omega_E\cos(k_sz)\Bigg[\sqrt{k(k-1)}A_{k-2}\exp(-iB_{k-2}) \\
&+ \sqrt{(k+1)(k+2)}A_{k+2}\exp(-iB_{k+2})\Bigg] \\
&+ \frac{1}{4}\mu V_1\alpha^4\cos(k_sz)\Bigg[\sqrt{k(k-1)(k-2)(k-3)}A_{k-4}\exp(-iB_{k-4}) \\
&+ \sqrt{(k+1)(k+2)(k+3)(k+4)}A_{k+4}\exp(-iB_{k+4}) \\
&+ (4k-2)\sqrt{k(k-1)}A_{k-2}\exp(-iB_{k-2}) \\
&+ (4k+6)\sqrt{(k+1)(k+2)}A_{k+2}\exp(-iB_{k+2})\Bigg] \\
&+ \frac{\mu}{2}\cos(k_sz)\frac{3}{4}\frac{V_1\alpha^4}{\hbar}(2k^2+2k+1)A_k\Bigg\}
\end{aligned} \tag{2.65}$$

Eqn. (2.65) can be written in the form

$$i\frac{d\hat{A}}{dz} = \mu\hat{H}\hat{A} \tag{2.66}$$

with

$$\hat{H} = \begin{pmatrix}
J & 0 & (u^*+6w^*)\sqrt{2} & 0 & v^*\sqrt{24} & ... \\
0 & 5J & 0 & (u^*+10w^*)\sqrt{6} & 0 & ... \\
(u+6w)\sqrt{2} & 0 & 13J & 0 & (u^*+14w^*)\sqrt{12} & ... \\
0 & (u+10w)\sqrt{6} & 0 & 25J & 0 & ... \\
v\sqrt{24} & 0 & (u+14w)\sqrt{12} & 0 & 41J & ... \\
... & ... & ... & ... & ... & ...
\end{pmatrix} \tag{2.67}$$

The above Hermitian matrix can be written in the form of recurrence relations given

by,

$$\begin{aligned} H_{k+2,k} &= H^*_{k,k+2} = [u + (4k+6)w]\sqrt{(k+1)(k+2)} \\ H_{k+4,k} &= H^*_{k,k+4} = v\sqrt{(k+1)(k+2)(k+3)(k+4)} \\ H_{k,k} &= J(2k^2+2k+1) \end{aligned} \tag{2.68}$$

where

$$J = \frac{3}{8}t\zeta_{ah}\mu\cos(k_s z), \qquad t = \frac{V_1\alpha^4}{\hbar}$$

and

$$\begin{aligned} u &= \frac{1}{4}\zeta_{ah}\omega_E\cos(k_s z)\exp\left\{i\zeta_{ah}\left(2\omega_E + \frac{3}{4}t(8k+12)\right)\left[z + \frac{\mu}{2}\frac{\sin(k_s z)}{k_s}\right]\right\} \\ v &= \frac{1}{4}t\zeta_{ah}\cos(k_s z)\exp\left\{2i\zeta_{ah}\left(2\omega_E + \frac{3}{4}t(8k+20)\right)\left[z + \frac{\mu}{2}\frac{\sin(k_s z)}{k_s}\right]\right\} \\ w &= \frac{1}{4}t\zeta_{ah}\cos(k_s z)\exp\left\{i\zeta_{ah}\left(2\omega_E + \frac{3}{4}t(8k+12)\right)\left[z + \frac{\mu}{2}\frac{\sin(k_s z)}{k_s}\right]\right\} \end{aligned} \tag{2.69}$$

Solving Eqn. (2.66) we get the total wave function. It is given as

$$\psi_{np_yE}(r) = \frac{1}{\sqrt{l_y l_z}}\exp\left(\frac{i}{\hbar}p_y y\right)\sum_{k=0}^{\infty} S_{kE}(x)Q_{kn}(z). \tag{2.70}$$

Resonant influence of hypersound

The superposed wavefunction due to effect of hypersound and anharmonicity is obtained from Eqn. (2.70) and is given by,

$$\psi_{np_yE} = \psi^{(-1)}_{np_yE} + \psi^{(0)}_{np_yE} + \psi^{(+1)}_{np_yE} \tag{2.71}$$

where

$$\psi^{(0)}_{np_yE} = \frac{1}{\sqrt{l_y l_z}}\ S_{nE}(x)\ \exp\left\{\frac{i}{\hbar}[p_y y + p_{nE} z]\right\}\left[1 - i\frac{3}{8}\mu^2\zeta_{ah}t(2n^2+2n+1)\frac{\sin(k_s z)}{k_s}\right] \tag{2.72}$$

$$\psi^{(\pm1)}_{npyE} = \frac{1}{\sqrt{l_y l_z}} \quad \Bigg[\quad b^{(\pm1)}_{n-4} S_{n-4,E}(x) + b^{(\pm1)}_{n-2} S_{n-2,E}(x)$$
$$+ \quad b^{(\pm1)}_{n} S_{n,E}(x) + b^{(\pm1)}_{n+2} S_{n+2,E}(x) + b^{(\pm1)}_{n+4} S_{n+4,E}(x) \Bigg]$$
$$\times \quad \exp\left\{ \frac{i}{\hbar}[p_y y + (p_{nE} \pm \hbar k_s) z] \right\} \tag{2.73}$$

During the above simplification, the amplitudes are found to be,

$$\begin{aligned}
b^{(\pm1)}_{n-4} &= \frac{\mu t \zeta_{ah} \sqrt{n(n-1)(n-2)(n-3)}}{8k_s(2\xi \mp 1)} \\
b^{(\pm1)}_{n-2} &= \frac{\mu \zeta_{ah}[\omega_E + (4n-2)t]\sqrt{n(n-1)}}{8k_s(\xi \mp 1)} \\
b^{(\pm1)}_{n} &= \mp \frac{\zeta_{ah}}{2\hbar k_s}\left(U_0 + \frac{1}{2}\mu \varepsilon'_{nE} \right) \\
b^{(\pm1)}_{n+2} &= -\frac{\mu \zeta_{ah}[\omega_E + (4n+6)t]\sqrt{(n+1)(n+2)}}{8k_s(\xi \pm 1)} \\
b^{(\pm1)}_{n+4} &= -\frac{\mu t \zeta_{ah} \sqrt{(n+1)(n+2(n+3)(n+4}}{8k_s(2\xi \pm 1)}
\end{aligned} \tag{2.74}$$

where $\xi = \frac{2\zeta_{ah}\omega_E}{k_s}$.

In addition to the resonance obtained for the harmonic case, it further follows from the above Eqn. (2.74) that $b^{(+1)}_{n-4} \to b^{(-1)}_{n+4} \to \infty$ when $2\xi = \frac{4\zeta_{ah}\omega_E}{k_s} \to 1$. Thus the absolute values of the amplitudes of the states with $p_z = p_{nE} \pm \hbar k_s$ show a sudden increase when the wavelength $\lambda_s = 2\pi/k_s$ decreases and reaches the critical value

$$\lambda^c_{ah} = \frac{\pi}{2\zeta_{ah}\omega_E} \tag{2.75}$$

which is just half of the corresponding resonance wavelength for the harmonic case. This leads to a variation in the intensity of the radiation, as discussed in the following sections.

The radiation frequency obtained by the Doppler formula after incorporating energy changes due to anharmonic effects leads to the modified formula as

$$\omega_{ah} = \frac{\Omega_{fi}\left[1+\left(\frac{3V_1}{4V_0}\right)\alpha^2(n_i+n_f+1)\right] - \nu k_s \zeta_{ah}^{-1}}{1-\beta_{\|}\cos\theta} \tag{2.76}$$

Thus the fractional change in the radiative frequency due to the anharmonicity is given by,

$$\frac{\Delta\omega}{\omega_h} = \frac{\Omega_{fi}\left(\frac{3V_1}{4V_0}\right)\alpha^2(n_i+n_f+1) - \nu k_s(\zeta_{ah}^{-1}-\zeta_h^{-1})}{\Omega_{fi}-\zeta_h^{-1}} \tag{2.77}$$

One can notice from the above expression that the fractional change in the resonance frequency $\rightarrow 0$ in the absence of anharmonic interactions.

Radiative transitions induced by hypersound

Let us consider the radiative transitions of the channeled positrons that are stimulated by the hypersound affected by the anharmonic interactions. The probability of transitions is given by Eqn. (2.32). The matrix elements $\vec{\alpha}_{fi}$ for the harmonic case are given in Eqn. (2.34) where the elements $\vec{D}_{fi}$ for the anharmonic case are given by,

$$\vec{D}_{fi}^{\nu} = \frac{1}{E}\sum_{\varepsilon_1,\varepsilon_2}\delta_{\nu,\varepsilon_2-\varepsilon_1}\int \exp(-iq_x x)\; F_f^{(\varepsilon_1)^*}\hat{\vec{p}}_{i\varepsilon_2}F_i^{(\varepsilon_2)}\; dx \tag{2.78}$$

where

$$F_{nE}^{(\varepsilon)} = \begin{cases} S_{nE}(x) & \varepsilon = 0 \\ b_{n-4}^{(\varepsilon)}S_{n-4,E}(x) + b_{n-2}^{(\varepsilon)}S_{n-2,E}(x) & \\ +b_n^{(\varepsilon)}S_{n,E}(x) + b_{n+2}^{(\varepsilon)}S_{n+2,E}(x) + b_{n+4}^{(\varepsilon)}S_{n+4,E}(x) & \varepsilon = \pm 1 \end{cases} \tag{2.79}$$

Angular and spectral distributions

ν represents the transition between different states. $\nu = 0$ corresponds to the case where there is no hypersound interaction and the matrix elements are given in Eqn. (2.42).

It needs to calculate the matrix elements for $\nu = \pm 1$. It is found that direct transitions are possible for $\xi[1 + (\frac{3V_1}{4V_0})\alpha^2(n_i + n_f + 1)] > 2$ and $\nu = \pm 1$. Direct as well as inverse transitions are possible for $\xi[1 + (\frac{3V_1}{4V_0})\alpha^2(n_i + n_f + 1)] < 2$ and $\nu = -1$. Table 1 shows the photon frequencies for $\nu = \pm 1$.

Table 1: Photon Frequencies for $\nu = \pm 1$ at direct and inverse transitions.

	ν	
$n_i - n_f$	-1	+1
+1	$\omega = \frac{\omega_E\{\xi[1+(\frac{3V_1}{4V_0})\alpha^2(n_i+n_f+1)]+2\}}{\xi(1-\beta\cos\theta)} = \omega'_{dir}$	$\omega = \frac{\omega_E\{\xi[1+(\frac{3V_1}{4V_0})\alpha^2(n_i+n_f+1)]-2\}}{\xi(1-\beta\cos\theta)} = \omega''_{dir}$
direct transition	for any ξ	$\xi[1 + (\frac{3V_1}{4V_0})\alpha^2(n_i + n_f + 1)] > 2$
-1	$\omega = \frac{\omega_E\{2-\xi[1+(\frac{3V_1}{4V_0})\alpha^2(n_i+n_f+1)]\}}{\xi(1-\beta\cos\theta)} = \omega_{inv}$	$\omega = -\frac{\omega_E\{\xi[1+(\frac{3V_1}{4V_0})\alpha^2(n_i+n_f+1)]+2\}}{\xi(1-\beta\cos\theta)} < 0$
inverse transition	$\xi[1 + (\frac{3V_1}{4V_0})\alpha^2(n_i + n_f + 1)] < 2$	not realized

We shall now analyze those transitions due to anharmonicity.

Substituting q_x from Eqn (2.43) and using equations (2.74) and (2.79),

$$\vec{D}_{fi}^{(\pm1)} \approx \pm\frac{ix_{fi}\mu\xi}{8c} \quad \left[\quad \frac{\sqrt{6}t}{4(2\xi \mp 1)} + \frac{\omega_E + 6t}{(\xi \mp 1)} \right] \left\{ \xi \left[1 + \left(\frac{3V_1}{4V_0} \right) \alpha^2 (n_i + n_f + 1) \right] \mp 2 \right\} \times \quad \left[1, \ 0, \ \frac{\beta \sin\theta \cos\varphi}{1 - \beta\cos\theta} \right] \tag{2.80}$$

for direct transitions, and

$$\vec{D}_{fi}^{(-1)} \approx \frac{ix_{fi}\mu\xi}{8c} \quad \left[\quad \frac{\sqrt{6}t}{4(2\xi - 1)} + \frac{\omega_E + 6t}{(\xi - 1)} \right] \left\{ 2 - \xi \left[1 + \left(\frac{3V_1}{4V_0} \right) \alpha^2 (n_i + n_f + 1) \right] \right\} \times \quad \left[1, \ 0, \ \frac{\beta \sin\theta \cos\varphi}{1 - \beta\cos\theta} \right] \tag{2.81}$$

for inverse transitions.

Performing integration over ω in Eqn. (2.40) and using equations (2.41), (2.80) and (2.81), we get,

$$\frac{dW_{fi}^{(\pm1)}}{d\Omega} = q_{3fi}^{(\pm1)} \ \frac{e^2\omega_E^3 x_{fi}^2}{2\pi\hbar c^3 (1 - \beta\cos\theta)^4} [(1 - \beta\cos\theta)^2 - (1 - \beta^2)\sin^2\theta\cos^2\varphi] \tag{2.82}$$

where the x_{fi} are given by,

$$\begin{aligned} x_{n,\ n-1} &= \alpha \left(\frac{n}{2} \right)^{1/2} \left(1 - n\frac{3}{4}\frac{V_1}{V_0}\alpha^2 \right) \\ \text{and} \qquad x_{n,\ n+1} &= \alpha \left(\frac{n+1}{2} \right)^{1/2} \left(1 - (n+1)\frac{3}{4}\frac{V_1}{V_0}\alpha^2 \right) \end{aligned}$$

and the q_{sfi} are given by,

$$q_{sfi}^{(\pm1)}(\xi) = \frac{\mu^2 \xi^{(4-s)} \{\xi[1 + (\frac{3V_1}{4V_0})\alpha^2(n_i + n_f + 1)] \mp 2\}^s}{64} \left[\frac{\sqrt{6}b}{4(2\xi \mp 1)} + \frac{1 + 6b}{(\xi \mp 1)} \right]^2 \tag{2.83}$$

for direct transitions, and

$$q_{sfi}^{(-1)}(\xi) = \frac{\mu^2 \xi^{(4-s)} \{2 - \xi[1 + (\frac{3V_1}{4V_0})\alpha^2(n_i + n_f + 1)]\}^s}{64} \left[\frac{\sqrt{6}b}{4(2\xi - 1)} + \frac{1 + 6b}{(\xi - 1)} \right]^2 \tag{2.84}$$

for inverse transitions, with $b = \frac{t}{\omega_E}$.

Performing integration over the solid angle in Eqn. (2.40), we get

$$\frac{dW_{fi}^{(\pm1)}}{d\omega} = q_{2fi}^{(\pm1)} \ \frac{e^2\omega_E^2 x_{fi}^2}{\hbar c^3}\left[1 - 2\frac{\omega}{\omega_{\pm fi}} + 2\left(\frac{\omega}{\omega_{\pm fi}}\right)^2\right] \tag{2.85}$$

where

$$\omega_{\pm fi} = 2\gamma^2\omega_E \begin{cases} [1 + (\frac{3V_1}{4V_0})\alpha^2(n_i + n_f + 1)] - \frac{2}{\xi} & \nu = +1 \\ n_i - n_f = +1 \qquad & \xi[1 + (\frac{3V_1}{4V_0})\alpha^2(n_i + n_f + 1)] > 2 \\ \\ \frac{2}{\xi} + [1 + (\frac{3V_1}{4V_0})\alpha^2(n_i + n_f + 1)] & \nu = -1 \\ n_i - n_f = +1 & \\ \\ \frac{2}{\xi} - [1 + (\frac{3V_1}{4V_0})\alpha^2(n_i + n_f + 1)] & \nu = -1 \\ n_i - n_f = -1 \qquad & \xi[1 + (\frac{3V_1}{4V_0})\alpha^2(n_i + n_f + 1)] < 2 \end{cases} \tag{2.86}$$

Multiplying equations (2.82) and (2.85) by $\hbar\omega$, we get the angular and spectral distribution of the radiation intensity as,

$$\frac{dI_{fi}^{(\pm1)}}{d\Omega} = q_{4fi}^{(\pm1)} \ \frac{e^2\omega_E^4 x_{fi}^2}{2\pi c^3(1 - \beta\cos\theta)^5}[(1 - \beta\cos\theta)^2 - (1 - \beta^2)\sin^2\theta\cos^2\varphi] \tag{2.87}$$

$$\frac{dI_{fi}^{(\pm1)}}{d\omega} = 3I_{fi}^{(\pm1)} \ \frac{\omega}{\omega_{\pm fi}^2}\left[1 - 2\frac{\omega}{\omega_{\pm fi}} + 2\left(\frac{\omega}{\omega_{\pm fi}}\right)^2\right] \tag{2.88}$$

where

$$I_{fi}^{(\pm1)} = \frac{4}{3}\frac{e^2\omega_E^4\gamma^4 x_{fi}^2}{c^3} \ q_{4fi}^{(\pm1)} \tag{2.89}$$

The expression for total intensity is proportional to the power of hypersound ($\sim \mu^2$). $q_{4fi}^{(\pm1)} \ll 1$ for $n_i - n_f = +1$. Comparing with the results in the harmonic case, the angular and spectral distributions of radiation differ by the anharmonic parameters given in equations (2.83) and (2.84).

2.2.3 Inverse radiative transitions

Inverse radiative transitions $n_i - n_f$ = -1 are excited by the hypersound. From equations (2.54) and (2.84) it is obvious that as $\xi \to 1$, $q_{4fi}^{(-1)} \gg 1$. This shows that there is a resonant amplification of the channeling radiation intensity due to inverse transitions. It is also found from Eqn. (2.84) that for the anharmonic case there is also an amplification of the radiation compared to the harmonic case. Figure 2.1 shows the influence of both hypersound and anharmonicity. The curves for a specific case $n_i = 0$, $n_f = 1$ are calculated using equations (2.58) and (2.88) for inverse transitions with ν = -1, μ= 0.1 and Eqn. (2.48) for direct transitions with $\nu = 0$ ($(s_{fi})^{-1} = 2e^2\omega_E^3\gamma^2 x_{fi}^2/c^3$). For the sake of comparison with the harmonic case, we take $\xi = 1.01$ and $\xi = 1.03$. The ratio of spectral distribution of radiation intensity in the anharmonic case to that in the harmonic case is about 1.16, which shows that the effect of the anharmonic term cannot be neglected.

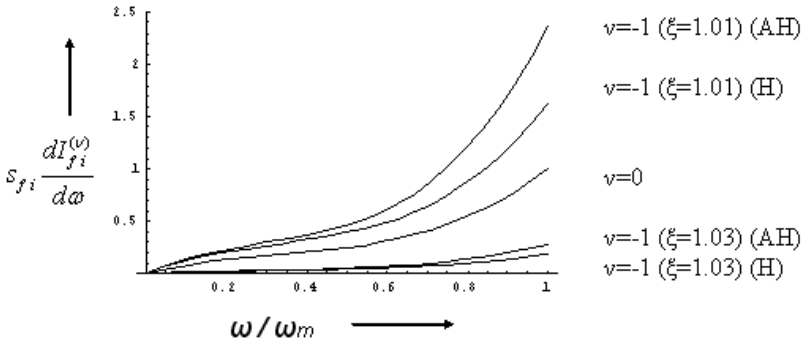

Figure 2.1: Spectral distributions in the case of inverse radiative transitions at $\nu = -1$ and ξ=1.01 and 1.03 for harmonic and anharmonic cases at $\nu = 0$.

2.3 Effects Transverse Periodic Perturbation

2.3.1 Harmonic Model

Influence on Wavefunction

When the transverse acoustic wave is propagating in the direction of z, the channel is bent and the atomic planes are displaced in the direction of x-axis by $a\ \cos(k'_s z)$ where $k'_s = \frac{2\pi}{\lambda'_s}$, a is the amplitude of bending and λ'_s is the wavelength of the transverse wave.

The planar potential after including the effects of the transverse acoustic wave is given by,

$$\begin{aligned} U(x,z) &= V_0\{x - a\ \cos(k'_s z)\}^2 \\ &= V_0 x^2 + V_0 a^2\ \cos^2(k'_s z) - 2V_0 xa\ \cos(k'_s z) \end{aligned} \tag{2.90}$$

If we consider the third term in Eqn. (2.90) as perturbation, the perturbed energy is given by

$$\begin{aligned} \varepsilon'_{nE} &= \varepsilon_{nE} + E' \\ \varepsilon_{nE} &= \left(n + \frac{1}{2}\right)\hbar\omega \\ E' &= -\frac{4V_0^2 a^2\ \cos^2(k'_s z)}{2m\omega^2} \end{aligned}$$

As seen from Eqn. (2.90), the positron planar potential is z-dependent. Therefore the wavefunction has the same form as in Eqn. (2.9). Using Eqn. (2.91) in Eqn. (2.10), we can write,

$$\begin{aligned} - &\left(\frac{E^2 - p_y^2 c^2 - m_0^2 c^4}{2E}\right)\psi + \varepsilon_{kE}\psi + \left[V_0 a^2\ \cos^2(k'_s z) - 2V_0 xa\ \cos(k'_s z)\right]\psi \\ - &\frac{\hbar^2 c^2}{2E}\frac{\partial^2}{\partial z^2}\sum_{k=0}^{\infty} C_{kE}(z)\ S_{kE}(x) = 0 \end{aligned} \tag{2.91}$$

Converting the x in the 3^{rd} term of Eqn. (2.91) to operator form, we get

$$\left[-\left(\frac{E^2-p_y^2c^2-m_0^2c^4}{2E}\right)+\varepsilon_{kE}+V_0a^2\ \cos^2(k_s'z)-\frac{\hbar^2c^2}{2E}\frac{\partial^2}{\partial z^2}\right]C_k$$
$$-\sqrt{\frac{2\hbar}{m\omega}}V_0a\ \cos(k_s'z)\left[\sqrt{k+1}\ C_{k+1}+\sqrt{k}\ C_{k-1}\right]=0 \tag{2.92}$$

As in the longitudinal case we write C_k in the form

$$C_k = A_k(z)\ \exp(iB_k(z)) \tag{2.93}$$
$$\hbar B_k = p_{_{kE}}z+\int\sigma_k(z)\ dz \tag{2.94}$$
$$i\hbar\frac{\partial\sigma_k}{\partial z} = \sigma_k(\sigma_k+2p_{_{kE}})+\frac{E}{c^2}\varepsilon_{kE}'a\ \cos(k_s'z) \tag{2.95}$$

Hence Eqn. (2.92) becomes

$$\begin{aligned}
&-\ \frac{\hbar^2c^2}{2E}\frac{\partial^2}{\partial z^2}\ A_k\ \exp(iB_k)\ +\ V_0a^2\ \cos^2(k_s'z)A_k\ \exp(iB_k)\\
&-\ \frac{p_{_{kE}}^2c^2}{2E}A_k\ \exp(iB_k)\\
&-\ \sqrt{\frac{2\hbar}{m\omega}}V_0a\ \cos(k_s'z)\left[\sqrt{k+1}\ A_{k+1}\ \exp(iB_{k+1})+\sqrt{k}\ A_{k-1}\ \exp(iB_{k-1})\right]\\
&=\ 0
\end{aligned} \tag{2.96}$$

which after simplification we get,

$$\begin{aligned}
&-\ \frac{\hbar^2c^2}{2E}A_k''\ -\ i\frac{\hbar c^2}{E}A_k'\left(p_{_{kE}}+\sigma_k(z)\right)\\
&-\ \frac{1}{2}A_k\ a\ \varepsilon_{kE}\ \cos(k_s'z)\ +\ V_0a^2\ \cos^2(k_s'z)A_k\\
&-\ \sqrt{\frac{2\hbar}{m\omega}}V_0a\ \cos(k_s'z)\ \exp(-iB_k)\left[\sqrt{k+1}\ A_{k+1}\ \exp(iB_{k+1})+\sqrt{k}\ A_{k-1}\ \exp(iB_{k-1})\right]\\
&=\ 0
\end{aligned} \tag{2.97}$$

The above equation can be written in a form similar to Eqn. (2.20) and is given by,

$$i\ \frac{dA_k}{dz}=\hat{H}A \tag{2.98}$$

where $\hat{H}$ is a Hermitian matrix, whose elements are found as,

$$\begin{aligned}
\int \hat{H}_{k+1,k} &= -\sqrt{k+1}\left(\frac{2}{m\hbar\omega}\right)^{1/2} V_0\zeta_h\ a\int \cos(k_s'z)\ \exp\left(i\zeta_h\ \omega\left[z+\frac{a}{2}\ \frac{\sin(k_s'z)}{k_s'}\right]\right)\ dz \\
&= i\sqrt{k+1}\ \frac{V_0\zeta_h a}{2k_s'}\left(\frac{2}{m\hbar\omega}\right)^{1/2}\left[\frac{e^{i(\xi+1)\tau}}{\xi+1}+\frac{e^{i(\xi-1)\tau}}{\xi-1}\right] \qquad (2.99) \\
\int \hat{H}_{k-1,k} &= -\sqrt{k}\left(\frac{2}{m\hbar\omega}\right)^{1/2} V_0\zeta_h\ a\int \cos(k_s'z)\ \exp\left(-i\zeta_h\ \omega\left[z+\frac{a}{2}\ \frac{\sin(k_s'z)}{k_s'}\right]\right)\ dz \\
&= -i\sqrt{k}\ \frac{V_0\zeta_h a}{2k_s'}\left(\frac{2}{m\hbar\omega}\right)^{1/2}\left[\frac{e^{-i(\xi-1)\tau}}{\xi-1}+\frac{e^{-i(\xi+1)\tau}}{\xi+1}\right] \qquad (2.100) \\
\int \hat{H}_{k,k} &= \frac{\zeta_h}{2\hbar}\left[V_0a^2z+\frac{V_0a^2}{2}\ \frac{\sin(2k_s'z)}{k_s'}-\varepsilon_{kE}\ a\ \frac{\sin(k_s'z)}{k_s'}\right] \qquad (2.101)
\end{aligned}$$

where $\tau = k_s'z$ and $\xi = \frac{\zeta_h\omega}{k_s'}$.

Including the above matrix elements and simplifying, we get the total wavefunction of positron channeling as,

$$\psi = \psi^{(-1)} + \psi^{(0)} + \psi^{(+1)} \qquad (2.102)$$

where

$$\begin{aligned}
\psi^{(0)} &= \frac{1}{\sqrt{l_yl_z}}\ S_{nE}\ \exp\left(\frac{i}{\hbar}[p_yy+p_{nE}z]\right) \\
&\quad \left(1-i\frac{\zeta_h}{2\hbar}\left[V_0a^2z+\frac{V_0a^2}{2}\ \frac{\sin(2k_s'z)}{k_s'}-\varepsilon_{nE}\ a\ \frac{\sin(k_s'z)}{k_s'}\right]\right) \qquad (2.103) \\
\psi^{(\pm1)} &= \frac{1}{\sqrt{l_yl_z}}\ \left[b_{n-1}^{'(\pm1)}S_{n-1,E}+b_n^{'(\pm1)}S_{n,E}+b_{n+1}^{'(\pm1)}S_{n+1,E}\right] \\
&\quad \exp\left(\frac{i}{\hbar}[p_yy+(p_{nE}\pm\hbar k_s'z)]\right) \qquad (2.104)
\end{aligned}$$

where

$$\begin{aligned}
b_{n-1}^{'(\pm1)} &= -\left(\frac{1}{2m\hbar\omega}\right)^{1/2}\ \frac{V_0\zeta_h a}{k_s'}\ \frac{\sqrt{n}}{\xi\mp1} \\
b_{n+1}^{'(\pm1)} &= \left(\frac{1}{2m\hbar\omega}\right)^{1/2}\ \frac{V_0\zeta_h a}{k_s'}\ \frac{\sqrt{n+1}}{\xi\pm1} \qquad (2.105) \\
b_n^{'(\pm1)} &= \mp\frac{\zeta_h a\ \varepsilon_{nE}}{4\hbar k_s'}
\end{aligned}$$

From the above equations, $b_{n+1}^{'(-1)} \rightarrow b_{n-1}^{'(+1)} \rightarrow 1$ when $\xi = \frac{\zeta_h \omega}{k_s'} \rightarrow 1$. This means that, the maximum amplitude is achieved when $\lambda_s' = \frac{2\pi}{\zeta_h \omega}$ which has its maximum value when $p_y = 0$. i. e., $(\lambda_s')_{max} = \frac{2\pi}{\omega} = \lambda$ $(c = 1)$, where $\lambda = \frac{2\pi}{\omega}$, the characteristic wavelength related to the transverse oscillation of the channeled particle, as predicted by Mkrtchyan *et. al* [33] as against $(\lambda_s')_{max} = \frac{\pi}{\omega} = \lambda/2$ in the longitudinal case. But the condition for the radiation due to the periodic bending (undulator radiation) is $\lambda_s' > \lambda$. At this resonance condition, the spectrum will not have a contribution from the undulator radiation but only channeling radiation prevails.

Radiative transitions induced by hypersound

To find the spectral distribution induced by the transverse hypersonic field, we use the general equation for probability of transitions given by Eqn. (2.40) which can be written in the integral form,

$$W_{fi}^{(\nu)} = \frac{e^2}{2\pi\hbar} \int \left(\left| \vec{\alpha'}_{fi}^{(\nu)} \ . \ \vec{e}_1 \right|^2 + \left| \vec{\alpha'}_{fi}^{(\nu)} \ . \ \vec{e}_2 \right|^2 \right) \ |q|^{-1} \ \delta(\omega_{fi} - \omega) \ dq \tag{2.106}$$

where α_{fi}' are given by,

$$\begin{aligned} \vec{\alpha'}_{fi} &= \delta_{\sigma_{iz} \ \sigma_{fz}} \delta_{p_{iy} \ p_{fy} + \hbar q_y} \Big[\vec{D}_{fi}^{'(-1)} \delta_{p_{n_i E_i - \hbar k_s}, \ p_{n_f E_f + \hbar q_z}} \\ &+ \vec{D}_{fi}^{'(0)} \delta_{p_{n_i E_i}, \ p_{n_f E_f + \hbar q_z}} + \vec{D}_{fi}^{'(+1)} \delta_{p_{n_i E_i + \hbar k_s}, \ p_{n_f E_f + \hbar q_z}} \Big] \end{aligned} \tag{2.107}$$

We integrate Eqn. (2.107) and use Eqn. (2.42) and

$$\left| \vec{D}_{fi}^{'(\pm 1)} \ . \ \vec{e}_1 \right|^2 = \frac{x_{fi}^2 \xi^2 a^2 \omega_E^2}{16 c^2} \ (\xi \mp 1)^2 \ \cos^2 \varphi \left[\frac{\cos\theta - \beta}{1 - \beta \ \cos\theta} \right]^2 \tag{2.108}$$

$$\left| \vec{D}_{fi}^{'(\pm 1)} \ . \ \vec{e}_2 \right|^2 = \frac{x_{fi}^2 \xi^2 a^2 \omega_E^2}{16 c^2} \ (\xi \mp 1)^2 \ \sin^2 \varphi \tag{2.109}$$

to get the angular and spectral distribution of probability and radiation intensity as,

$$\frac{dW^{(\pm1)}}{d\Omega} = q_{3fi}^{'(\pm1)} \frac{e^2 x_{fi}^2 \omega_E^3}{2\pi\hbar c^3(1-\beta\ \cos\theta)^4} \left[(1-\beta\ \cos\theta)^2 - (1-\beta^2)\sin^2\theta\ \cos^2\varphi\right] \tag{2.110}$$

$$\frac{dI^{(\pm1)}}{d\Omega} = q_{4fi}^{'(\pm1)} \frac{e^2 x_{fi}^2 \omega_E^4}{2\pi(1-\beta\ \cos\theta)^5} \left[(1-\beta\ \cos\theta)^2 - (1-\beta^2)\sin^2\theta\ \cos^2\varphi\right] \tag{2.111}$$

$$\frac{dW^{(\pm1)}}{d\omega} = q_{2fi}^{'(\pm1)} \frac{e^2 x_{fi}^2 \omega_E^2}{\hbar c^3} \left[1 - 2\left(\frac{\omega}{\omega'_{\pm fi}}\right) + 2\left(\frac{\omega}{\omega'_{\pm fi}}\right)^2\right] \tag{2.112}$$

$$\frac{dI^{(\pm1)}}{d\omega} = 3\ I_{fi}^{'(\pm1)} \frac{\omega}{\omega_{\pm fi}^2} \left[1 - 2\left(\frac{\omega}{\omega'_{\pm fi}}\right) + 2\left(\frac{\omega}{\omega'_{\pm fi}}\right)^2\right] \tag{2.113}$$

where

$$\omega'_{\pm fi} = 2\gamma^2\omega_E \begin{cases} 1-\frac{1}{\xi} & \nu=+1,\ \ n_i-n_f=+1 \\ 1+\frac{1}{\xi} & \nu=-1,\ \ n_i-n_f=+1 \\ \frac{1}{\xi}-1 & \nu=-1,\ \ n_i-n_f=-1 \end{cases} \tag{2.114}$$

$$q_{sf}^{'(\pm1)} = \xi^{4-s} \frac{a^2(\xi\mp1)^s}{16} \tag{2.115}$$

$$q_{sfi}^{'(-1)} = \xi^{4-s} \frac{a^2(1-\xi)^s}{16} \tag{2.116}$$

for direct and indirect transitions respectively and

$$I_{fi}^{'(\pm1)} = \frac{4}{3} \frac{e^2 x_{fi}^2 \omega_E^4 \gamma^4}{c^3} q_{4fi}^{'(\pm1)} \tag{2.117}$$

From the above equations it is clear that, the spectrum depends on the value of the amplitude of bending 'a' and is proportional to 'a^2'. Since we are considering the small amplitude regime, $q_{4fi}^{'(-1)} \ll 1$. The radiation intensity due the periodic bending at the low amplitude is negligible. With the decrease of $'a'$, the amplitude of the transverse oscillation increases, and correspondingly an increase in channeling radiation is predicted here.

2.3.2 Effects of Anharmonicity

Introducing anharmonicity to the positron planar potential potential in Eqn. (2.90), will make the potential more complicated as,

$$U(x,z) = V_0\{x - a\ \cos(k_s' z)\}^2 + V_1\{x - a\ \cos(k_s' z)\}^4 \tag{2.118}$$

where V_1 is given by Eqn. (2.61). As we have seen in the previous cases, due to the transverse perturbations and anharmonicity, the total wavefunction can be written as,

$$\psi = \psi^{(-1)} + \psi^{(0)} + \psi^{(+1)}$$

where

$$\begin{aligned}\psi^{(0)} &= \frac{1}{\sqrt{l_y l_z}}\ S_{nE}\ \exp\left(\frac{i}{\hbar}[p_y y + p_{nE} z]\right) \\ &\quad \left(1 - i\frac{\zeta_{ah}}{2\hbar}\left[V_0 a^2 z + \frac{V_0 a^2}{2}\ \frac{\sin(2k_s' z)}{k_s'} - \varepsilon_{nE}'\ a\ \frac{\sin(k_s' z)}{k_s'}\right]\right)\end{aligned} \tag{2.119}$$

$$\begin{aligned}\psi^{(\pm 1)} &= \frac{1}{\sqrt{l_y l_z}}\ \Big[b_{n-3}^{'(\pm 1)} S_{n-3,E} + b_{n-2}^{'(\pm 1)} S_{n-2,E} + b_{n-1}^{'(\pm 1)} S_{n-1,E} + b_n^{'(\pm 1)} S_{n,E} \\ &+ b_{n+1}^{'(\pm 1)} S_{n+1,E} + b_{n+2}^{'(\pm 1)} S_{n+2,E} + b_{n+3}^{'(\pm 1)} S_{n+3,E}\Big] \\ &\quad \exp\left(\frac{i}{\hbar}[p_y y + (p_{nE} \pm \hbar k_s' z)]\right)\end{aligned} \tag{2.120}$$

where

$$\begin{aligned} b_{n-3}^{'(\pm 1)} &= -\left(\frac{\hbar}{3m\omega}\right)^{3/2}\ \frac{9V_1\zeta_{ah}a}{2\hbar k_s'}\ \frac{[\omega_E + t(n-1)]\sqrt{n(n-1)(n-2)}}{3\xi \mp 1} \\ b_{n-2}^{'(\pm 1)} &= -\frac{6V_1\zeta_{ah}a^2}{4m\omega_E k_s'}\ \frac{[\omega_E + 3t(n-1)]\sqrt{n(n-1)}}{\xi \mp 1} \\ b_{n-1}^{'(\pm 1)} &= -\left(\frac{1}{2m\hbar\omega}\right)^{1/2}\ \frac{V_0\zeta_{ah}a}{k_s'}\ \frac{[\omega_E + 3tn]\sqrt{n}}{\xi \mp 1}\end{aligned} \tag{2.121}$$

$$
\begin{aligned}
b_n^{\prime(\pm 1)} &= \mp \frac{\zeta_{ah} a\ \varepsilon'_{nE}}{4\hbar k'_s} \\
b_{n+1}^{\prime(\pm 1)} &= \left(\frac{1}{2m\hbar\omega}\right)^{1/2} \frac{V_0 \zeta_{ah} a}{k'_s} \frac{[\omega_E + 3t(n+1)]\sqrt{n+1}}{\xi \pm 1} \\
b_{n+2}^{\prime(\pm 1)} &= \frac{3V_1 \zeta_{ah} a^2}{4m\omega_E k'_s} \frac{[2\omega_E + 3t(2n+3)]\sqrt{(n+1)(n+2)}}{\xi \pm 1} \\
b_{n+3}^{\prime(\pm 1)} &= \left(\frac{\hbar}{3m\omega}\right)^{3/2} \frac{9V_1 \zeta_{ah} a}{2\hbar k'_s} \frac{[\omega_E + 3t(n+2)]\sqrt{(n+1)(n+2)(n+3)}}{\xi \pm 1}
\end{aligned}
$$

where ζ_{ah} is given by Eqn. (2.64)

$$
\begin{aligned}
\zeta_{ah} &= \frac{E}{p'_{kE} c^2} \qquad (2.122) \\
\text{Also} \qquad \xi &= \frac{\zeta_{ah} \omega_E}{k'_s} \\
\text{and} \qquad t &= \frac{V_1 \alpha^4}{\hbar}
\end{aligned}
$$

This change in the amplitudes change the corresponding values of q'_{sfi} in equations (2.115) and (2.116). They are calculated as

$$
q_{sf}^{\prime(\pm 1)} = \xi^{4-s} a^2 \frac{\left(\xi\left[1+\left(\frac{3V_1}{4V_0}\alpha^2(n_i+n_f+1)\right)\right] \mp 1\right)^s}{16} \qquad (2.123)
$$

$$
q_{sfi}^{\prime(-1)} = \xi^{4-s} a^2 \frac{\left(1-\xi\left[1+\left(\frac{3V_1}{4V_0}\alpha^2(n_i+n_f+1)\right)\right]\right)^s}{16} \qquad (2.124)
$$

for direct and indirect transitions respectively.

As discussed in the previous section; the a^2 dependence of the q_{sfi} values weakens the radiative transitions for a periodically bent crystal with low amplitude of bending. Only radiation due to the channeling oscillation is prevailing in the spectrum. Even the proportional amplification due to the anharmonic parameters are having less impact on the spectrum.

2.4 Results and Discussions

In this chapter, we have studied the effects of a hypersonic field on the positron planar channeling radiation. We first considered the effects of longitudinal field. The anharmonic effects (quartic term) of the interplanar transverse potential seen by the positron have been included in the problem. The corresponding eigen spectrum is calculated from the Dirac equation. The wavefunction of the positron gets modified by these effects and changes the observable parameters like frequency and intensity of radiation. The fractional change in the frequency of the emitted radiation from that in the harmonic case is found to be directly proportional to the strength of the anharmonic term. The spectral distribution of radiation intensity is found for both harmonic and anharmonic cases. A resonant amplification of radiation intensity is observed in the inverse transitions for both the cases whereas the direct transitions are weakly influenced by the hypersonic field. Also a considerable variation of radiation intensity due to the anharmonic effects is observed as plotted in Figure 2.1: an increase by a factor 1.16 over harmonic case. This intensity amplification shows that the anharmonic terms cannot be neglected.

We found that the amplitudes (Eqn. (2.74)), responsible for the intensity of the emitted radiation, show a resonance when the hypersonic field wavelength λ_s approaches a value $\pi/2\zeta_{ah}\omega_E$ which is exactly half of the corresponding quantity for the harmonic case. This means that the resonance takes place at higher frequencies in the anharmonic case.

We also studied the influence of a transverse acoustic wave on the positron planar channeling radiation. The planar potential gets modified and the corresponding eigen spectrum is calculated using the Dirac equation. The wavefunction is calculated after including these effects and the intensity of radiation is found. It is found that

the spectral distribution of radiation intensity due to the periodic bending of the channel depends on the value of the amplitude of bending 'a' and is proportional to 'a^2'. Since we are considering the small amplitude regime, $q_{4fi}^{\prime(-1)} \ll 1$. Hence, the transverse perturbation have weak influence on undulator radiation spectrum in the low amplitude regime. Correspondingly an increase in channeling radiation intensity is expected, since the amplitude of channeling oscillation increases with decrease in a.

The influence of the anharmonicity on the effects of transverse perturbation has been studied. Though there is a proportional magnification due to the anharmonicity terms, it is not strong enough to overcome the strong a^2 dependence. As predicted in the theory of undulator radiation, we have found that only channeling radiation prevails in a low amplitude regime. Effects of higher amplitude case for these waves will be discussed in chapter 5.

We found that the amplitude equations (2.105) show a resonance at $\lambda_s' = \frac{2\pi}{\zeta\omega}$. The maximum value of λ is $(\lambda_s')_{max} = \frac{2\pi}{\omega} = \lambda$, the characteristic wavelength related to the transverse oscillation of the channeled particle, which is double the value found for longitudinal case as predicted by Mkrtchyan [33].

If we compare the longitudinal and transverse perturbations, we can conclude that for the case of channeling radiation, amplification of radiation intensity is maximum for the longitudinal case. Transverse perturbation has its dependencies on the amplitude of the acoustic waves depending on which the corresponding radiation intensity is varied.

APPENDIX

The equation of motion of a relativistic positron in the scalar field $U(x,z)$ is given by the Dirac equation,

$$i\hbar\frac{\partial\Phi}{\partial t} = [\vec{\alpha}.\vec{p} + \beta m_0 c^2 + U(x,z)]\Phi \tag{2.125}$$

where

$$\Phi = \begin{pmatrix} \varphi \\ \chi \end{pmatrix}$$

is a bispinor, m_0 is the rest mass of the positron, $\vec{p} = -i\hbar\partial/\partial r$ and $\vec{\alpha}$ and β are given by,

$$\vec{\alpha} = \begin{pmatrix} 0 & \vec{\sigma} \\ \vec{\sigma} & 0 \end{pmatrix} \text{ and } \quad \beta = \begin{pmatrix} I & 0 \\ 0 & -I \end{pmatrix}$$

where $\vec{\sigma}$ are the Pauli matrices given by,

$$\vec{\sigma}_x = \begin{pmatrix} 0 & 1 \\ 1 & 0 \end{pmatrix} \ , \ \vec{\sigma}_y = \begin{pmatrix} 0 & -i \\ i & 0 \end{pmatrix} \text{ and } \vec{\sigma}_z = \begin{pmatrix} 1 & 0 \\ 0 & -1 \end{pmatrix}$$

Substituting in above equations in Eqn. (2.125), we get

$$i\hbar\frac{\partial}{\partial t}\begin{pmatrix} \varphi \\ \chi \end{pmatrix} = \left[\begin{pmatrix} 0 & \vec{\sigma} \\ \vec{\sigma} & 0 \end{pmatrix} .\vec{p} + \begin{pmatrix} I & 0 \\ 0 & -I \end{pmatrix} m_0 c^2 + U(x,z) \right] \begin{pmatrix} \varphi \\ \chi \end{pmatrix} \tag{2.126}$$

Eqn. (2.126) hence delivers two sets of equations,

$$\begin{aligned} i\hbar\frac{\partial\varphi}{\partial t} &= \vec{\sigma}.\vec{p}\chi + m_0 c^2\varphi + U(x,z)\varphi \\ i\hbar\frac{\partial\chi}{\partial t} &= \vec{\sigma}.\vec{p}\varphi - m_0 c^2\chi + U(x,z)\chi \end{aligned}$$

With $E = i\hbar\partial/\partial t$, rearranging the above equations, we get

$$\begin{aligned} \Big[E - U(x,z) - m_0 c^2\Big]\varphi &= \vec{\sigma}.\vec{p}\,\chi \\ \Big[E - U(x,z) + m_0 c^2\Big]\chi &= \vec{\sigma}.\vec{p}\,\varphi \end{aligned}$$

Simplifying the above equations we get,

$$\left[(E-U)^2 - m_0^2c^2\right]\varphi = \left[- i\hbar c(\vec{\sigma}.\bigtriangledown)(\vec{\sigma}.\vec{p}) + \frac{i\hbar c(\vec{\sigma}.\bigtriangledown U)(\vec{\sigma}.\vec{p})}{E-U+m_0c^2}\right]\varphi \tag{2.127}$$

Solving,

$$\left[(E-U)^2 - m_0^2c^2 + \hbar^2c^2\Delta^2 - \frac{i\hbar c}{E-U+m_0}\left\{(\bigtriangledown U)\vec{p} + i\sigma(\bigtriangledown \times \vec{p})\right\}\right]\varphi = 0 \tag{2.128}$$

At energies >10MeV, the influence of spin on the interaction with channeled particles is neglected. So one can omit the last term in Eqn. (2.128), which gives the Dirac equation as,

$$[(E-U)^2 - m_0^2c^4 + \hbar^2c^2\bigtriangledown^2]\varphi = 0.$$

CHAPTER 3

Quantum Calculations for the Effects of Dislocations on Channeling

3.1 Introduction to Crystal Defects and Dechanneling

One of the main applications of ion channeling is the studies of various kinds of defects. It is well known that real crystals are never perfect. The most common kinds of defects found in solids are point defects which include lattice vacancies, interstitials, color centres etc, line defects like edge dislocations, screw dislocations etc and plane defects like grain boundaries, stacking faults etc.

A particle propagating through real solids can 'see' the presence of the defects through their effects in the solids. Classically, particles can see the presence of defects either by direct obstruction of the particle path or through the distortion produced

in the crystal or even both. When the projectile directly hits the defect sites or is scattered in the potential field of the defects obstructing the open channels and the trajectory gets modified as a consequence, the effects are said to be of obstruction type. Examples are stacking faults, interstitial atoms, grain or twin boundaries. If, on the other hand, the defects give rise to distortion in a certain region of the crystal, disturbing the regularity of the material in that region, the effects are of distortion type. The most important example here is that of dislocations. These two qualitatively different types of defects give rise to obstruction dechanneling and distortion dechanneling respectively.

Dechanneling may also be caused by a combination of both the types of defects. In such cases dechanneling is neither purely of obstruction type nor of distortion type. This phenomena is called composite dechanneling. This happens because of the fact that the defects produced in the solid are not uniquely of one type but a combination of different kinds of defects or because the defect itself gives rise partially to obstruction effects and partially to distortion effects. Examples are gas bubbles [51, 52], Guinier-Preston zones [53], voids and antiphase boundaries. The simultaneous use of channeling, back scattering and TEM [54] can correlate the dechanneling observations with damage configurations.

Classically, the dechanneling effects depend on the transverse energy. Transverse energy is increased when the particles are in the vicinity of the defects and when it exceeds a critical value ($E\psi_c^2$), the particles get dechanneled [55]. Quantum mechanically, this transverse energy is quantized. Due to the influence of defects, transverse energy is increased and the particles go to one of the excited states. If this influence is strong, the particles go above the *barrier*, and are no longer bounded. Therefore quantum mechanically, dechanneling means transition from *bound state* to *scattering state* due to the increase in transverse energy.

Such effects and transitions to scattering states leading to dechanneling take place due to distortions in the channels situated in the vicinity of dislocation core. Here the atomic rows and planes exhibit curvature which alters the trajectory of the channeled particle and can dechannel the particle altogether if the curvature is large enough to severely modify the trajectory. This distortion is maximum near the dislocation core and decreases as one moves away from the core [56]. Thus one can think of a cylindrical region around the dislocation axis, called 'dechanneling cylinder' [57]. Figure 3.1 illustrates how the distortion of channels outside a particular region of radius r_0 around the dislocation core; i.e., the dechanneling cylinder, decreases. The effects of dislocations are introduced through the curvature of the channels. The effect of this curvature is to introduce a transverse centrifugal force on the propagating particles. This force should therefore be combined with the force due to the continuum potential (longitudinal).

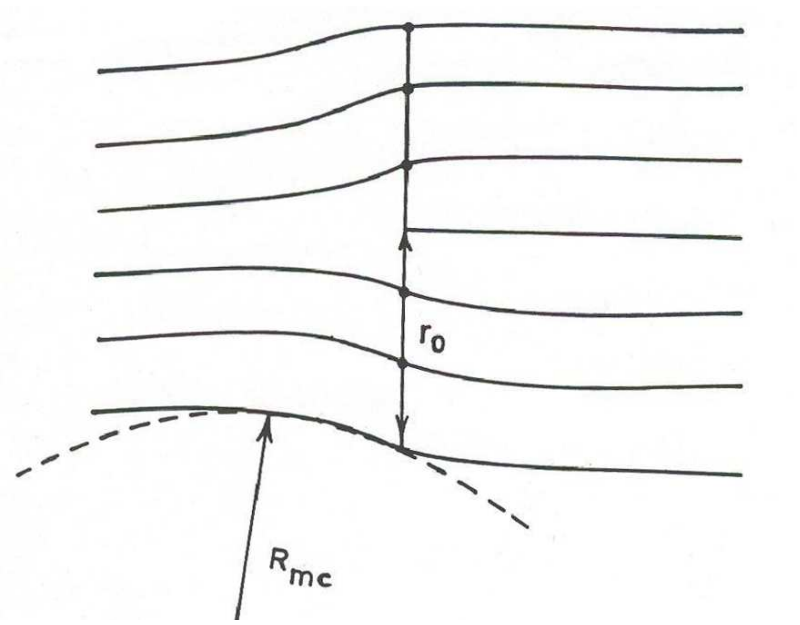

Figure 3.1: The dislocation affected planar channel. R_{mc} is the minimal radius of curvature of the channel at a distance r_0 from the dislocation core.

Classical description of the dislocation effects on the channeling of positrons in the planar and axial cases [58, 59] has also been used to estimate the effects of such defects on the overall rate of energy loss of channeled particles. The corresponding quantum mechanical treatment of the effects of dislocations on channeling were given later [47, 60, 61]. In these investigations, a detailed relativistic framework was used to derive dechanneling probability and its energy dependence.

In this chapter, we consider a quantum mechanical model for the effects of dislocations on the initially well-channeled particles in a planar channel by considering both the transverse and longitudinal motion of the particles in the channel. We first consider the effects on positron planar channeling and later on electron channeling.

3.2 Electron and Positron Channeling

As mentioned in chapter 1, positively charged particles channeling along various crystallographic directions are bound to oscillate between the atomic rows or planes of atoms and are repelled by these rows or planes during its propagation. The corresponding transverse motion can be described by harmonic oscillator potential with equally spaced energy levels. On the other hand, the negatively charged particles like electrons are attracted towards the atomic planes or axes and cross them. Hence the electrons have increased probability for hard collisions with atoms and the transverse potential is approximated to one dimensional hydrogen atom [62]. Hence one can say that the continuum potential is simply the negative of that governing the motion of positrons. Figure 3.2 shows the transverse potentials of both positrons and electrons. Also Figure 3.3 illustrates the motion of electrons along a string of atoms. This helical motion of negatively charged particles is named "rosette motion" [50, 63, 64, 65, 66].

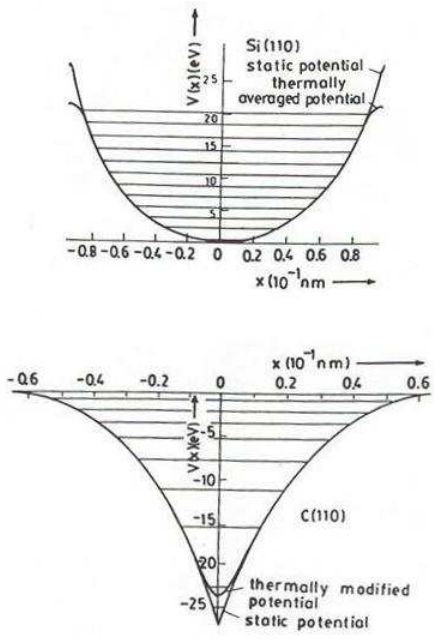

Figure 3.2: Planar potentials for 54.5 MeV positrons and electrons along (110) planes of Si and C respectively. For positrons the energy levels are equally spaced, whereas for electrons, it is not equally spaced.

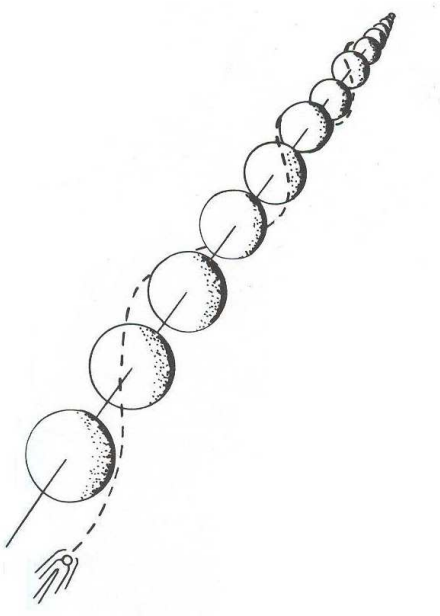

Figure 3.3: Channeling trajectory of an electron along a string of atoms.

3.3 Effects of Dislocations on Positron Channeling

We consider a typical channel at some distance from the dislocation core, outside the dechanneling cylinder so that the motion is influenced by the distortions but does not result in complete dechanneling. When the particles enter from an undistorted region of the channel to the distorted region, they see the curvature of the channel and experience additional centrifugal force. This results in modification of their trajectory following the curvature. The model is shown in Figure 3.4. The whole channel is divided into four regions. The dislocation affected parts of the channel are regions II and III. ρ_0 corresponds to the radial co-ordinate of the channel center as measured from the origin and φ_0 is the corresponding angular co-ordinate.

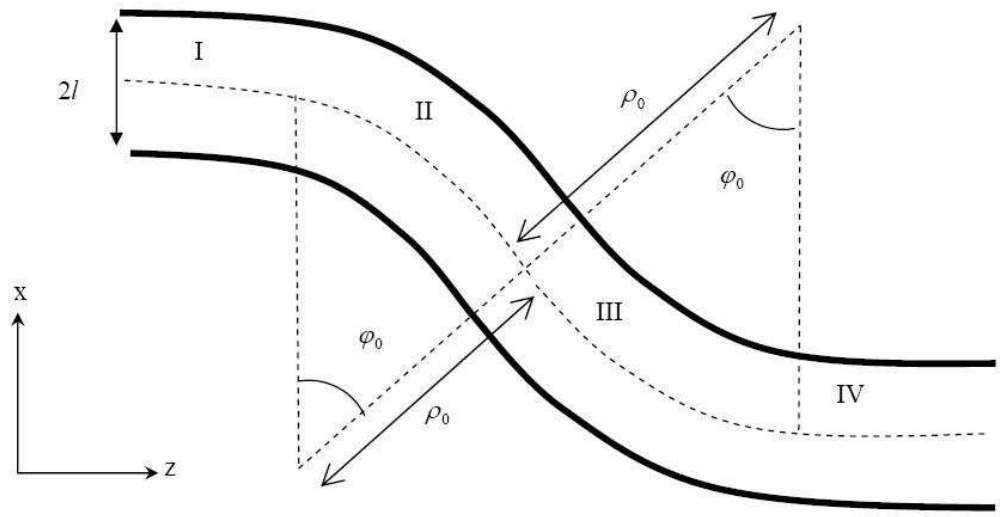

Figure 3.4: The dislocation affected channel.

3.3.1 Shift in Potential Minima

We consider the particle motion in the four regions separately, considering both the longitudinal and transverse motions. The Schrodinger equation for planar channeling for a particle of mass m moving in region I (perfect channel) can be written as,

$$-\frac{\hbar^2}{2m}\left(\frac{\partial^2}{\partial x^2}+\frac{\partial^2}{\partial z^2}\right)\Psi^I(x,z)+\frac{1}{2}m\omega^2x^2\Psi^I(x,z)=E^I\Psi^I(x,z) \tag{3.1}$$

where E^I is the total energy and can be written as $E^I = E_T^I + E_L^I$ (with E_T^I and E_L^I, the energy components associated with the transverse and longitudinal motion, respectively).

$$\begin{aligned} E_T^I(n,\omega) &= \left(n+\frac{1}{2}\right)\hbar\omega \\ E_L^I &= \frac{\hbar^2k^2}{2m} \end{aligned} \tag{3.2}$$

where ω is the characteristic frequency obtained from the harmonic approximation to the planar potential

$$V_p(x) = V_0x^2 \tag{3.3}$$

i.e.,

$$\omega = \sqrt{\frac{2V_0}{m}} \tag{3.4}$$

After separation of variables, the equation of motion in the transverse and longitudinal directions can be written as,

$$-\frac{\hbar^2}{2m}X^{''I}(x) + \frac{1}{2}m\omega^2 x^2 X^I(x) = E_T^I X^I(x) \tag{3.5}$$

$$-\frac{\hbar^2}{2m}Z^{''I}(z) = E_L^I Z^I(z) \tag{3.6}$$

whose solutions are given by,

$$X^I(x) = \frac{\exp(-x^2/2\alpha^2)}{\sqrt{2^n n!\alpha\sqrt{\pi}}}\ H_n(x/\alpha) \tag{3.7}$$

$$Z^I(z) = Ae^{ikz} + B^{-ikz} \tag{3.8}$$

where

$$\alpha = \sqrt{\frac{\hbar}{m\omega}}$$

The total wave function for the region I can be written as

$$\Psi^I(x,z) = X_n^I(x - x_0)\ Z^I(z) \tag{3.9}$$

where x_0 is the initial amplitude of the channelon. Assuming that an initially well-channeled particle coming from left, interacts and undergoes reflections at the boundary (between I and II regions), the actual wavefunction in the first region has the effects of excited sates also. Hence the total wavefunction can be written as,

$$\Psi^I(x,z) = A_0 X_0^I e^{ik_0 z} + \sum_{n=0}\ B_n X_n^I e^{-ik_n z} \tag{3.10}$$

Now consider the dislocation affected parts of the channel. We have two curved regions which are due to the centrifugal force proportional to $\frac{\mu^2}{\rho^2}$, where $\mu\hbar$ is the angular momentum with $\mu^2 = l(l+1)$ with l as the orbital angular momentum quantum number and ρ is the radius of curvature of the channel.

In the second region of the channel, the Schrodinger equation is written in terms of the polar co-ordinates ρ and φ and is given by,

$$-\frac{\hbar^2}{2m}\bigtriangledown^2_{\rho,\varphi}\,\Psi^{II}(\rho,\varphi)+V(\rho)\Psi^{II}(\rho,\varphi)=E^{II}\Psi^{II}(\rho,\varphi) \tag{3.11}$$

where the potential in this region is given by,

$$V(\rho)=\frac{1}{2}m\omega^2(\rho-\rho_0)^2 \tag{3.12}$$

Here the distance 'x' in the transverse direction is replaced by $\rho-\rho_0$, the corresponding distance in the ρ-direction. In this region, the *x, y, z* components are written in terms of ρ and φ and are given by,

$$\begin{aligned} x &= \rho\cos\varphi \\ y &= y \\ z &= \rho\sin\varphi \end{aligned}$$

The particle motion is in the *x*-*z* plane. Therefore, the 'y' component remains the same. Now, Eqn. (3.11) can be re-written as,

$$-\frac{\hbar^2}{2m}\left[\frac{1}{\rho}\frac{\partial}{\partial\rho}\left(\rho\frac{\partial}{\partial\rho}\right)+\frac{1}{\rho^2}\frac{\partial^2}{\partial\varphi^2}\right]\Psi^{II}(\rho,\varphi)+\frac{1}{2}m\omega^2(\rho-\rho_0)^2\;\Psi^{II}(\rho,\varphi)=E^{II}\;\Psi^{II}(\rho,\varphi) \tag{3.13}$$

Separating variables gives azimuthal equation,

$$F''^{II}(\varphi)=-\mu^2F^{II}(\varphi) \tag{3.14}$$

with solution

$$F^{II}(\varphi)=Ce^{i\mu\varphi}+De^{-i\mu\varphi} \tag{3.15}$$

and radial equation,

$$R''^{II}(\rho)+\frac{2m}{\hbar^2}\left[E^{II}-\frac{1}{2}m\omega^2(\rho-\rho_0)^2-\frac{\hbar^2}{2m}\frac{\mu^2}{\rho^2}\right]R^{II}(\rho)=0 \tag{3.16}$$

From the above equation, we can write the effective potential in the region II as,

$$V_{eff}(\rho) = \frac{1}{2}m\omega^2(\rho - \rho_0)^2 + \frac{\hbar^2}{2m}\frac{\mu^2}{\rho^2} \tag{3.17}$$

Putting $\xi = \rho - \rho_0$,

$$V_{eff}(\xi) = \frac{1}{2}m\omega^2\xi^2 + \frac{\hbar^2}{2m}\frac{\mu^2}{(\xi + \rho_0)^2}$$

Since $\xi \ll \rho_0$, we may expand V_{eff} to second order around ξ=0,

$$V_{eff}(\xi) = V(0) + \left(\frac{dV_{eff}}{d\xi}\right)_{\xi=0}\xi + \frac{1}{2}\left(\frac{d^2V_{eff}}{d\xi^2}\right)_{\xi=0}\xi^2 \tag{3.18}$$

Putting $a = \sqrt{\frac{m\omega}{\hbar}}$,

$$V_{eff} = \frac{\hbar^2}{2m}\left[a^4\xi^2 + \frac{\mu^2}{(\xi + \rho_0)^2}\right] \tag{3.19}$$

The above equation gives,

$$V(0) = \frac{\hbar^2\mu^2}{2m\rho_0^2} \tag{3.20}$$

$$\frac{dV_{eff}}{d\xi} = \frac{\hbar^2}{2m}\left[2a^4\xi - \frac{2\mu^2}{(\xi + \rho_0)^3}\right] \tag{3.21}$$

$$\frac{d^2V_{eff}}{d\xi^2} = \frac{\hbar^2}{2m}\left[2a^4 + \frac{6\mu^2}{(\xi + \rho_0)^4}\right] \tag{3.22}$$

Substituting the above values in Eqn. (3.18), we get the effective potential for the region II given by,

$$V_{eff}(\xi) = \frac{\hbar}{2m}\left[\left(\frac{\lambda}{\rho_0^4}\right)(\xi - a_p)^2 + U_{min}\right] \tag{3.23}$$

where

$$\lambda = a^4\rho_0^4 + 3\mu^2$$

$$a_p = \frac{\mu^2\rho_0}{\lambda}$$

$$U_{min} = \frac{\mu^2(\lambda - \mu^2)}{\rho_0^2\lambda} = \frac{2m}{\hbar^2}V_{min}$$

This equation of effective potential (Eqn. (3.23)) corresponds to a harmonic oscillator with frequency,

$$\omega' = \frac{\hbar}{m}\left(\frac{\lambda}{\rho_0^4}\right)^{1/2} \tag{3.24}$$

The qualitative shape of the potential is shown in Figure 3.5. It is observed that the effect of centrifugal force shifts the potential curve; the new curve is centered at a_p with a shift V_{min} in energy minimum. Furthermore, the effective transverse potential is no longer completely harmonic.

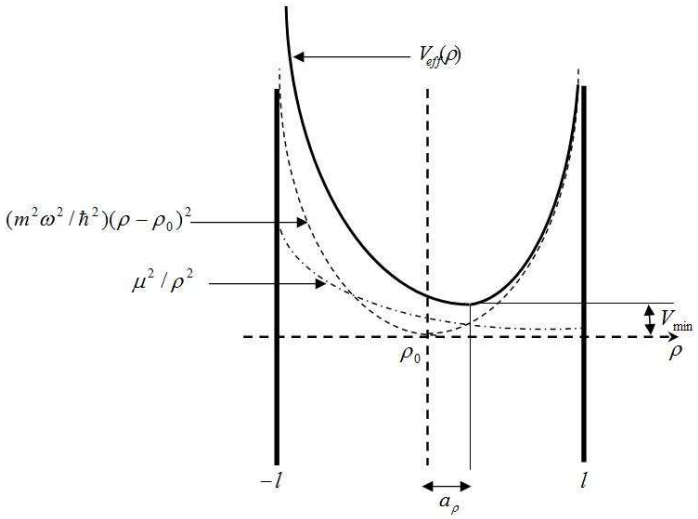

Figure 3.5: The shape of the effective potential in the third region of the dislocation affected channel (region II) for positrons.

The wavefunction for region II can be written as,

$$\Psi^{II}(\rho,\varphi) = \sum_{m=0} R_m^{II}\left[C_m e^{i\mu\varphi} + D_m e^{-i\mu\varphi}\right] \tag{3.25}$$

Putting $\eta = \xi - a_p = \rho - \rho_0 - a_p$, the radial equation in Eqn. (3.16) can now be written as,

$$R''^{II}(\eta) + \left[\frac{\hbar^2}{2m}E^{II} - \frac{\lambda}{\rho_0^4}\eta^2 + U_{min}\right]R^{II}(\eta) = 0 \tag{3.26}$$

with solution,

$$R_{n'}^{II}(\eta) = \left(\frac{m\omega'}{\pi\hbar}\right)^{1/4}(2^{n'}n!)^{-1/2}H_{n'}(b\eta)e^{-b^2\eta^2/2} \tag{3.27}$$

where $b = (m\omega'/\hbar)^{1/2}$.

For the third region, the Schrodinger equation in polar coordinates becomes,

$$-\frac{\hbar^2}{2m}\left[\frac{1}{\rho}\frac{\partial}{\partial\rho}\left(\rho\frac{\partial}{\partial\rho}\right)+\frac{1}{\rho^2}\frac{\partial^2}{\partial\varphi^2}\right]\Psi^{III}(\rho,\varphi)+\frac{1}{2}m\omega^2(\rho-\rho_0)^2\Psi^{III}(\rho,\varphi)=E^{III}\ \Psi^{III}(\rho,\varphi) \tag{3.28}$$

Separating variables gives azimuthal equation,

$$F''^{III}(\varphi)=-\mu^2F^{III}(\varphi) \tag{3.29}$$

with solution,

$$F^{III}(\varphi)=Ge^{i\mu\varphi}+He^{-i\mu\varphi}$$

and radial equation,

$$R''^{III}(\rho)+\frac{2m}{\hbar^2}\left[E^{III}-\frac{1}{2}m\omega^2(\rho-\rho_0)^2+\frac{\hbar^2}{2m}\frac{\mu^2}{\rho^2}\right]R^{III}(\rho)=0 \tag{3.30}$$

The effective potential, in the third region can be written as

$$V'_{eff}(\rho)=\frac{1}{2}m\omega^2(\rho-\rho_0)^2-\frac{\hbar^2}{2m}\frac{\mu^2}{\rho^2} \tag{3.31}$$

Using the Eqn. (3.18), the corresponding equations for (3.20 to 3.22) are given by,

$$V'(0) = -\frac{\hbar^2\mu^2}{2m\rho_0^2} \tag{3.32}$$

$$\frac{dV'_{eff}}{d\xi} = \frac{\hbar^2}{2m}\left[2a^4\xi+\frac{2\mu^2}{(\xi+\rho_0)^3}\right] \tag{3.33}$$

$$\frac{d^2V'_{eff}}{d\xi^2} = \frac{\hbar^2}{2m}\left[2a^4-\frac{6\mu^2}{(\xi+\rho_0)^4}\right] \tag{3.34}$$

which give the effective potential in the IIIrd region as,

$$V'_{eff}(\xi)=\frac{\hbar}{2m}\left[\left(\frac{\lambda'}{\rho_0^4}\right)(\xi-a'_p)^2+U'_{min}\right] \tag{3.35}$$

where

$$\begin{aligned}\lambda' &= a^4\rho_0^4-3\mu^2\\ a'_p &= \frac{\mu^2\rho_0}{\lambda'}\\ U'_{min} &= -\frac{\mu^2(\lambda'+\mu^2)}{\rho_0^2\lambda'}=-\frac{2m}{\hbar^2}V'_{min}\end{aligned}$$

The potential equation; Eqn. (3.35) corresponds to a harmonic oscillator with frequency,

$$\omega'' = \frac{\hbar}{m}\left(\frac{\lambda'}{\rho_0^4}\right)^{1/2} \tag{3.36}$$

The shape of this potential is shown in Figure 3.6. It is observed that the effect of the centrifugal force shifts the potential curve as in region II, but in a direction opposite to it. The new curve is centered at a'_p with a negative shift of V'_{min} in energy minimum.

It is observed from the above calculations that the curvature of the channel induces a shift in the equilibrium axis for channeling which changes the frequency of oscillation from ω to ω' and ω'' in the first and second regions of the curved channel respectively.

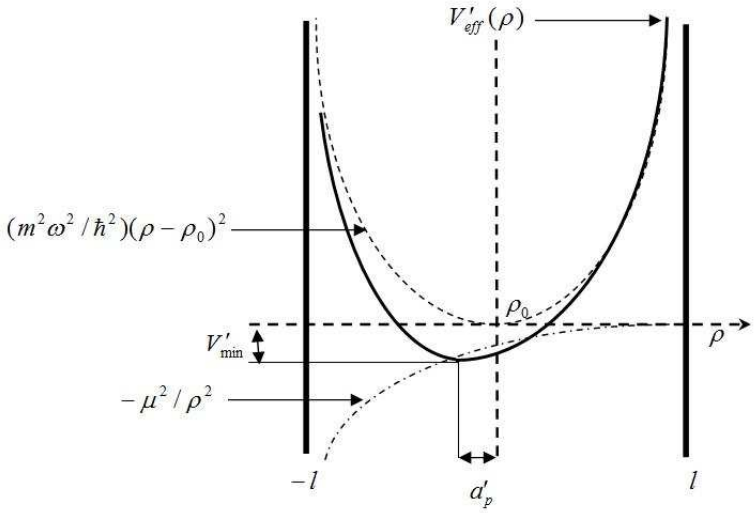

Figure 3.6: The shape of the effective potential in the second region of the dislocation affected channel (region III) for positrons.

The total wavefunction in the third region can be written as

$$\Psi^{III}(\rho,\varphi) = \sum_{m=0} R_m^{III}\left[G_m e^{i\mu\varphi} + H_m e^{-i\mu\varphi}\right] \tag{3.37}$$

where

$$R_{n'}^{III}(\eta') = \left(\frac{m\omega''}{\pi\hbar}\right)^{1/4} (2^{n'}n!)^{-1/2} H_{n'}(b'\eta') e^{-b'^2\eta'^2/2} \tag{3.38}$$

with $b' = (m\omega''/\hbar)^{1/2}$ and $\eta' = \xi + a'_p = \rho - \rho_0 + a'_p$.

In the fourth region (i.e., the perfect channel), there will be only the transmitted wave and the wave function in this region is given by,

$$\Psi^{IV}(x,z) = X_n^{IV}\ I_n\ e^{ik_n z} \tag{3.39}$$

3.3.2 Channeling and Dechanneling Probabilities

Now we proceed to find the reflection and transmission coefficients. We have 4 regions and 3 boundaries separating them. The boundary conditions across these regions are given by the following equations,

$$\Psi^{I}|_{z=0} = \Psi^{II}|_{\varphi=0} \tag{3.40}$$

$$\left.\frac{\partial\Psi^{I}}{\partial z}\right|_{z=0} = \frac{1}{\rho_0}\left.\frac{\partial\Psi^{II}}{\partial\varphi}\right|_{\varphi=0} \tag{3.41}$$

$$\Psi^{II}|_{\varphi=\varphi_0} = \Psi^{III}|_{\varphi=0} \tag{3.42}$$

$$\left.\frac{\partial\Psi^{II}}{\partial\varphi}\right|_{\varphi=\varphi_0} = \left.\frac{\partial\Psi^{III}}{\partial\varphi}\right|_{\varphi=0} \tag{3.43}$$

$$\Psi^{III}|_{\varphi=\varphi_0} = \Psi^{IV}|_{z=t} \tag{3.44}$$

$$\frac{1}{\rho_0}\left.\frac{\partial\Psi^{III}}{\partial\varphi}\right|_{\varphi=\varphi_0} = \left.\frac{\partial\Psi^{IV}}{\partial z}\right|_{z=t} \tag{3.45}$$

We use the above boundary conditions in the wavefunction of the 4 regions given by the equations, (3.10), (3.25), (3.37) and (3.39).

$$\text{Eqn. (3.40)} \Rightarrow AX^I + BX^I = R_m^{II}(C+D) \tag{3.46}$$

$$\text{Eqn. (3.41)} \Rightarrow \frac{k\rho_0}{\mu}AX^I - BX^I = R_m^{II}(C-D) \tag{3.47}$$

$$\text{Eqn. (3.42)} \Rightarrow R_m^{II}[Ce^{i\mu\varphi_0} + De^{-i\mu\varphi_0}] = R_m^{III}(G+H)$$

which gives,

$$G + H =< R_m^{III}|R_m^{II} > [Ce^{i\mu\varphi_0} + De^{-i\mu\varphi_0}] \tag{3.48}$$

$$\text{Eqn. (3.43)} \Rightarrow R_m^{II}[Ce^{i\mu\varphi_0} - De^{-i\mu\varphi_0}] = R_m^{III}(G-H)$$

which gives,

$$G - H =< R_m^{III}|R_m^{II} > [Ce^{i\mu\varphi_0} - De^{-i\mu\varphi_0}] \tag{3.49}$$

$$\text{Eqn. (3.44)} \Rightarrow R_m^{III}[Ge^{i\mu\varphi_0} + He^{-i\mu\varphi_0}] = IX^{IV}e^{ikt} \tag{3.50}$$

$$\text{Eqn. (3.45)} \Rightarrow \frac{i\mu R_m^{III}}{\rho_0}[Ge^{i\mu\varphi_0} - He^{-i\mu\varphi_0}] = ikIX^{IV}e^{ikt} \tag{3.51}$$

From the above equations we need to find $|\frac{B}{A}|^2$ which gives the reflection co-efficient. From Equations (3.46) and (3.47), we get,

$$C = \frac{1}{2} < R_m^{II}|X^I > \left[A\left(1 + \frac{k\rho_0}{\mu}\right) + B\left(1 - \frac{k\rho_0}{\mu}\right)\right] \tag{3.52}$$

$$D = \frac{1}{2} < R_m^{II}|X^I > \left[A\left(1 - \frac{k\rho_0}{\mu}\right) + B\left(1 + \frac{k\rho_0}{\mu}\right)\right] \tag{3.53}$$

which gives the value of $\frac{B}{A}$ as,

$$\frac{B}{A} = \frac{\frac{k\rho_0}{\mu}\left(\frac{C}{D}+1\right) - \left(\frac{C}{D}-1\right)}{\frac{k\rho_0}{\mu}\left(\frac{C}{D}+1\right) + \left(\frac{C}{D}-1\right)} \tag{3.54}$$

From equations (3.48) and (3.49) we have,

$$G = < R_m^{III} | R_m^{II} > Ce^{i\mu\varphi_0} \tag{3.55}$$

$$H = < R_m^{III} | R_m^{II} > De^{-i\mu\varphi_0} \tag{3.56}$$

The above equations (3.55) and (3.56) give,

$$\frac{C}{D} = \frac{G}{H} e^{-2i\mu\varphi_0} \tag{3.57}$$

Finally from equations (3.50) and (3.51) we have

$$\frac{G}{H} = \frac{\mu + k\rho_0}{\mu - k\rho_0} e^{-2i\mu\varphi_0} \tag{3.58}$$

Substituting Eqn. (3.58) in (3.57), we get the value of $\frac{C}{D}$ as,

$$\frac{C}{D} = \frac{\mu + k\rho_0}{\mu - k\rho_0} e^{-4i\mu\varphi_0} \tag{3.59}$$

Substituting Eqn. (3.59) in Eqn. (3.54), we get,

$$\frac{B}{A} = \frac{(k^2\rho_0^2 - \mu^2)[1 - e^{-4i\mu\varphi_0}]}{(k^2\rho_0^2 + \mu^2)[1 - e^{-4i\mu\varphi_0}] - 2k\rho_0\mu[1 - e^{-4i\mu\varphi_0}]} \tag{3.60}$$

Now substituting,

$$1 - e^{-4i\mu\varphi_0} = 2ie^{2i\mu\varphi_0} \sin(2\mu\varphi_0)$$

$$1 + e^{-4i\mu\varphi_0} = 2ie^{2i\mu\varphi_0} \cos(2\mu\varphi_0)$$

and solving, we get the reflection co-efficient as

$$\left|\frac{B}{A}\right|^2 = |R|^2 = \frac{(-\mu^2 + k^2\rho_0^2)^2 \ \sin^2(2\mu\varphi_0)}{4k^2\mu^2\rho_0^2 \cos^2(2\mu\varphi_0) + (\mu^2 + k^2\rho_0^2)^2 \ \sin^2(2\mu\varphi_0)} \tag{3.61}$$

The transmission co-efficient is given by,

$$1 - |R|^2 = |T|^2 = \frac{4k^2\rho_0^2\mu^2}{4k^2\mu^2\rho_0^2 \cos^2(2\mu\varphi_0) + (\mu^2 + k^2\rho_0^2)^2 \ \sin^2(2\mu\varphi_0)} \tag{3.62}$$

The reflection and transmission co-efficients given in the above equations give us the values of dechanneling and channeling probabilities respectively. These can be written, in terms of energy as

$$|R|^2 = \frac{(-\mu^2\hbar^2 + 2mE\rho_0^2)^2 \ \sin^2(2\mu\varphi_0)}{8mE\mu^2\rho_0^2\cos^2(2\mu\varphi_0) + (\mu^2\hbar^2 + 2mE\rho_0^2)^2 \ \sin^2(2\mu\varphi_0)} \tag{3.63}$$

$$|T|^2 = \frac{8mE\rho_0^2\mu^2}{8mE\mu^2\rho_0^2\cos^2(2\mu\varphi_0) + (\mu^2\hbar^2 + 2mE\rho_0^2)^2 \ \sin^2(2\mu\varphi_0)} \tag{3.64}$$

The dependence of these probabilities on the parameters E and ρ_0 are given in figures 3.7 and 3.8, taking the average values of $\sin^2(2\mu\varphi_0)$ and $\cos^2(2\mu\varphi_0)$ as 0.5. Here ρ_0 is inversely related to the density of dislocations.

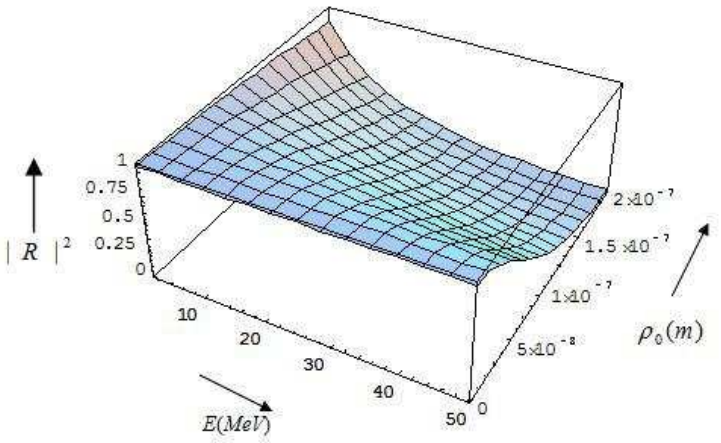

Figure 3.7: The E and ρ_0 dependence of dechanneling probability for positrons.

Now let us consider the case of maximum and minimum dechanneling probabilities. The maximum dechanneling takes place when the value of ρ_0 is very small, i.e., when the curvature of the channel is very large. The figures 3.7 and 3.8 also show the channeling and dechanneling probabilities for the least value of ρ_0 which

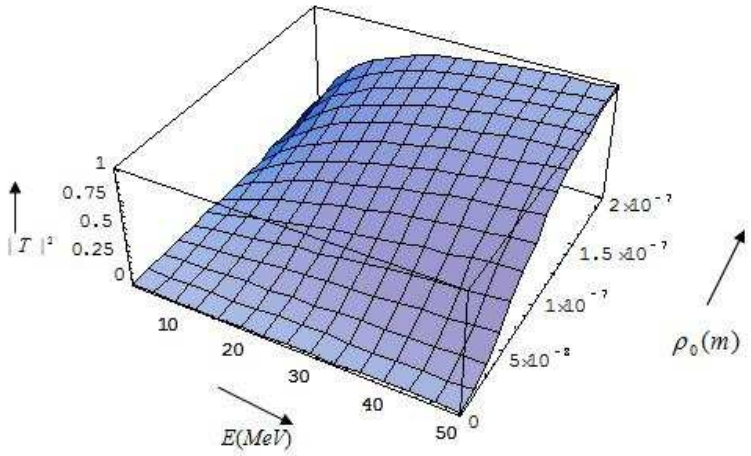

Figure 3.8: The E and ρ_0 dependence of channeling probability for positrons.

gives maximum dechanneling and minimum channeling probabilities. The minimum dechanneling takes place at φ_0=0, i.e., when the channel is straight. The maximum value of φ_0 is found to be $\pi/(4\sqrt{2})$.

3.4 Effects of Dislocations on Electron Channeling

Here, we consider the effects of dislocations on planar channeling of electrons. Electrons, as mentioned in section 3.3, are confined to move around the planes or axes where their potential minima lies. Just like in the case of positron case, both the transverse and longitudinal motion of the particles are considered.

3.4.1 Shift in Potential Minima

The Schrodinger Equation for planar channeling for a particle of mass m moving in region I (perfect channel) can be written as:

$$-\frac{\hbar^2}{2m}\left(\frac{\partial^2}{\partial x^2}+\frac{\partial^2}{\partial z^2}\right)\ \Psi^I(x,z)+U(x)\ \Psi^I(x,z)=E^I\ \Psi^I(x,z) \tag{3.65}$$

For electron the transverse potential is given by [62, 67, 68],

$$U(x) = -\frac{V_0}{x + a_{TF}} \tag{3.66}$$

where

$$V_0 = 2\pi Z_1 Z_2 e^2 N d_p C a_{TF}^2 \tag{3.67}$$

After separation of variables, the total wavefunction for region I becomes,

$$\Psi^I(x, z) = A_0 X_0^I e^{ik_0 z} + \sum_{n=0} B_n X_n^I e^{-ik_n z} \tag{3.68}$$

Now consider the two regions in the channel which are affected by dislocation. These curved regions are due the centrifugal force proportional to $\frac{\mu^2}{\rho^2}$.

The Schrodinger equation for the region II in terms of the polar coordinates ρ and φ,

$$-\frac{\hbar^2}{2m}\left[\frac{1}{\rho}\frac{\partial}{\partial\rho}\left(\rho\frac{\partial}{\partial\rho}\right) + \frac{1}{\rho^2}\frac{\partial^2}{\partial\varphi^2}\right]\Psi^{II}(\rho,\varphi) - \frac{V_0}{(\rho-\rho_0)+a_{TF}}\Psi^{II}(\rho,\varphi) = E^{II}\ \Psi^{II}(\rho,\varphi) \tag{3.69}$$

Separating variables gives azimuthal equation,

$$F''^{II}(\varphi) = -\mu^2 F^{II}(\varphi) \tag{3.70}$$

with solution similar to that in the positron case (Eqn. (3.15)) and radial equation,

$$R''^{II}(\rho) + \frac{2m}{\hbar^2}\left[E^{II} + \frac{V_0}{(\rho-\rho_0)+a_{TF}} - \frac{\hbar^2}{2m}\frac{\mu^2}{\rho^2}\right]R^{II}(\rho) = 0 \tag{3.71}$$

From the above radial equation, the effective potential for region II can be written as

$$V_{eff}(\rho) = -\frac{V_0}{(\rho-\rho_0)+a_{TF}} + \frac{\hbar^2}{2m}\frac{\mu^2}{\rho^2} \tag{3.72}$$

Keeping $\xi = \rho - \rho_0$ and simplifying the above equation we get the effective potential and is given by,

$$V_{eff}(\xi) = \frac{\hbar}{2m}\left\{\frac{\lambda_1'^3}{\lambda_1^2\rho_0^4 a_{TF}^3[2\xi + \frac{\lambda_1'}{\lambda_1}]} - \frac{\lambda_1'^2}{\lambda_1\rho_0^4 a_{TF}^3} + \frac{\lambda_1''}{\rho_0^4 a_{TF}^3}\right\} \tag{3.73}$$

where

$$\lambda_1 = -2a^4\rho_0^4 + 3\mu^2 a_{TF}^3 \tag{3.74}$$

$$\lambda_1' = -a^4\rho_0^4 a_{TF} + \mu^2 a_{TF}^3 \rho_0 \tag{3.75}$$

$$\lambda_1'' = -2a^4\rho_0^4 a_{TF}^2 + \mu^2 a_{TF}^3 \rho_0^2 \tag{3.76}$$

From Eqn. (3.73) we can see a shift in the minimum of the potential, which is due to the shift in the equilibrium axis due to dislocations. Figure 3.9 shows the potential shift in this region. The wavefunction of region II can be written in a form given by Eqn. (3.25),

$$\Psi^{II}(\rho,\varphi) = \sum_{m=0} R_m^{II}\left[C_m e^{i\mu\varphi} + D_m e^{-i\mu\varphi}\right] \tag{3.77}$$

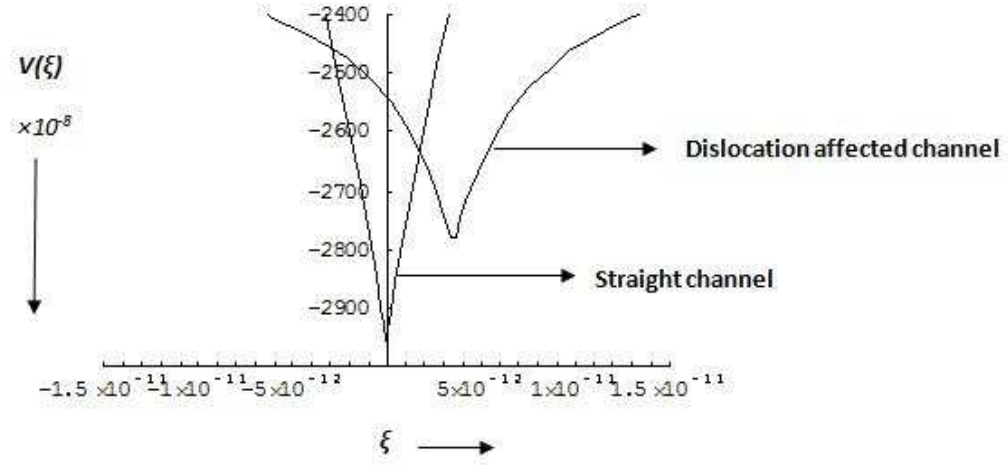

Figure 3.9: The shift in potential due to dislocations for electrons.

Similarly, proceeding to the region III, the Schrodinger equation can be written as

$$-\frac{\hbar^2}{2m}\left[\frac{1}{\rho}\frac{\partial}{\partial\rho}\left(\rho\frac{\partial}{\partial\rho}\right) + \frac{1}{\rho^2}\frac{\partial^2}{\partial\varphi^2}\right]\Psi^{III}(\rho,\varphi) - \frac{V_0}{(\rho-\rho_0)+a_{TF}}\Psi^{III}(\rho,\varphi) = E^{III}\ \Psi^{III}(\rho,\varphi) \tag{3.78}$$

Separating variables gives azimuthal and radial equations as,

$$F''^{III}(\varphi) = -\mu^2 F^{III}(\varphi) \tag{3.79}$$

$$R''^{III}(\rho) + \frac{2m}{\hbar^2}\left[E^{III} + \frac{V_0}{(\rho-\rho_0)+a_{TF}} + \frac{\hbar^2}{2m}\frac{\mu^2}{\rho^2}\right]R^{III}(\rho) = 0 \tag{3.80}$$

The effective potential for region III can be written as

$$V_{eff}(\rho) = -\frac{V_0}{(\rho-\rho_0)+a_{TF}} - \frac{\hbar^2}{2m}\frac{\mu^2}{\rho^2} \tag{3.81}$$

which, upon simplification,

$$V_{eff}(\xi) = \frac{\hbar}{2m}\left\{\frac{\lambda_2'^3}{\lambda_2^2\rho_0^4 a_{TF}^3[2\xi + \frac{\lambda_2'}{\lambda_2}]} - \frac{\lambda_2'^2}{\lambda_2\rho_0^4 a_{TF}^3} + \frac{\lambda_2''}{\rho_0^4 a_{TF}^3}\right\} \tag{3.82}$$

where

$$\lambda_2 = -2a^4\rho_0^4 - 3\mu^2 a_{TF}^3 \tag{3.83}$$

$$\lambda_2' = -a^4\rho_0^4 a_{TF} - \mu^2 a_{TF}^3\rho_0 \tag{3.84}$$

$$\lambda_2'' = -2a^4\rho_0^4 a_{TF}^2 - \mu^2 a_{TF}^3\rho_0^2 \tag{3.85}$$

The above equation (3.82) shows a shift in the potential minimum, but in the reverse direction of that of region II and the shifts in both the regions are in accordance with the direction of the centrifugal force. The wavefunction of region III can be written as,

$$\Psi^{III}(\rho,\varphi) = \sum_{m=0} R_m^{III}\left[G_m e^{i\mu\varphi} + H_m e^{-i\mu\varphi}\right] \tag{3.86}$$

The fourth region is the perfect channel as discussed in the previous section and the wavefunction is,

$$\Psi^{IV}(x,z) = X_n^{IV}\ I_n\ e^{ik_n z} \tag{3.87}$$

To find the reflection and transmission coefficients, we use the boundary conditions across the 3 boundaries are given by equations (3.40) to (3.45). From these we get $|R|^2$ and $|T|^2$ as,

$$|R|^2 = \frac{(-\mu^2 + k^2\rho_0^2)^2 \ \sin^2(2\mu\varphi_0)}{4k^2\mu^2\rho_0^2\cos^2(2\mu\varphi_0) + (\mu^2 + k^2\rho_0^2)^2 \ \sin^2(2\mu\varphi_0)} \tag{3.88}$$

$$|T|^2 = \frac{4k^2\rho_0^2\mu^2}{4k^2\mu^2\rho_0^2\cos^2(2\mu\varphi_0) + (\mu^2 + k^2\rho_0^2)^2 \ \sin^2(2\mu\varphi_0)} \tag{3.89}$$

These give the dechanneling and channeling probabilities respectively. The variation of these co-efficients with the value of ρ_0 and incident energy E is given in figures 3.10 and 3.11.

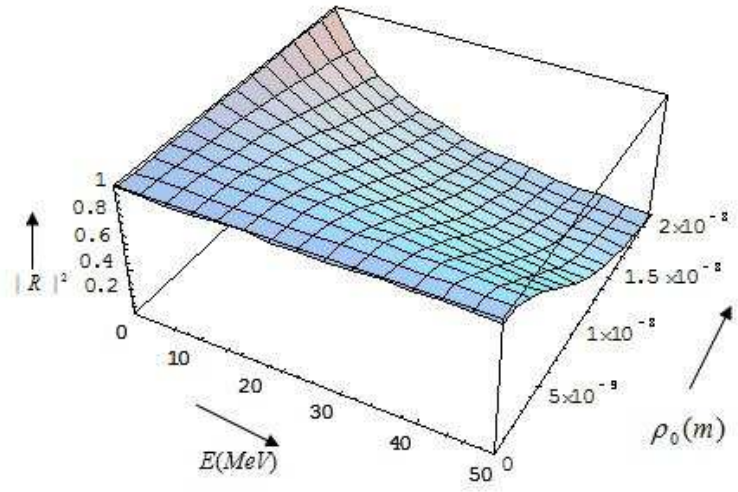

Figure 3.10: Variation of the reflection co-efficient / dechanneling probability with ρ_0 and Incident energy E of electron

The above equations (3.88) and (3.89) look similar to those of the positron channeling case since we consider the same channel with same dislocation effects. From the figures 3.7 and 3.10, and from 3.8 and 3.11, it is found that for electron channeling,

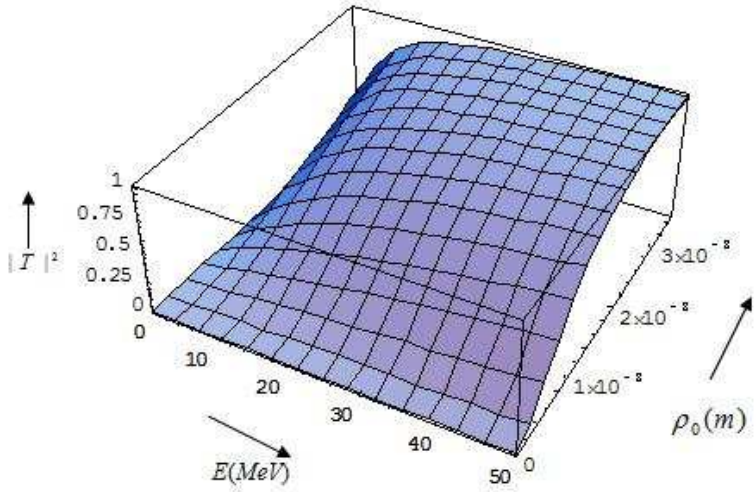

Figure 3.11: Variation of the transmission co-efficient / channeling probability with ρ_0 and Incident energy E of electron

channeling starts at a smaller value of ρ_0 compared to that of positron channeling. It means that at a particular value of ρ_0, the probability of the particles to dechannel is less for electrons when compared to positrons. This is due to the fact that the electrons have its transverse motion bound to an atomic row or plane of atoms.

3.4.2 Spectral Distribution of Radiation Intensity

The eigen spectrum of electron channeling is given by [67, 68],

$$|E_n| = \frac{V_0^2}{2\hbar^2(n+\delta n)^2} \tag{3.90}$$

$$\delta n = 2a_T/a_{TF} \tag{3.91}$$

$$a_T = \sqrt{a_{TF}^2 + u^2} \tag{3.92}$$

where u^2 is the mean-square vibrational amplitude. The additional centrifugal force due to the dislocation changes the spectrum. This change in energy due to channeling of electrons in a dislocation affected channel for various materials and various

energies are given in Table 1 and compared with that in a straight channel for a value of ρ_0=0.5 $\times$ 10^{-7}m.

Table 1 : The change in energy (in eV) for various materials for electrons channeling along the (110) direction at different incident energies for a value of ρ_0=0.5 $\times$ 10^{-7}m.

	50 MeV		20 MeV		10 MeV	
	Straight Channel	Dislocation affected Channel	Straight Channel	Dislocation affected Channel	Straight Channel	Dislocation affected Channel
Si	2.83 $\times 10^{-3}$	2.861 $\times 10^{-3}$	0.93 $\times 10^{-3}$	0.942 $\times 10^{-3}$	0.476 $\times 10^{-3}$	0.481 $\times 10^{-3}$
Cu	3.257 $\times 10^{-3}$	3.293 $\times 10^{-3}$	1.3 $\times 10^{-3}$	1.31 $\times 10^{-3}$	0.651 $\times 10^{-3}$	0.658 $\times 10^{-3}$

Now we consider the effects of dislocations on the spectral distribution of the radiation intensity. The probability of transition from an initial state (i) to a final state (f) of the electron per unit time is determined by the well-known formula,

$$W_{fi} = \frac{4\pi^2 e^2}{\hbar V} \sum_{\vec{q}} |\vec{q}|^{-1} |\vec{\alpha}_{fi}.\vec{e}_k|^2 \ \delta(\omega_{fi} - \omega) \tag{3.93}$$

Where V is the volume of the system, $\vec{q}$ and $\vec{e}_k$ are the wave vector and polarization vector of a quantum of electromagnetic field as discussed in chapter 2.

$$\hbar\omega_{fi} = E_{ni} - E_{nf} \tag{3.94}$$

The matrix elements $\vec{\alpha}_{fi}$ are given by

$$\vec{\alpha}_{fi} = \delta_{\sigma_{iz}\sigma_{fz}} \delta_{p_{iy}, p_{fy}+\hbar q_y} \vec{D}_{fi} \tag{3.95}$$

$$\vec{D}_{fi} = -i x_{fi} (\Omega_{fi}, 0, q_x\beta) \tag{3.96}$$

$$x_{fi} = \int_{\infty}^{-\infty} x S_{n_f E_f}(x) S_{n_i E_i}(x) \ dx \tag{3.97}$$

where S_{nE} are oscillatory wavefunctions which obeys the Schrodinger equation given by

$$\left[-\frac{\hbar^2}{2E}\frac{d^2}{dx^2} + U(x)\right] S_{nE}(x) = E S_{nE}(x) \tag{3.98}$$

Let us define a vector of polarization $\vec{e}_1$ in the plane having the wave vector $\vec{q}$ and the z-axis and a vector $\vec{e}_2 \perp \vec{e}_1$ in the plane having the axes x and y. If φ and θ are the azimuth and polar angle of the wave vector $\vec{q}$,

$$\vec{e}_1 = (\cos\theta\cos\varphi, \cos\theta\sin\varphi, -\sin\theta) \tag{3.99}$$

$$\vec{e}_2 = (-\sin\varphi, \cos\varphi, 0) \tag{3.100}$$

The summation in Eqn. (3.93) is written in the integral form as

$$W_{fi} = \frac{e^2}{2\pi\hbar}\int \left(|\vec{\alpha}_{fi}.\vec{e}_1|^2 + |\vec{\alpha}_{fi}.\vec{e}_2|^2 \right) |\vec{q}|^{-1}|\ \delta(\omega_{fi} - \omega)\ d\vec{q} \tag{3.101}$$

Solving we get the transmission probabilities as

$$\frac{dW_{fi}}{d\Omega} = \frac{e^2 x_{fi}^2 \Omega_{fi}^3}{2\pi\hbar(1-\beta\cos\theta)^4}[(1-\beta\cos\theta)^2 - (1-\beta^2)\sin^2\theta\cos^2\varphi] \tag{3.102}$$

$$\frac{dW_{fi}}{d\omega} = x_{fi}^2\Omega_{fi}^2\frac{e^2}{2\hbar\beta^3}\left[1+\beta^2 - 2(1+\beta)\frac{\omega}{\omega_{0fi}} + 2(1+\beta)^2\left(\frac{\omega}{\omega_{0fi}}\right)^2\right] \tag{3.103}$$

$$\frac{dI_{fi}}{d\Omega} = \frac{e^2 x_{fi}^2 \Omega_{fi}^3}{2\pi(1-\beta\cos\theta)^5}[(1-\beta\cos\theta)^2 - (1-\beta^2)\sin^2\theta\cos^2\varphi] \tag{3.104}$$

$$\frac{dI_{fi}}{d\omega} = e^2 x_{fi}^2\Omega_{fi}^2\frac{\omega}{2\beta^3}\left[1+\beta^2 - 2(1+\beta)\frac{\omega}{\omega_{0fi}} + 2(1+\beta)^2\left(\frac{\omega}{\omega_{0fi}}\right)^2\right] \tag{3.105}$$

where

$$\omega_{0fi} \approx 2\Omega_{fi}\gamma^2 \tag{3.106}$$

The spectral intensity of radiation of a channeled electron in the case of a straight and dislocation affected channels are plotted in figures 3.12 and 3.13 with

$$s = \frac{3e^2 x_{fi}^2}{8\beta^3\gamma^2} \tag{3.107}$$

It is found that the change in the effective potential and frequency of oscillations proportionally changes the spectral distribution of radiation intensity. But the change is small and owes to the small dechanneling probability of electrons due to its motion in a symmetry direction (around the strings of atoms).

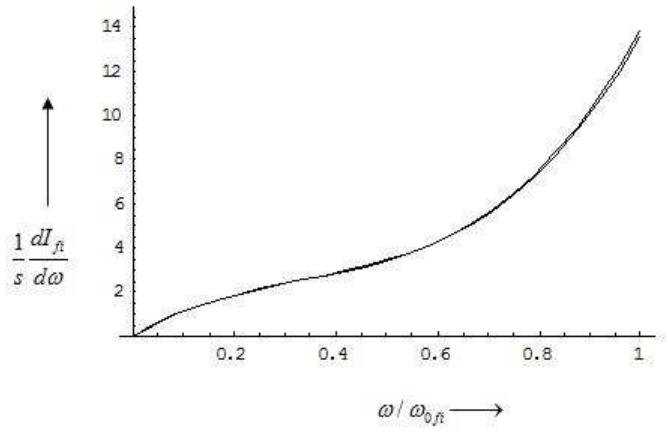

Figure 3.12: Spectral distribution of radiation intensity

3.5 Results and Discussions

We have developed a quantum mechanical model for the effects of dislocations on positron and electron channeling. The effects of centrifugal force developed due to the distorted channel have been discussed by including the effects of longitudinal motion of the particle using polar co-ordinates. The shift in potential due to the additional influence of longitudinal motion is thus found, in this dynamic formalism. The transverse potential and the frequency of channeling radiation in the perfect channel and the two regions of dislocation affected channels are also calculated. The wave functions for the transverse and longitudinal motions are calculated by using continuity of wave functions and their derivatives at the three boundaries. The reflection and

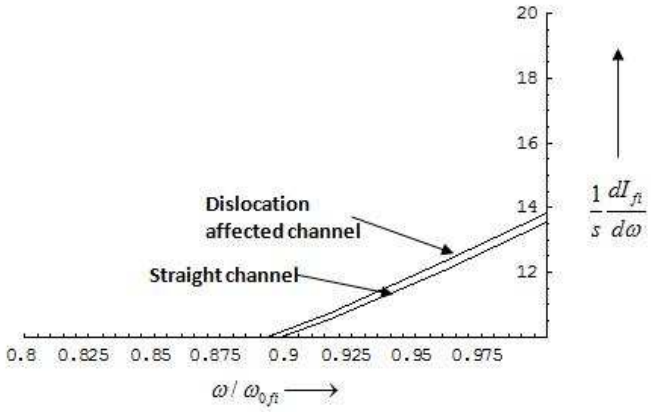

Figure 3.13: Spectral distribution of radiation intensity, showing clearly the fractional change due to the effects of dislocations

transmission coefficients are found using these boundary conditions which are the dechanneling and channeling probabilities respectively.

Comparing the positron and electron channeling cases, it is found from the figures 3.7 and 3.10 and also 3.8 and 3.11 that, for a given radius of curvature of the channels, the dechanneling probability is less for electrons than that for positrons. This is due to the property of electron channeling, where the transverse motion of electrons is bound to an atomic row or plane of atoms. Hence the dechanneling of the particles is less in this case when compared to the positively charged particles where transverse oscillation is between two planes or several rows of atoms. Due to this, the effects of dislocations are lesser for an electron channeling case than that for positrons.

For the electron case, the energy change is calculated for few materials like Si and Cu and for various incident energies and are given in Table 1. A comparison with the straight channel values is also made here. The change in spectral distribution

of radiation intensity is also calculated as seen from Figures 3.12 and 3.13. With the dechanneling probability being small for electrons, the spectral distribution of radiation intensity also has only small influence from the dislocations.

Summing up, the quantum mechanical model developed here for the effects of dislocations is applicable for channeling of both positive and negatively charged particles. This model is general and is likely to be basis for the explanation of the channeling/dechanneling phenomena due to any kind of distortion effects in crystalline materials.

CHAPTER 4

Dechanneling of Positrons by Dislocations: Effects of Anharmonic Interactions

4.1 Introduction

The potential usefulness of charged particle probes to study the materials for their purity had induced interest in the study on the effects of defects on channeling from the very beginning. Various classical [8, 57] as well as quantum mechanical models [16] have been developed to study the dechanneling due to defects, especially the dislocations. In the previous chapter we have derived a quantum model to study the effects of dislocations on positive and negatively charged particles propagating in single crystals. The dislocation affected regions of the channel and the unaffected straight regions were modelled as regions separated by boundaries. By using proper boundary conditions on wavefunctions and their derivatives, we could find the channeling (transmission) and dechanneling (reflection) co-efficients. In the present chapter, we

concentrate on specific case of positron planar channeling and use quantum model for the effects of dislocations. The anharmonic effects in the continuum potential have been included in these calculations and compared with the earlier results based on harmonic approximation for potential [60].

The dislocations induce distortion effects in the channels which affect the channeling radiation spectrum. These effects are incorporated by including the energy term $(2E/R)x$ due to the transverse centrifugal force, where E is the average energy in the curved part of the channel with radius of curvature R and x is the position of the particle in the transverse direction. This deflecting term is added to the continuum planar potential, which acts as a restoring force. Dechanneling of particles takes place when they are within some distance from the dislocation core (critical radius) where the distortion is maximum and hence large centrifugal deflecting force. The critical minimum radius of curvature R_{mc} of channels below which the particle will dechannel completely (shown in Figure 3.1 in chapter 3) can be obtained by equating the deflecting centrifugal force to the restoring planar potential and is given by;

$$R_{mc} = \frac{4E}{\pi Z_1 Z_2 e^2 C N_p} \tag{4.1}$$

Particles entering the channels with radius of curvature greater than R_{mc} will only be channeled. The corresponding critical distance of channels from dislocation core r_0 is given by,

$$r_0 = \sqrt{\frac{bR_{mc}}{10}} \tag{4.2}$$

where b as the Burgers vector [69]. This r_0 is called the mean dechanneling radius. Channels outside this region of radius r_0 around the dechanneling core (dechanneling cylinder) [8, 57, 58, 59] are distorted only slightly and do not lead to dechanneling.

An initially well channeled particle in the undistorted region oscillates around the equilibrium axis of the channel. But once it enters the distorted region, the potential

minima (about which the particle oscillates) shifts due to the centrifugal force term. Let this be denoted as a_r as shown in Figure 4.1. The effect of this shift on the continuum potential is calculated for both harmonic and anharmonic cases. Also the transitions among the energy levels in the transverse continuum potential induced due to dislocations are discussed.

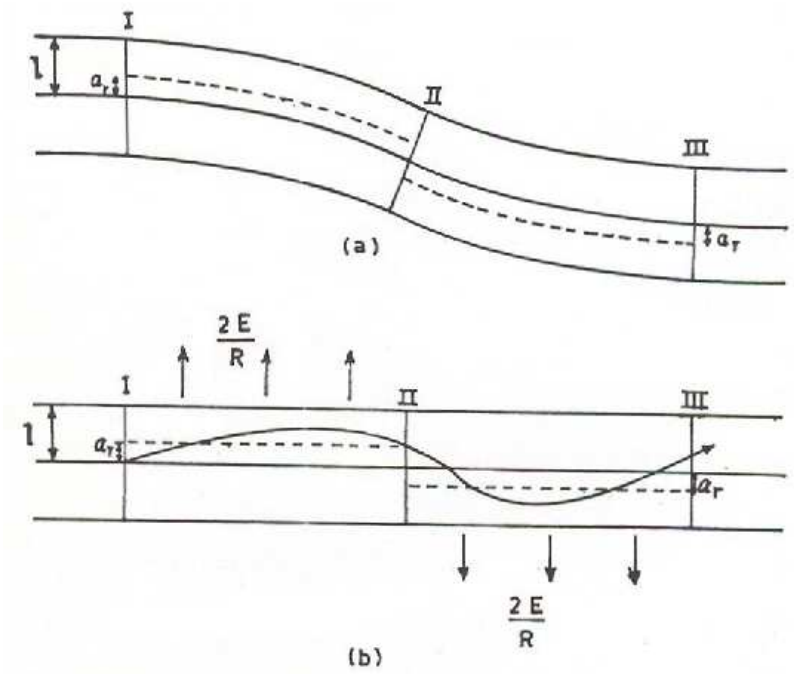

Figure 4.1: (a) A Channel with radius of curvature R and a shift a_r in the equilibrium position due to dislocations. (b) The curved channel is replaced by straight one to show the direction of the centrifugal force.

4.2 Harmonic Model

For the planar channeling of positrons, we use the continuum potential discussed in chapter 1. The transverse potential is given by [58, 59],

$$V(x) = \frac{4V_0 L a_{TF}}{L^2 - x^2} \tag{4.3}$$

which can be approximated as,

$$V(x) = U_0 + \frac{1}{2}k_1 x^2 \tag{4.4}$$

for the harmonic case, where $U_0 = \frac{4V_0 a_{TF}}{L}$ and $k_1 = \frac{8V_0 a_{TF}}{L^3}$. Also $L = l + a_{TF}$ as mentioned in the previous chapters.

4.2.1 Effects of Distortion

The centrifugal force due to the curvature of the channel affects the transverse potential. The effective potential in the distorted part of the channel is obtained by including an energy term corresponding to this centrifugal force and is given by [47, 60, 61],

$$V_{eff} = \frac{4V_0 L a_{TF}}{L^2 - x^2} - \frac{2E}{R}x \tag{4.5}$$

Expanding around the shifted minimum,

$$V_{eff}(x) = V_{eff}(a_r) + (x - a_r)\frac{dV_{eff}}{dx}\bigg|_{x=a_r} + \frac{1}{2}(x - a_r)^2 \frac{d^2 V_{eff}}{dx^2}\bigg|_{x=a_r} \tag{4.6}$$

$$\frac{dV_{eff}}{dx} = 0 \quad \Longrightarrow \quad a_r = \sqrt{\left(\frac{B}{L}\right)^2 - \frac{L^2}{2}} - \frac{B}{L} \tag{4.7}$$

with

$$B = \frac{RV_0 a_{TF}}{E}$$

which gives the effective potential as,

$$V_{eff}(x) = V_{eff}(a_r) + \frac{1}{2}(x - a_r)^2 \frac{d^2 V_{eff}}{dx^2}\bigg|_{x=a_r} \tag{4.8}$$

From Eqn. (4.5), we can write

$$\frac{d^2 V_{eff}}{dx^2} = \frac{8V_0 a_{TF} L}{(L^2 - x^2)^3}\,[L^2 + 3x^2] \tag{4.9}$$

Substituting, Eqn. (4.9) in (4.8), we get the co-efficient of x^2 which gives the effective force constant and can be written as,

$$k_1^{eff} = \frac{8V_0 a_{TF} L}{(L^2 - a_r^2)^3}\,[L^2 + 3a_r^2] \tag{4.10}$$

The maximum number of bound states can be obtained from the relation [60],

$$(n + 1/2)\hbar\omega = \frac{1}{2}k_1 x^2 \tag{4.11}$$

At $x = x_{max}$, we have maximum number of states, $n = j_{max}$, where $x_{max} = l - a_{TF} - a_r$. Substituting $\omega = \sqrt{\frac{k_1}{\gamma m}}$, Eqn. (4.11) can be rewritten as,

$$j_{max} = \frac{1}{2}\left[\sqrt{\gamma m k_1^{eff}}\ \frac{x_{max}^2}{\hbar} - 1\right] \tag{4.12}$$

Substituting k_1^{eff} from Eqn. (4.10) we get,

$$j_{max} = \frac{1}{2}\left[\sqrt{\frac{\gamma m 8 V_0 a_{TF} L}{(L^2 - a_r^2)^3}\ [L^2 + 3a_r^2]}\ \ \frac{(l - a_{TF} - a_r)^2}{\hbar} - 1\right] \tag{4.13}$$

The transition probability among the energy levels in the transverse continuum potential are to be calculated. These transitions are induced by the distortions created due to dislocations.

We take the example of a positron with incident energy $12.45MeV(\gamma = 25)$ channeling along $Al(111)$ planes with dislocations. Using the above equations, we can find $j_{max} = 3$. It is shown in Figure 4.2 (plotted in comparison with the anharmonic case).

Due to the change in the force constant in the distortion region, the coupling constant $\alpha = \sqrt{\frac{m\omega}{\hbar}}$ gets modified to α' and is given from Eqn.(4.13) as,

$$\alpha'^2 = \sqrt{\gamma m 8 V_0 a_{TF} L\ \frac{L^2 + 3a_r^2}{(L^2 - a_r^2)^3}} = \sqrt{\frac{\gamma m 8 V_0 a_{TF}}{L^3}\ \left\{\frac{1 + 3(a_r/L)^2}{1 - (a_r/L)^2}\right\}} \tag{4.14}$$

$$\alpha'^2 = \tau^2 \alpha^2 \tag{4.15}$$

$$\alpha^2 = \sqrt{\frac{\gamma m 8 V_0 a_{TF}}{L^3}} \tag{4.16}$$

where the distortion parameter $\tau = \alpha'/\alpha$ is given by

$$\tau^2 = \sqrt{\frac{1 + 3(a_r/L)^2}{1 - (a_r/L)^2}} \tag{4.17}$$

When the distortion in the channels is least, the shift in the potential minima is almost zero. It is obvious from the above Eqn. (4.17); at a_r =0, $\tau^2 = 1$. Figure 4.3 illustrates the variation of the distortion parameter with respect to the distance from the dislocation core in the harmonic as well as anharmonic cases. It is observed that, as the distance from the dislocation core increases, the curvature of the channels increases and the distortion parameters approaches 1 (zero distortion).

4.2.2 Channeling probabilities across the interfaces

As shown in Figure 4.1, the whole region is divided into four with three boundaries through which the particle has to cross during its passage through the distorted channel. We use the sudden approximation to calculate the transition probabilities across these three boundaries. The wavefunction of the particles in the four regions can be written as,

$$\psi_i = \left(\frac{\alpha}{\sqrt{\pi}\ 2^i i!}\right)^{1/2} \exp\left\{\frac{-\alpha^2 x^2}{2}\right\} H_i(\alpha x) \tag{4.18}$$

$$\psi_j^{(1)} = \left(\frac{\alpha'}{\sqrt{\pi}\ 2^j j!}\right)^{1/2} \exp\left\{\frac{-\alpha'^2 (x+a_r)^2}{2}\right\} H_j(\alpha' x + \alpha' a_r) \tag{4.19}$$

$$\psi_k^{(2)} = \left(\frac{\alpha'}{\sqrt{\pi}\ 2^k k!}\right)^{1/2} \exp\left\{\frac{-\alpha'^2 (x-a_r)^2}{2}\right\} H_k(\alpha' x - \alpha' a_r) \tag{4.20}$$

$$\psi_f = \left(\frac{\alpha}{\sqrt{\pi}\ 2^f f!}\right)^{1/2} \exp\left\{\frac{-\alpha^2 x^2}{2}\right\} H_f(\alpha x) \tag{4.21}$$

The maximum number of bound states is $j_{max} = 3$. From a fixed initial state the particle can occupy any of the final states in the distorted regions of the channel. The possible transitions are;

$$\begin{array}{llll} 0 \to 0\ ; & 0 \to 1\ ; & 0 \to 2\ ; & 0 \to 3 \\ 1 \to 0\ ; & 1 \to 1\ ; & 1 \to 2\ ; & 1 \to 3 \\ 2 \to 0\ ; & 2 \to 1\ ; & 2 \to 2\ ; & 2 \to 3 \\ 3 \to 0\ ; & 3 \to 1\ ; & 3 \to 2\ ; & 3 \to 3 \end{array}$$

The transition probability across the first interface [70]; i.e., probability of the particle with initial state $|i\rangle$ to cross to the state $|j\rangle$ in the first distorted region, is given by,

$$p_{i\to j} = |\langle\psi_j^{(1)}|\psi_i\rangle|^2 \tag{4.22}$$

The overlap integral of the transitions across the first interface written as,

$$\langle\psi_j^{(1)}|\psi_i\rangle = \left(\frac{\alpha\alpha'}{\pi 2^{j+i} j!\ i!}\right)^{1/2} I_{n,m} \tag{4.23}$$

where

$$I_{n,m} = \int_{-\infty}^{\infty} H_i(\alpha x)\ H_j(\alpha' x + \alpha' a_r)\ \exp\left\{ -\frac{1}{2}(\alpha^2 x^2 + \alpha'^2 (x + a_r)^2)\right\} \tag{4.24}$$

Solving the above equation we get the individual transition amplitudes $|\langle j^{(1)}|i\rangle|^2$ and are given by,

$$\begin{aligned} |\langle j^{(1)}|i\rangle|^2 &= \left(\frac{\alpha\alpha'}{\pi 2^{j+i} j!\ i!}\right)\ \exp\left\{-\left(\frac{\alpha'^2}{\alpha^2+\alpha'^2}\right)\alpha^2 a_r^2\right\} \\ &\times \left| \int_{-\infty}^{\infty} \exp\left\{ -\frac{1}{2}(\alpha^2+\alpha'^2)\left[x + \frac{\alpha'^2}{\alpha^2+\alpha'^2} a_r\right]^2\right\}\right. \\ &\left. H_j(\alpha' x + \alpha' a_r)\ H_i(\alpha x)\right|^2 \end{aligned} \tag{4.25}$$

The total probability of the particle in the initial state $|i\rangle$ to occupy any of the final states $|j\rangle$ ($j_{max} < i_{max}$) in the first region of distortion affected channel is given by

$$p_i^I = \sum_{j=0}^{j_{max}} |\langle j^{(1)}|i\rangle|^2 \tag{4.26}$$

So the dechanneling probability across the first interface is written as,

$$\chi_i^I = 1 - p_i^I \tag{4.27}$$

Similarly channeling and dechanneling probabilities across II and III regions are given by,

$$p^{II}_{j^{(1)}} = \sum_{k=0}^{k_{max}} |\langle k^{(2)}|j^{(1)}\rangle|^2 \tag{4.28}$$

$$\chi^{II}_{j} = 1 - p^{II}_{j^{(1)}} \tag{4.29}$$

$$p^{III}_{k^{(2)}} = \sum_{f=0}^{f_{max}} |\langle f|k^{(2)}\rangle|^2 \tag{4.30}$$

$$\chi^{III}_{j} = 1 - p^{III}_{k^{(2)}} \tag{4.31}$$

The total channeling probability of the particle with an initial state $|i\rangle$ to find itself in the straight channel with final state $|f\rangle$ after passing through the two regions of dislocation affected channel is written as,

$$p_{i\to f} = \sum_{k^{(2)}=0}^{k^{(2)}_{max}} \left(p_{k^{(2)}\to f} \left[\sum_{j^{(1)}=0}^{j^{(1)}_{max}} p_{i\to j^{(1)}} \times p_{j^{(1)}\to k^{(2)}} \right] \right) = p_{f\to i} \tag{4.32}$$

The variation of the channeling probability with distance from dislocation core for an initially well-channeled particle and a particle in the first excited state are plotted in figures 4.5 and 4.6 respectively in comparison with the anharmonic case. As the distance from the dislocation core increases, the probability of channeling also increases and attains a maximum value. The distance r_0 at which the probability of channeling attains a finite value corresponds to the radius of the dechanneling cylinder and it can be found from these figures 4.5 and 4.6.

4.3 Effects of Anharmonicity

We now consider the effects of anharmonicity and its relevance to positron planar channeling with dislocations. We analyze how various parameters in channeling get affected by the additional anharmonic term in the positron planar potential.

Including the anharmonic term for the transverse periodic potential of the positron, the potential equation can be written as,

$$\begin{aligned} V(x) &= \frac{4V_0 a_{TF}}{L}\left(1-\frac{x^2}{L^2}\right)^{-1} \\ &= \frac{4V_0 a_{TF}}{L}\left(1+\frac{x^2}{L^2}+\frac{x^4}{L^4}\right) \\ V(x) &= U_0+\frac{1}{2}k_1x^2+\frac{1}{4}k_2x^4 \end{aligned} \tag{4.33}$$

where

$$k_2 = \frac{16V_0 a_{TF}}{L^5} \tag{4.34}$$

4.3.1 Effects on the distortion parameter

Expanding around the shifted potential minimum, a_r, the effective potential is written as,

$$V_{eff}(x) = V_{eff}(a_r) + \frac{1}{2}(x-a_r)^2\frac{d^2V_{eff}}{dx^2}\bigg|_{x=a_r} + \frac{1}{4}(x-a_r)^4\frac{d^4V_{eff}}{dx^4}\bigg|_{x=a_r} \tag{4.35}$$

Using Eqn. (4.5), we can write,

$$\frac{d^4V_{eff}}{dx^4} = 8V_0 a_{TF} L\left[\frac{60x^4+12x^2L^2+12L^4}{(L^2-x^2)^5}\right] \tag{4.36}$$

which gives co-efficient of x^4 and hence the effective value of k_2.

$$k_2^{eff} = 8V_0 a_{TF} L\left[\frac{60a_r^4+12a_r^2L^2+12L^4}{(L^2-a_r^2)^5}\right] \tag{4.37}$$

The energy spectrum including the effects of anharmonicity is given by,

$$E_n = \hbar\omega_0\left[(n+1/2)+\frac{\varepsilon}{4}(2n^2+2n+1)\right] \tag{4.38}$$

where

$$\varepsilon = \frac{3\hbar k_2}{4\gamma m\omega_0 k_1} \tag{4.39}$$

The maximum number of quantum states, j_{max} are given from the equation,

$$\hbar\omega_0\left[(j_{max}+1/2)+\frac{\varepsilon^{eff}}{4}(2j_{max}^2+2j_{max}+1)\right]=\frac{1}{2}k_1^{eff}x_{max}^2+\frac{1}{4}k_2^{eff}x_{max}^4 \tag{4.40}$$

which gives, after solving,

$$j_{max}=\left(\frac{1}{2}+\frac{1}{\varepsilon^{eff}}\right)\left[-1+\left(1-\frac{2\varepsilon^{eff}}{\varepsilon^{eff}+2}+\frac{4\varepsilon^{eff}}{(\varepsilon^{eff}+2)^2}\,\frac{k_1^{eff}x_{max}^2+1/2k_2^{eff}x_{max}^4}{\hbar\omega_0}\right)^{1/2}\right] \tag{4.41}$$

We can find from the above equation that anharmonicity changes the number of maximum bound states from 3 to 5. It is shown in Figure 4.2.

With the increase of the number of bound states, we can expect more transitions between these states. The possible transitions are,

$$\begin{array}{lllll}
0\to 0\,; & 0\to 1\,; & 0\to 2\,; & 0\to 3 & 0\to 4\,; \quad 0\to 5\\
1\to 0\,; & 1\to 1\,; & 1\to 2\,; & 1\to 3 & 1\to 4\,; \quad 1\to 5\\
2\to 0\,; & 2\to 1\,; & 2\to 2\,; & 2\to 3 & 2\to 4\,; \quad 2\to 5\\
3\to 0\,; & 3\to 1\,; & 3\to 2\,; & 3\to 3 & 3\to 4\,; \quad 3\to 5\\
4\to 0\,; & 4\to 1\,; & 4\to 2\,; & 4\to 3 & 4\to 4\,; \quad 4\to 5\\
5\to 0\,; & 5\to 1\,; & 5\to 2\,; & 5\to 3 & 5\to 4\,; \quad 5\to 5
\end{array}$$

The frequency of oscillation with the effects of anharmonicity is calculated as,

$$\omega_{ah}=\omega_0\left[1+\frac{\varepsilon}{4}\right] \tag{4.42}$$

which changes the coupling constant to $\alpha'=\sqrt{\frac{m\omega_{ah}}{\hbar}}$. Hence the distortion parameter is given by,

$$\tau^2=\frac{\alpha'^2}{\alpha^2}=\sqrt{\frac{k_1^{eff}}{k_1}}\,\frac{\left(1+\frac{\varepsilon^{eff}}{4}\right)}{\left(1+\frac{\varepsilon}{4}\right)} \tag{4.43}$$

where

$$\varepsilon^{eff}=\frac{3\hbar k_2^{eff}}{4\gamma m\omega_0 k_1^{eff}} \tag{4.44}$$

Figure 4.3 illustrates the effects of dislocations on the distortion parameter for a positron incident with incident energy $12.45MeV(\gamma = 25)$ channeling along $Al(111)$ planes. With anharmonicity the distortion increases as shown in this figure 4.3. As the distance from the dislocation core increases, the distortion parameter decreases. But unlike in the harmonic case, it is not reducing to 1. This is due to the fact that anharmonicity, by itself, is inducing some perturbations in the channel.

Also Figure 4.4 shows the effects of anharmonicity on the frequency of oscillation. For the harmonic model, as the distance from the dislocation core is large, the channel is almost straight and $\frac{\omega}{\omega_0}$ approaches 1. But in the anharmonic case, it has always have a finite value > 1. A percentage increase of 17% in the frequency of oscillation is found from the harmonic to anharmonic model.

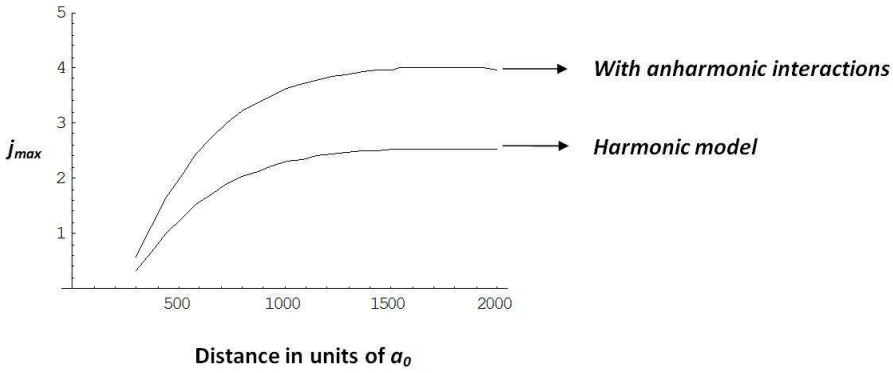

Figure 4.2: The variation of number of states supported by a planar channel with distortion of the channel.

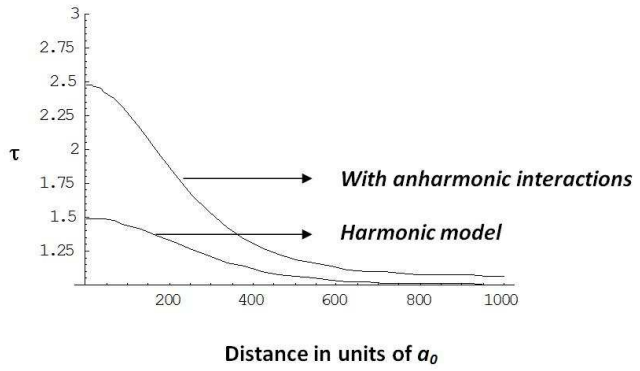

Figure 4.3: The variation of distortion parameter as a function of distance from dislocation, in comparison with the harmonic case.

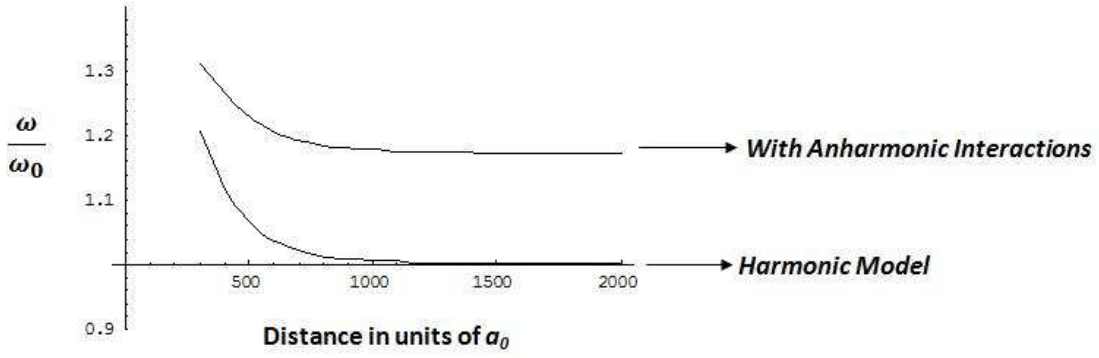

Figure 4.4: The variation of the frequency of oscillation.

4.3.2 Effects on Channeling probabilities

Now we consider the effects of anharmonicity on the channeling and dechanneling probabilities. The first order perturbed wavefunction is given by the equation [60, 61, 71],

$$\begin{aligned} |\psi\rangle = |n\rangle + \frac{\varepsilon^{eff}}{48} \quad \Bigg[& \quad \sqrt{n(n-1)(n-2)(n-3)}|n-4\rangle \\ & + \quad 4(2n-1)\sqrt{n(n-1)}|n-2\rangle \\ & - \quad 4(2n+3)\sqrt{(n+1)(n+2)}|n+2\rangle \\ & - \quad \sqrt{(n+1)(n+2)(n+3)(n+4)}|n+4\rangle \Bigg] \end{aligned} \tag{4.45}$$

which can be written as,

$$|\psi_n\rangle = |n\rangle + \frac{\varepsilon^{eff}}{48}\Big[A_n|n-4\rangle + B_n|n-2\rangle - C_n|n+2\rangle - D_n|n+4\rangle\Big] \tag{4.46}$$

where the constants $A_n,\ B_n,\ C_n$ and D_n are given by,

$$\begin{aligned} A_n &= \sqrt{n(n-1)(n-2)(n-3)} \\ B_n &= 4(2n-1)\sqrt{n(n-1)} \\ C_n &= 4(2n+3)\sqrt{(n+1)(n+2)} \\ D_n &= \sqrt{(n+1)(n+2)(n+3)(n+4)} \end{aligned} \tag{4.47}$$

From the above equations, the overlap integral corresponding to the anharmonic potential for two states M and N represented by ψ_m and ψ_n is written as,

$$
\begin{aligned}
\langle M|N\rangle = \langle m|n\rangle \;&+\; \frac{\varepsilon^{eff}}{48}\Big[A_n\langle m|n-4\rangle + B_n\langle m|n-2\rangle \\
&-\; C_n\langle m|n+2\rangle - D_n\langle m|n+4\rangle\Big] \\
&+\; \frac{\varepsilon^{eff}}{48}\Big[A_m\langle m-4|n\rangle + B_m\langle m-2|n\rangle \\
&-\; C_m\langle m+2|n\rangle - D_m\langle m+4|n\rangle\Big] \\
&+\; \left(\frac{\varepsilon^{eff}}{48}\right)^2\Big[A_nA_m\langle m-4|n-4\rangle + B_nA_m\langle m-4|n-2\rangle \\
&-\; C_nA_m\langle m-4|n+2\rangle - D_nA_m\langle m-4|n+4\rangle\Big] \\
&+\; \left(\frac{\varepsilon^{eff}}{48}\right)^2\Big[A_nB_m\langle m-2|n-4\rangle + B_nB_m\langle m-2|n-2\rangle \\
&-\; C_nB_m\langle m-2|n+2\rangle - D_nB_m\langle m-2|n+4\rangle\Big] \\
&+\; \left(\frac{\varepsilon^{eff}}{48}\right)^2\Big[A_nC_m\langle m+2|n-4\rangle + B_nC_m\langle m+2|n-2\rangle \\
&-\; C_nC_m\langle m+2|n+2\rangle - D_nC_m\langle m+2|n+4\rangle\Big] \\
&+\; \left(\frac{\varepsilon^{eff}}{48}\right)^2\Big[A_nD_m\langle m+4|n-4\rangle + B_nD_m\langle m+4|n-2\rangle \\
&-\; C_nD_m\langle m+4|n+2\rangle - D_nD_m\langle m+4|n+4\rangle\Big]
\end{aligned}
\tag{4.48}
$$

Now, by using Eqn. (4.48) and (4.25), we can find the channeling probability from Eqn. (4.22).

Let us consider two cases; particles in the ground state (initially well channeled particles) and in the first excited states. The transition probabilities are found for these two cases; $p_{0\to0}$ and $p_{1\to0}$ respectively.

Transition probability across the first interface; i.e., the probability of the particle in the initial state $|0\rangle$ to occupy any of the final states $|M\rangle \quad (M_{max} = j_{max})$ in the first region of dislocation affected channel is given by,

$$p_0^I = \sum_{M=0}^{5} |\langle M^{(1)}|0\rangle|^2 \tag{4.49}$$

The individual amplitudes $\langle m|n\rangle$ etc, on the right hand side of Eqn (4.48) are calculated using Eqn. (4.25). The probabilities across the II^{nd} and III^{rd} interfaces are similarly calculated and the total channeling probability, $p_{0\to0}$ thus can be found using Eqn. (4.32).

For the particles in the first excited state, the transition probability $p_{1\to0}$ is calculated in the same way. Figures 4.5 and 4.6 illustrate the channeling probabilities for initially well-channeled particle and first excited state respectively. It is found that the probability of channeling is increased due anharmonicity in both the cases. Also it can be noticed that the value of r_0 which corresponds to the radius of dechanneling cylinder is increased with the effect of anharmonicity.

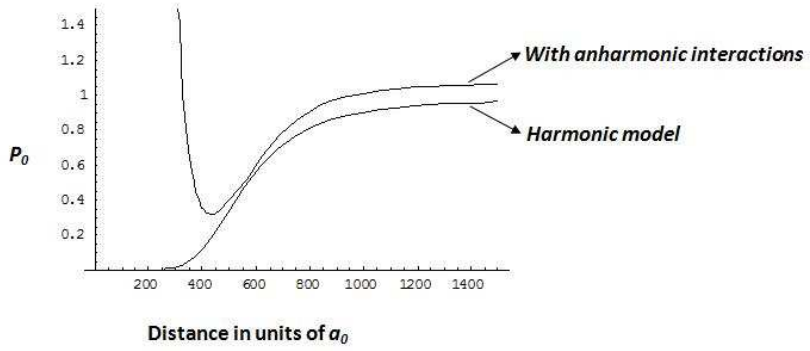

Figure 4.5: Influence of channel distance from dislocation on channeling probability corresponding to an initially well-channeled particle ($P_{0\to0}$)

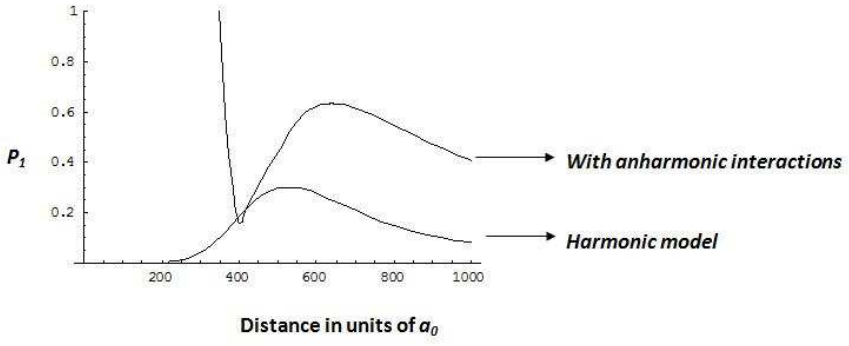

Figure 4.6: Influence of channel distance from dislocation on channeling probability corresponding to initial state $|1\rangle$ ($P_{1\to 0}$)

4.4 Results and Discussions

We have developed a quantum theory of dechanneling due to dislocations with the effects of anharmonic term in the positron planar potential. The effects of dislocations and anharmonicity on the planar channeling potential are estimated. The above calculations are performed for positrons with incident energy 12.45 MeV channeled in Al in the planar direction (111). We have considered a typical dislocation density of 10^8 dislocations / cm^2. It is found that anharmonicity changes the channeling parameters and distortion parameters considerably. If the material has disordered regions, then the transition of positrons from normal to disordered region is affected according to the variation in the planar continuum potential.

The number of states supported by the planar channel too varies with anharmonicity. It changes from 3 to 5 as plotted in Figure 4.2. As a result the number of transitions increases. We have found a considerable amount of change in the distortion parameter due to the anharmonic effects as shown in Figure 4.3. In a straight, normal channel with zero distortion, the value of distortion parameter is set as 1. In a dislocation affected region, as the distance from the dislocation core increases,

the radius of curvature of the channels increases which results in the decrease of curvature. The decrease in the curvature thus decreases the distortion as plotted. Anharmonicity increases the distortion parameter as shown, but decreases with the distance from the dislocation core. It can be noticed from the Figure 4.3 that the value of the distortion parameter never goes to 1. This is due to the fact that anharmonicity itself is inducing some perturbations in the channel. The change in the frequency of oscillations due dislocation is also studied. As shown the Figure 4.4 the effects of anharmonicity increases frequency of oscillations by 17%. This is in good agreement with the changes in the spectral distribution of radiation intensity discussed in chapter 2.

We have considered the channeling probabilities corresponding to an initially well-channeled particle ($|i\rangle = |0\rangle$) and that corresponding to an initial state $|i\rangle = |1\rangle$. The anharmonic term increases these transition probabilities considerably as shown in figures 4.5 and 4.6. This is due to the increased transitions between the additional states due to the anharmonicity. The value of r_0 at which the probabilities p_0 and p_1 increases and then reaches a maximum corresponds to the radius of the dechanneling cylinder. It is found that anharmonicity causes the increase of this radius as shown in the figures.

From the above calculations we have found that the channeling parameters are affected considerably by anharmonicity. The fact that anharmonicity itself is inducing perturbations in the channel, it adds to the already existing distortions due to dislocations. In conclusion, the effects of anharmonicity should be included in any realistic treatment of the problem.

CHAPTER 5

Effects of Dislocations on Channeling Radiation from a Periodically Bent Crystal

5.1 Introduction to Crystalline Undulator

Ever since its discovery about 30 years back, channeling radiation has been investigated extensively and has been used successfully in the study of defects such as dislocations. Dislocations, as discussed in chapters 3 and 4, is the most important example of defects that produce distortions in the channel. The effects of these dislocations on channeling radiation have been studied both theoretically [60, 61] and experimentally [72] and one finds an increase in channeling radiation frequency and decrease of intensity with increase of the distortions induced by these dislocations. In chapter 3, a detailed study of the effects of dislocations on the channeling of positive and negative particles is given and we concluded that the effects of defects like dislocations are very important and cannot be neglected in the study of charged particle

propagation through solids.

Channeling in a **periodically** bent crystal is of recent interest in connection with the undulator problem. A crystalline undulator is basically a periodically bent channel with ultrarelativistic charged particles undergoing channeling through it (Figure 5.1). In a crystalline undulator, in addition to the channeling radiation, there occurs radiation due to the motion of particle which follows the periodic bending of crystallographic planes. This radiation is called undulator radiation as mentioned in chapter 2. Crystalline undulator serves as an efficient source for coherent high energy photon emission [30, 73],[40-46]. The parameter of the undulator can be tuned by varying the energy and type of projectile and by choosing different crystallographic channels. Also wide range of frequencies and bending amplitudes in crystals allow one to generate crystalline undulator radiation with energies from eV to MeV region. Several investigators have studied this theoretically [41-46] and few others have used this in making undulators [74-82].

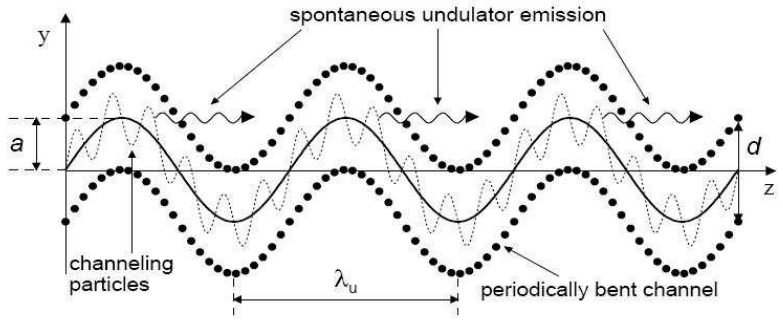

Figure 5.1: A schematic representation of a crystalline undulator.

The necessary conditions to be satisfied by a crystalline undulator to become a source of radiation are discussed by various authors [41, 83, 84]. These are given by;

$$\begin{aligned} C &= 4\pi^2\varepsilon a/U'_{max}\lambda_u^2 < 1 && \text{- stable channeling} \\ d &\ll a \ll \lambda_u && \text{- large amplitude regime} \\ N &= L/\lambda \gg 1 && \text{- large number of undulator periods} \\ L &< \min[L_d(C), L_a(\omega)] && \text{- account for channeling and photon attenuation} \\ \Delta\varepsilon/\varepsilon &\ll 1 && \text{- low radiative losses} \end{aligned} \tag{5.1}$$

where a is the amplitude of bending of the channel, $\varepsilon = \gamma mc^2$, the energy of the particle, λ_u is the wavelength of the undulator, L, the undulator length, L_d, dechanneling length, L_a, attenuation length and d, the interplanar spacing.

Stable channeling of a projectile in a periodically bent crystal occurs if the maximum centrifugal force $F_{cf} = \gamma mc^2/R_{min}$ (R_{min} being the minimum curvature of radius of the bent channel) is less than the maximal restoring force due to the interplanar field F_{int}. i.e, $C = F_{cf}/F_{int} < 1$. A crystalline undulator should be considered in high amplitude regime. In the limit $a/d > 1$, the undulator and channeling radiation frequencies are well-separated. The term 'undulator' implies the number of periods to be large so that the emitted radiation spectrum is narrow with well-separated peaks.

The fourth condition in Eqn. (5.1) puts a severe limitation on the allowed values of crystalline undulator length L due to dechanneling and attenuation represented by dechanneling length L_d and attenuation length L_a respectively. A particle entering the channel undergoes scattering by electrons and nuclei of the crystal. The dechanneling effect stands for a gradual increase in the transverse energy of a channeled particle due to these inelastic collisions. At the the distance L_d, from the entrance point, the particle gains a transverse energy higher than the planar potential barrier

and leaves the channel. L_a is defined as the scale at which the intensity of the photon flux is decreased by a factor e due to the process of absorption and scattering. Commenting on the last condition in Eqn. (5.1), the coherence of undulator radiation is only possible when the energy loss $\Delta\varepsilon$ of the particle during its passage through the undulator is small.

Various methods have been proposed to realize a crystalline undulator. It can be done either by using ultrasonic waves [42] or by gradient crystals [74, 75, 76] or by using substrates with periodically deposited strips of alternating stresses [77]. This last method has been tried recently in the works of Guidi *et.al.* and Lanzoni *et.al.* [79, 80, 81]. Methods like making regularly spaced grooves on crystal surfaces [78, 79, 82] and using crystals with periodic surface deformations [82] have also been proposed to achieve periodic bending in a crystal. However an actual crystalline undulator has still not been completely realized.

On the other hand, all the theoretical models for crystalline undulators vis-a-vis channeling radiation have ignored the presence of defects and damage which is invariably present in the materials. As mentioned above, the dislocations are the most important defects, having long range effects on channeling phenomena because of the distortions they produce. These distortions are also likely to have very significant effects on the analysis of the channeling in periodically bent crystals. In the present analysis, we investigate the effects of dislocations on the particle propagating in a periodically bent crystal.

In chapter 2, an attempt was made to study the effects of periodically bent crystal on channeling radiation. The study was focussed only on the effect of transverse acoustic wave interactions with lower amplitudes. In this chapter, we first consider a periodically bent channel with a reasonable amplitude of bending 'a' ($a \gg d$). Both

the dislocation affected region and the periodically bent channel are represented by their radii of curvature and wavelengths (represented by λ_d and λ_u respectively) and we consider the modulation of these effects of dislocation over the periodicity of the channel. Two cases of high and low dislocation densities are considered. The varying dislocation densities change these modulation effects. We divide the channel into four regions; beginning and ending with perfect periodically bent regions with two dislocation affected regions between them.

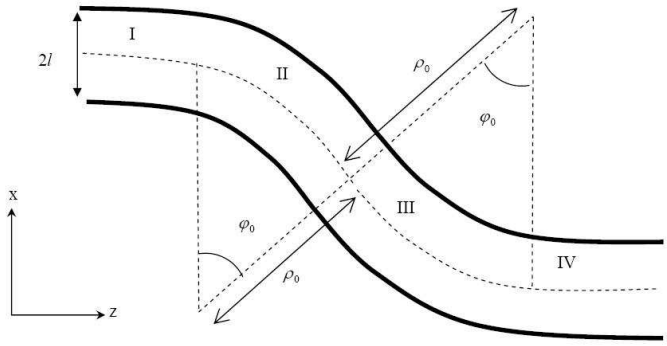

Figure 5.2: The Model for the channel affected with dislocation. Instead of the straight channels as in the figure, for the present study the whole region is considered as periodically bent.

5.2 Effects of dislocations

Let us consider a crystal whose planes are periodically bent following a perfect harmonic shape $x(z) = a\ \sin(k_u z)$. The transverse and longitudinal coordinates of a channeled particle in such a periodically bent crystal can be written as [45],

$$\tilde{x} = x - a\ \sin(k_u z) \tag{5.2}$$

where

$$k_u = \frac{2\pi}{\lambda_u} \tag{5.3}$$

We consider now, the effects of dislocations on such a typical channel situated at some finite distance from the dislocation core, outside the dechanneling cylinder [57]. The dislocation induced distortions in the crystallographic channels are divided into two regions [85] namely region II and III which smoothly join the perfect region I and region IV, as shown in Figure 5.2. The centrifugal forces act in opposite directions in regions II and III. Here ρ_0 corresponds to the radial coordinate of the channel center as measured from the origin and φ_0 is the corresponding angular co-ordinate.

Consider the Ist region, which is part of the normal periodically bent channel. The Schrodinger equation can be written as,

$$-\frac{\hbar^2}{2m}\left(\frac{\partial^2}{\partial x^2}+\frac{\partial^2}{\partial z^2}\right)\ \Psi^I(x,z)+U(x)\ \Psi^I(x,z)=E^I\ \Psi^I(x,z) \tag{5.4}$$

Where E^I is the total energy and can be written as

$$E^I = E_T^I + E_L^I \tag{5.5}$$

with E_T^I and E_L^I, the energy components associated with the transverse and longitudinal motion, respectively.

$$E_T^I = \left(n+\frac{1}{2}\right)\hbar\omega \tag{5.6}$$

$$E_L^I = \frac{\hbar^2 k^2}{2m} \tag{5.7}$$

where, $\alpha = \sqrt{\frac{\hbar}{m\omega}}$ and $\omega = \sqrt{\frac{2V_0}{m}}$. The positron planar potential in this region is written as,

$$\begin{aligned} U(x) &= V_0\tilde{x}^2 \\ &= V_0(x - a\ \sin(k_u z))^2 \end{aligned} \tag{5.8}$$

Now consider the dislocation affected regions of the channel. Centrifugal force proportional to μ^2/ρ^2 becomes operative in the curved regions of the channel. Here $\mu\hbar$

is the angular momentum with $\mu^2 = l(l+1)$ with l as the orbital angular momentum quantum number and ρ is the radius of curvature of the channel. For the two regions of dislocation affected channel these forces are acting in directions opposite to each other. Schrodinger equations for both these regions are written in terms of the polar co-ordinates ρ and φ.

5.2.1 Low dislocation density ($\lambda_d > \lambda_u$)

Now assume that a finite number of undulator periods are there in one period of the dislocation affected region of the channel. Let x_d be the amplitude of the wave corresponding to the dislocation affected region with a wavelength λ_d and that there is a phase difference of ϕ between the dislocation affected channel and the undulator wave. Now we can write,

$$\lambda_d = n\ \lambda_u \tag{5.9}$$

$$k_u = n\ k_d \tag{5.10}$$

Both these waves can be written in the form,

$$r_1 = a\ \sin(nk_d z) \tag{5.11}$$

$$r_2 = x_d\ \sin(k_d z + \phi) \tag{5.12}$$

Superposition of the waves gives

$$r = r_1 + r_2 = A\ \sin(k_d z + \Phi) \tag{5.13}$$

Where A and Φ are the effective amplitude and phase of the final wave and are given by,

$$A^2 = a^2 + x_d^2 + 2ax_d\ \cos[(n-1)k_d z - \phi] \tag{5.14}$$

$$\tan\ \Phi = \frac{a\ \sin[(n-1)k_d z] + x_d\ \sin\phi}{a\ \cos[(n-1)k_d z] + x_d\ \cos\phi} \tag{5.15}$$

Consider region II, i.e., the first curved part of the dislocation affected channel. Schrodinger equation for this region in terms of the polar coordinates ρ and φ is given by,

$$-\frac{\hbar^2}{2m}\left[\frac{1}{\rho}\frac{\partial}{\partial\rho}\left(\rho\frac{\partial}{\partial\rho}\right)+\frac{1}{\rho^2}\frac{\partial^2}{\partial\varphi^2}\right]\Psi^{II}(\rho,\varphi)+U(\rho)\Psi^{II}(\rho,\varphi)=E^{II}\ \Psi^{II}(\rho,\varphi) \qquad (5.16)$$

With the channel periodically bent, ρ_0 can be written as

$$\tilde{\rho_0}=\rho_0-x_d\ \sin(k_dz)+A\ \sin(k_uz) \qquad (5.17)$$

The variation of both the amplitude of bending and the radius of curvature of the dislocation affected regions depends on both the waves; dislocation affected region and the undulator represented by λ_d and λ_u respectively. The following tables show how these parameters depend on each others values. Table 1 gives the variation of the parameters of the dislocation affected region; radius and length of the curved region, $R_d=\rho_0$ and $\lambda_d=2z$ respectively with dislocation density. We have [58, 59],

$$\begin{aligned} R_d &= \frac{2\pi^2r_0^2}{b\cos^3\varphi} \\ \lambda_d &= \frac{2\pi r_0}{\cos\varphi} \end{aligned}$$

For channeling in Si (110) direction, the burgers vector $b=3.84\mathring{A}$.

Table 2 gives the range of various parameters of the periodically bent channel affected by dislocations corresponding to a dislocation density of $10^8/cm^2$.

Table 1: Parameters of a dislocation affected region for channeling in $< 110 >$ direction for Si

Dislocation density	r_0 (nm)	R_d (nm)	λ_d (nm)
$10^{10}/cm^2$	0.5×10^2	10.28×10^5	6.28×10^2
$10^9/cm^2$	1.58×10^2	$10.26\ 6\times 10^6$	9.92×10^2
$10^8/cm^2$	0.5×10^3	10.28×10^7	6.28×10^3

Table 2: The relation between a periodically bent channel and the dislocation affected region for channeling in a periodically bent region at a dislocation density $10^8/cm^2$.

a (nm)	λ_u (nm)	R_u (nm)	E (MeV)	x_d (nm)
1	3.14×10^3	2.5×10^5	142.363	2.198×10^4
10	3.14×10^3	$2.5\ 6\times 10^4$	14.236	2.198×10^3
100	3.14×10^3	2.5×10^3	1.412	2.198×10^2

Also figures 5.3 and 5.4 show the variation of the amplitude of bending of the channel and the radius of curvature of the dislocation affected region respectively. We consider the low dislocation density case of $10^8/cm^2$. The radius R_d of the dislocation affected region is taken as $10.28 \times 10^7\ nm$ and λ_d as $6.28 \times 10^3\ nm$. From Figure 5.3, it is found that the amplitude is no longer constant but varies periodically with respect to the depth. Figure 5.4 shows that larger the values of amplitude of bending 'a', larger is the variation of $\tilde{\rho}_0$ with z.

We consider the phase difference, $\Phi = 0$ and n=2 for the sake of simplicity of calculation. The potential equation can be written as

$$U(\rho) = V_0(\rho - \tilde{\rho_0})^2 \tag{5.18}$$

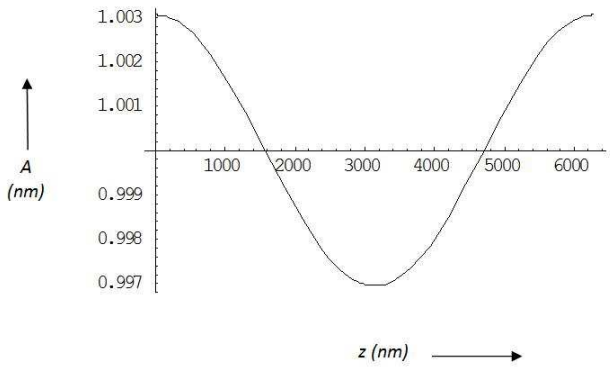

Figure 5.3: The change in amplitude of bending with respect to the depth of the crystal. The amplitude is no longer constant but varies periodically with the length of the dislocation affected region.

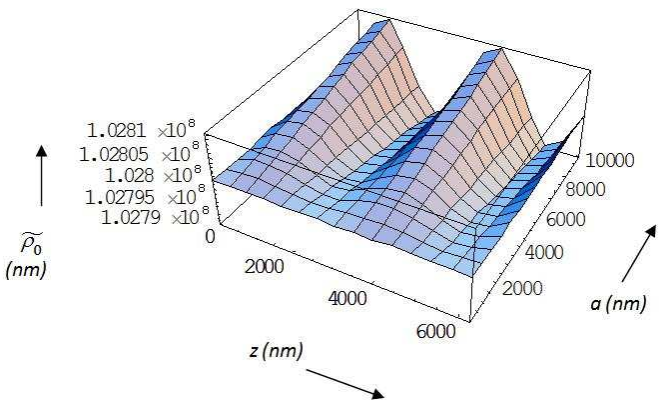

Figure 5.4: The change in radius of curvature of the dislocation affected channel with respect to amplitude of bending and depth. Here we find that larger the value of 'a', larger is the variation of $\tilde{\rho}_0$ with z.

Separating variables gives azimuthal and radial equations from the Schrodinger equation (5.16) as given by,

$$F''^{II}(\varphi) = -\mu^2 F^{II}(\varphi) \tag{5.19}$$

$$R''^{II}(\rho) + \frac{2m}{\hbar^2}\left[E^{II} - V_0(\rho - \tilde{\rho_0})^2 - \frac{\hbar^2}{2m}\frac{\mu^2}{\rho^2}\right]R^{II}(\rho) = 0 \tag{5.20}$$

The effective potential after including the centrifugal force term can be written as

$$V_{eff} = V_0(\rho - \tilde{\rho_0})^2 + \frac{\hbar^2}{2m}\frac{\mu^2}{\rho^2}$$

Let

$$\xi = \rho - \tilde{\rho_0} \tag{5.21}$$

Simplifying and solving, we get the effective potential as,

$$V_{eff}(\xi) = \frac{\hbar^2}{2m}\left[\frac{\lambda}{\tilde{\rho_0}^4}(\xi - \tilde{a_p})^2 + U_{min}\right] \tag{5.22}$$

where

$$\lambda = 3\mu^2 + b^4\tilde{\rho_0}^4 \tag{5.23}$$

$$\tilde{a_p} = \frac{\tilde{\rho_0}\mu^2}{\lambda} \tag{5.24}$$

$$U_{min} = \frac{\mu^2}{\lambda\tilde{\rho_0}^2}(\lambda - \mu^2) \tag{5.25}$$

$$b = \left(\frac{m\omega}{\hbar}\right)^{1/2} \tag{5.26}$$

Above equations show that the shape of the potential changes due to the effects of dislocations. The minima of the potential gets shifted due to these effects of dislocations in the channel and it is dependent on the undulator parameters as well.

The frequency of oscillation in the region II is obtained as

$$\omega' = \left(\frac{\hbar}{m}\right)\sqrt{\frac{\lambda}{\tilde{\rho_0}^4}} \tag{5.27}$$

The total radial equation can be written as

$$R''^{II}(\eta)+\left[\frac{2m}{\hbar^2}E^{II}-\frac{\lambda}{\tilde{\rho_0}^4}\eta^2-U_{min}\right]R^{II}(\eta)=0 \tag{5.28}$$

with solution,

$$R^{II}(\eta)=\frac{\exp(-b\eta^2/2)}{\sqrt{2^n n!(1/b)\sqrt{\pi}}}\ H_n(b\eta) \tag{5.29}$$

$$\eta=\xi-\tilde{a_p} \tag{5.30}$$

Consider region III, i.e., the second curved part of the dislocation affected channel. The centrifugal force is acting in the opposite direction of that in the first curved region. Solving this part of the distorted region as in the region II, we get the effective potential as

$$V_{eff}(\xi)=\frac{\hbar^2}{2m}\left[\frac{\lambda'}{\tilde{\rho_0}^4}(\xi+\tilde{a'_p})^2+U'_{min}\right] \tag{5.31}$$

where

$$\lambda'=-3\mu^2+b^4\tilde{\rho_0}^4 \tag{5.32}$$

$$\tilde{a'_p}=\frac{\tilde{\rho_0}\mu^2}{\lambda'} \tag{5.33}$$

$$U'_{min}=-\frac{\mu^2}{\lambda'\tilde{\rho_0}^2}(\lambda'+\mu^2) \tag{5.34}$$

The minima of the potential gets shifted in the opposite direction as in the region II and is dependent on the undulator parameters. The frequency of oscillation in the region III is obtained as,

$$\omega''=\left(\frac{\hbar}{m}\right)\sqrt{\frac{\lambda'}{\tilde{\rho_0}^4}} \tag{5.35}$$

The total radial equation can be written as,

$$R''^{III}(\eta')+\left[\frac{2m}{\hbar^2}E^{III}-\frac{\lambda'}{\tilde{\rho_0}^4}\eta'^2-U'_{min}\right]R^{III}(\eta')=0 \tag{5.36}$$

with solution,

$$R^{III}(\eta') = \frac{\exp(-b''\eta'^2/2)}{\sqrt{2^n n!(1/b'')\sqrt{\pi}}}\ H_n(b''\eta') \tag{5.37}$$

where

$$\eta' = \xi + \tilde{a_p'} \tag{5.38}$$

$$b'' = \left(\frac{m\omega''}{\hbar}\right)^{1/2} \tag{5.39}$$

Region IV is dislocation free and like any other channel which is periodically bent. It has only transmitted wave and the wavefunction is similar to that in region I.

We have 4 regions and the wavefunction corresponding to these regions are written as [85],

$$\Psi^I(x,z) = A_0 X_0^I e^{ik_0 z} + \sum_{n=0}\ B_n X_n^I e^{-ik_n z} \tag{5.40}$$

$$\Psi^{II}(\rho,\varphi) = \sum_{m=0} R_m^{II}\left[C_m e^{i\mu\varphi} + D_m e^{-i\mu\varphi}\right] \tag{5.41}$$

$$\Psi^{III}(\rho,\varphi) = \sum_{m=0} R_m^{III}\left[G_m e^{i\mu\varphi} + H_m e^{-i\mu\varphi}\right] \tag{5.42}$$

$$\Psi^{IV}(x,z) = X_n^{IV} I_n e^{ik_n z} \tag{5.43}$$

To find the reflection and transmission coefficients, we use the boundary conditions across the 3 boundaries and are obtained as

$$|R|^2 = \frac{(-\mu^2 + k^2{\tilde{\rho_0}}^2)^2\ \sin^2(2\mu\varphi_0)}{4k^2\mu^2{\tilde{\rho_0}}^2\cos^2(2\mu\varphi_0) + (\mu^2 + k^2{\tilde{\rho_0}}^2)^2\ \sin^2(2\mu\varphi_0)} \tag{5.44}$$

$$|T|^2 = \frac{4k^2\mu^2{\tilde{\rho_0}}^2}{4k^2\mu^2{\tilde{\rho_0}}^2\cos^2(2\mu\varphi_0) + (\mu^2 + k^2{\tilde{\rho_0}}^2)^2\ \sin^2(2\mu\varphi_0)} \tag{5.45}$$

The above equations (5.44) and (5.45) are the dechanneling and channeling coefficients

respectively. Comparing with the usual dislocation affected channel we find that dislocations in a periodically bent crystal changes the channeling and dechanneling coefficients by the parameters of the crystalline undulator.

For a dislocation density $10^8/cm^2$, the value of $\rho_0 = 10.28 \times 10^7\ cm$. The variation of the dechanneling and channeling probabilities corresponding to this fixed value of radius of curvature is same as that of any normal channel affected with dislocations. Figures 5.5 and 5.6 show the variation of these probability values with incident energy. It is found that transmission of particles is maximum for incident energies close to 140 MeV.

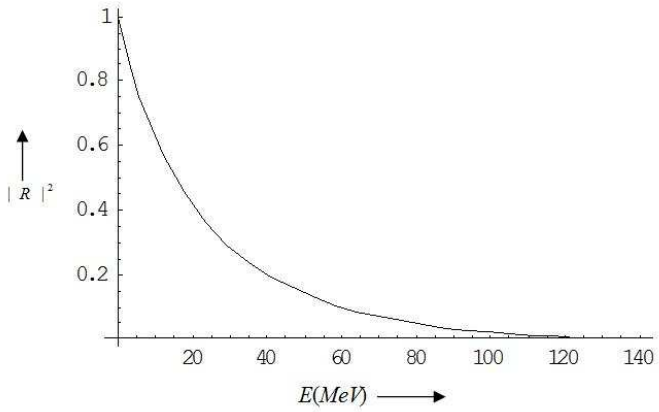

Figure 5.5: The change in the dechanneling probability with incident energy.

We fix the incident energy at 150 MeV so that most of the particles are in the channeling regime. The variation of the modulated radius of curvature $\tilde{\rho_0}$ with the amplitude of bending and depth changes channeling probability as seen in Figure 5.7. This variation directly follows the variation of the amplitude of bending with the depth.

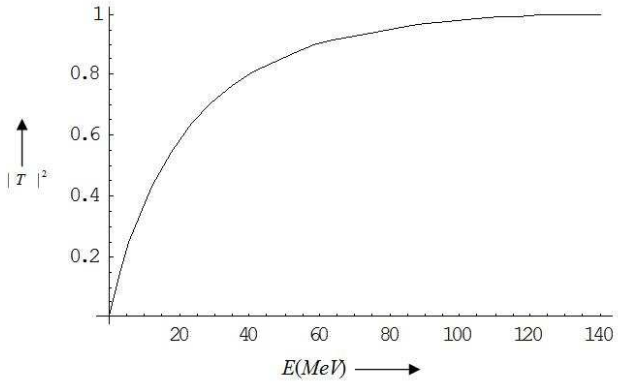

Figure 5.6: The change in the channeling probability with incident energy.

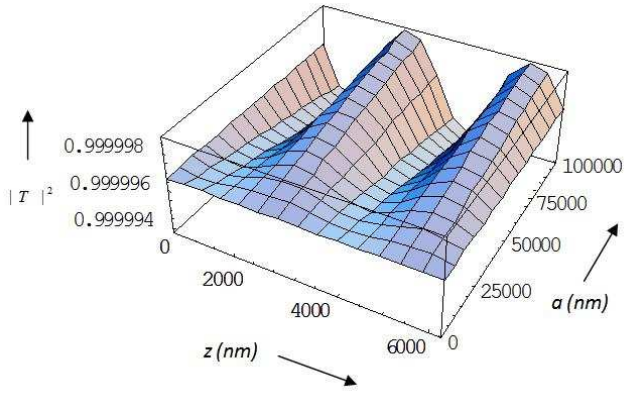

Figure 5.7: The change in channeling probability with z and the amplitude of bending a.

Now we proceed to find the spectral distribution of radiation intensity. The probability of transition from an initial state i to the final state f per unit time is determined by the well-known formula,

$$W_{fi} = \frac{4\pi^2 e^2}{\hbar V} \sum_{\vec{q}} |\vec{q}|^{-1} |\vec{\alpha}_{fi}.\vec{e}_k|^2 \ \delta(\omega_{fi} - \omega) \tag{5.46}$$

Where V is the volume of the system, $\vec{q}$ and $\vec{e}_k$ are the wave vector and polarization vector of a quantum of electromagnetic field.

$$\hbar\omega_{fi} = E_{ni} - E_{nf} \tag{5.47}$$

The matrix elements $\vec{\alpha}_{fi}$ are given by

$$\vec{\alpha}_{fi} = \delta_{\sigma_{iz}\sigma_{fz}} \delta_{p_{iy}, p_{fy}+\hbar q_y} \vec{D}_{fi} \tag{5.48}$$

$$\vec{D}_{fi} = -ix_{fi}(\Omega_{fi}, 0, q_x\beta) \tag{5.49}$$

$$\Omega_{fi} = \frac{\omega}{1 - \beta cos\theta} \tag{5.50}$$

$$x_{fi} = \int_{\infty}^{-\infty} x S_{n_f E_f}(x) S_{n_i E_i}(x) \ dx \tag{5.51}$$

where S_{nE} are oscillatory wavefunctions which obey the Schrodinger equation given by

$$\left[-\frac{\hbar^2}{2E}\frac{d^2}{dx^2} + U(x) \right] S_E(x) = E S_E(x) \tag{5.52}$$

Let us define a vector of polarization $\vec{e}_1$ in the plane having the wave vector $\vec{q}$ and the z-axis and a vector $\vec{e}_2 \perp \vec{e}_1$ in the plane having the axes x and y. If φ and θ are the azimuthal and polar angles of the wave vector $\vec{q}$,

$$\vec{e}_1 = (\cos\theta\cos\varphi, \cos\theta\sin\varphi, -\sin\theta) \tag{5.53}$$

$$\vec{e}_2 = (-\sin\varphi, \cos\varphi, 0) \tag{5.54}$$

The summation in Eqn. (5.46) is written in the integral form as

$$W_{fi} = \frac{e^2}{2\pi\hbar} \int \left(|\vec{\alpha}_{fi}.\vec{e}_1|^2 + |\vec{\alpha}_{fi}.\vec{e}_2|^2 \right) |\vec{q}|^{-1}| \ \delta(\omega_{fi} - \omega) \ d\vec{q} \tag{5.55}$$

Solving this we get the transition probabilities as

$$\frac{dW_{fi}}{d\Omega} = \frac{e^2 x_{fi}^2 \Omega_{fi}^3}{2\pi\hbar(1-\beta\cos\theta)^4}[(1-\beta\cos\theta)^2 - (1-\beta^2)\sin^2\theta\cos^2\varphi] \tag{5.56}$$

$$\frac{dW_{fi}}{d\omega} = x_{fi}^2\Omega_{fi}^2\frac{e^2}{\hbar}\left[1 - 2\frac{\omega}{\omega_m} + \left(\frac{\omega}{\omega_m}\right)^2\right] \tag{5.57}$$

$$\frac{dI_{fi}}{d\Omega} = \frac{e^2 x_{fi}^2 \Omega_{fi}^4}{2\pi(1-\beta\cos\theta)^5}[(1-\beta\cos\theta)^2 - (1-\beta^2)\sin^2\theta\cos^2\varphi] \tag{5.58}$$

$$\frac{dI_{fi}}{d\omega} = 3I_{fi}^{(0)}\left[1 - 2\frac{\omega}{\omega_m} + 2\left(\frac{\omega}{\omega_m}\right)^2\right] \tag{5.59}$$

where

$$\omega_m \approx 2\gamma^2\Omega_{fi} \tag{5.60}$$

$$I_{fi}^{(0)} = \frac{4}{3}e^2\Omega_{fi}^4\gamma^4 x_{fi}^2 \tag{5.61}$$

Unlike in the other dislocation problems, the value of Ω_{fi} changes periodically since the shifted equilibrium axis is periodically bent. Also the frequencies of oscillation in both the dislocation affected regions are not constant. Figure 5.8 shows the combined change in the spectral distribution of radiation intensity due to the periodicity of the channel and dislocation in comparison with the straight channel where $s = 4e^2\Omega_{fi}^4\gamma^4 x_{fi}^2$. We find a considerable amount of change in the spectral distribution due to dislocations. This is due to the fact that when the amplitude of bending of a periodically bent channel is high, undulator radiation intensity starts increasing.

5.2.2 High dislocation density ($\lambda_d < \lambda_u$)

Now consider a case where the dislocation affected region is a (small) part of one undulator wavelength. Such a situation arises when the dislocation density is high. In this case, the periodicity of the crystalline undulator is affected in just few regions of the undulator wavelength. Just like in the case of the straight channel, where a part of the channel is shifted due to the dislocation, here a region of the periodically bent channel is shifted.

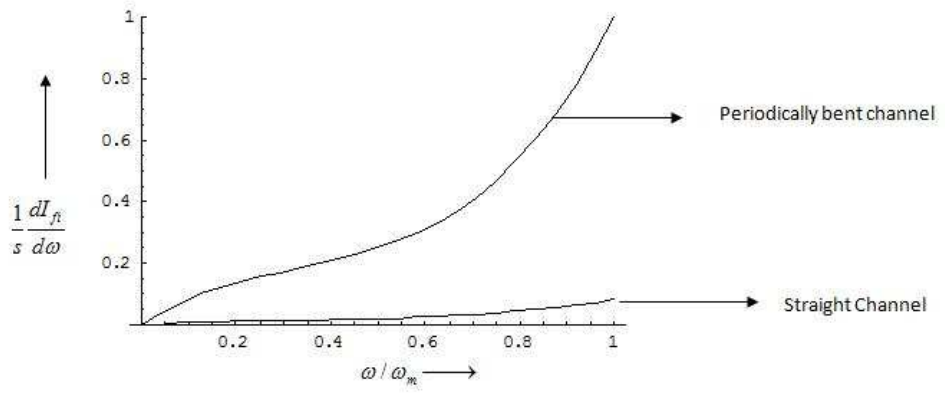

Figure 5.8: The change in the spectral distribution of radiation intensity due to the periodicity of the channel. $s = 4e^2\Omega_{fi}^4\gamma^4 x_{fi}^2$.

Eqn. (5.2) can be written as,

$$\tilde{x} = x - a\ \sin(k_u v t) \tag{5.62}$$

which gives

$$\ddot{\tilde{x}} = \ddot{x} + a k_u^2 v^2\ \sin(k_u v t) \tag{5.63}$$

keeping

$$\frac{1}{R} = a k_u^2\ \sin(k_u v t) \tag{5.64}$$

we get,

$$\ddot{\tilde{x}} = \ddot{x} + \frac{v^2}{R} \tag{5.65}$$

Rewriting Eqn. (5.63), we get

$$\gamma m \ddot{\tilde{x}} = \dot{p} + \gamma m \frac{v^2}{R} \tag{5.66}$$

where,

$$\dot{p} = -\frac{\partial H}{\partial \tilde{x}} \tag{5.67}$$

where H is given by,

$$H = \sqrt{c^2p^2 + m^2c^4} + qe\ U(\tilde{x}) \tag{5.68}$$

solving the above equation, we get,

$$\frac{\partial H}{\partial \tilde{x}} = qe\frac{\partial U(\tilde{x})}{\partial \tilde{x}} \tag{5.69}$$

Hence Eqn. (5.66) can be written as,

$$\ddot{\tilde{x}} + \frac{qe}{m\gamma}U(\tilde{x}) - \frac{v^2}{R}\tilde{x} = 0 \tag{5.70}$$

Integrating from $\tilde{x}$ to $\tilde{x}_m$, and solving we get the maximum amplitude of oscillation of the particle as,

$$\tilde{x}_m = \frac{m\gamma v^2}{qeV_0R} \tag{5.71}$$

and the new equilibrium axis is shifted to

$$\tilde{x}_0 = \frac{m\gamma v^2}{2qeV_0R} \tag{5.72}$$

In this case, since $\lambda_d < \lambda_u$, the dislocation affected region is just a part of the undulator wavelength. Hence we can consider the region affected as almost like a straight channel. The slight periodicity of the region is reflected in the *sin* terms of x_m and x_0. The period of oscillation of the particle in the channel can be found in the same way as in a straight channel [58, 59].

Solving Eqn. (5.70), we get

$$dt = \frac{d\tilde{x}}{\left[\frac{2v^2}{R}\tilde{x} - \frac{2qe}{m\gamma}U(\tilde{x})\right]^{1/2}} \tag{5.73}$$

Solving the above equation, we get the period of oscillation as,

$$T = \left(\frac{m\gamma}{2qeV_0}\right)^{1/2} \sin^{-1}\left\{1 - \frac{2qeV_0R}{m\gamma v^2}\cos(k_u z)\right\} \tag{5.74}$$

Table 3 shows the values of the various parameters of the channel affected with dislocation. In this case, the dislocation density is high in comparison with the previous case for a similar range of E and its value is found to be close to $1.5\times10^9/cm^2$.

Table 3: The various parameters of the undulator and dislocation affected regions at high dislocation density; when λ_u=2λ_d.

Dislocation density	λ_d (nm)	λ_u (nm)	a (nm)	R_u (nm)	E (MeV)
$1.5\times10^9/cm^2$	1.66× 10^3	3.32× 10^3	1	2.8× 10^5	150
			10	2.8× 10^4	15
			100	2.8× 10^3	1.5

5.3 Results and Discussions

We have developed a quantum mechanical model for the effects of dislocations on positron channeling along a periodically bent channel. It is clear from the calculations that the curvature of the channel due to dislocations shifts the potential minima even for a periodically bent channel. This results in the change of the frequency of oscillations in different regions of dislocation affected channel. In the case of periodic bending the shift in potential minima and the frequency of oscillations depends on the undulator parameters which are varying with the amplitude of bending and wavelength of the undulator. This means the shift is not a constant throughout the undulator but varies periodically with the length.

We first considered a case of low dislocation density with $\lambda_d = 2\lambda_u$. The frequency of channeling radiation as well as the undulator radiation are affected by the dislocations as expected. Figures 5.3 and 5.4 show the change in the amplitude of bending of the periodically bent channels and radius of curvature of the dislocation affected

region. We choose a dislocation density in the lower regime of $10^8/cm^2$. The corresponding radius of curvature of the dislocation affected region is $10.28\times10^7\ nm$. The incident energy is taken to be around 142 MeV to get most of the particles channeled. The amplitude of bending is modulated by the curvatures of the dislocation affected regions of the channel. It is found that this amplitude of bending is no longer a constant, but varies periodically with the amplitude and wavelength of the dislocation affected region. Also, the radius of curvature of the dislocation affected region changes with the amplitude of bending and wavelength of the undulator. Larger the value of amplitude of bending, larger is the variation of the radius of curvature with the length of the undulator.

The reflection and transmission coefficients calculated from the boundary conditions correspond to the values of dechanneling and channeling coefficients respectively. These are dependent on the undulator parameters via their dependence on the modulated radius of curvature of the dislocation affected region as seen in equations (5.44) and (5.45). Figures 5.5, 5.6 and 5.7 show the the variation of these probability values with incident energy and with the depth and amplitude of bending of the channel. It is noted from Figure 5.7 that, the variation of the channeling probability follows the variation in the curved regions modulated one over the other.

The spectral distribution of radiation intensity is calculated and plotted in Figure 5.8. We find a considerable amount of change in the spectral distribution of radiation intensity. It is to be noted that the change in radiation parameters are mainly due to the periodic bending of the channel. i.e., crystalline undulator plays a major role in the case of low dislocation density.

For the sake of completeness and comparison, we consider the complimentary case of $\lambda_d < \lambda_u$ corresponding to high dislocation density. All possible range of values

for both the undulator and dislocation wavelengths are discussed in detail and corresponding channeling parameters are calculated. The period of oscillation of the particle in the dislocation affected region for high values of dislocation density is found. It is observed from the calculations that in this case of high dislocation density, the change in various parameters of channeling in dislocation affected region is least affected by undulator parameters.

Since no crystal is perfect and study of crystalline undulators is incomplete without the consideration of defects like dislocations, the present study is crucial for investigations related with crystalline undulators.

CHAPTER 6

Summary and Concluding Remarks

Channeling and channeling radiation have been studied and reviewed by various authors classically and in quantum mechanical frameworks. Study of defects has been one of the main applications of this channeling phenomena from the very beginning. The effects of defects on the charged particle motion in solids in general and on channeling in particular have been studied extensively during last 4 decades. In most of the analytical calculations, continuum model for axial and planar channeling has been used as starting point. The influence of external fields on the channeling process is of recent interest mainly due to its relevance and usefulness in the phenomena of emission of electromagnetic radiation such as undulator radiation.

The basic motivation of the work presented in this thesis has been to study the interactions of both internal and external perturbations on the channeling process. The internal perturbations are defects like dislocations and the external ones are mechanical periodic perturbations like hypersonic/acoustic waves (both longitudinal

and transverse). We have investigated the quantum aspects of all these processes.

The motion of a positively charged particle is usually represented by a harmonic oscillator potential. In our formulations we have included the anharmonicity effects and found considerable variation in the channeling and channeling radiation parameters due to it. In all previous analytical investigations on the effects of dislocations on channeling, the distortion induced curvature is assumed to give rise to an additional centrifugal force term. Thus the equations for transverse motion were solved with this centrifugal term without incorporating longitudinal motion. We have successfully developed an improved model to include the longitudinal motion by using the polar co-ordinate system. The continuity of the particle wavefunction in the longitudinal motion are the main highlights of this formulation. These same ideas are extended to investigate the effects of dislocations on undulator radiation problem.

Summing up the results, the presentation is divided into three parts:

(i) Effects of hypersonic field on channeling radiation

The effects of both longitudinal and transverse hypersonic waves on channeling radiation are considered. Also the influence of anharmonicity of the planar transverse continuum potential on the wavefunction of the positron and the fractional change in frequency due to these anharmonic effects are calculated. The spectral distribution of radiation intensity which is affected by the external hypersonic field and additionally by anharmonicity, proves the earlier predictions that radiation intensity can be increased by the interaction of external fields [86]. The transverse perturbation effects (with acoustic waves of lower amplitudes) are to be given special mention, which is a first step in the study of undulator radiation, where waves of higher amplitudes are being used [87].

(ii) Effects of dislocations on channeling radiation

Effects of dislocations on channeling are studied for both positron and electron channeling. A quantum mechanical model, where the affected region is divided into four parts separated by 3 boundaries, has been developed. Continuity of wave functions and their derivatives across these boundaries gave channeling and dechanneling co-efficients [85]. A comparison of the dechanneling probabilities due to electron and positron channeling in a dislocation effected region is done in detail in this study [88]. The effects of anharmonic term in the positron planar potential on the distortion co-efficient and number of bound states and other channeling parameters like frequency of radiation, are studied and compared with those obtained in the harmonic case. The change in the channeling probabilities for particle in the ground state (an initially well-channeled particle) and that in the first excited state due to anharmonicity are calculated. We found an increase in the radius of dechanneling cylinder due to anharmonicity [89].

(iii) Effects of dislocations on channeling in a periodically bent crystal

The effects of dislocations on channeling phenomena in a periodically bent crystal (crystalline undulator) are studied for the first time. The distortion effects of both the dislocation affected regions and the periodically bent channels are represented in terms of waves with comparable amplitudes and wavelengths. Therefore, the distortion effects due to dislocations can be modulated on the periodic distortions (resulting for example due to undulators). In this analysis, we consider both the situations namely; $\lambda_d > \lambda_u$ (low dislocation density) and $\lambda_d < \lambda_u$ (high dislocation density), where λ_d and λ_u represent the wavelength of both dislocation affected region and periodically bent channel respectively. It is found that for low dislocation density,

the crystalline undulator parameters play a major role where as in the case of high dislocation density, undulator parameters have minimal effects on the radiation [90].

In summary, since no crystal is perfect (just as no human being is perfect!) any study of channeling/channeling radiation and crystalline undulators is incomplete without the consideration of defects and other field interactions. The present work is a broad study of these effects of distortions and field interactions on channeling of both positive and negative particles through crystals.

Future outlook

In our study on the effects of internal and external perturbations, we have used various aspects of quantum formulations of the positive and negative charged particle propagation in a crystal. The theoretical methods we have developed can be used in the study of various other applications of channeling and channeling radiation. The formulations on the study of the effects of longitudinal hypersonic field on channeling radiation were helpful in the analysis of the effects of transverse perturbations (lower amplitude) as in section 2.3 of chapter 2. The same theory can be extended to study the crystalline undulator which was previously based on classical assumptions.

The method developed in chapter 3 to study the effects of the curvature due to dislocations were extended to study its effects on a periodically bent channel (chapter 5). This methodology can form the basis to study the channeling and dechanneling phenomena due to any kinds of distortions in the crystal. Focussing of beams by the bent channels is well known application of this formulation where one uses bent crystal channeling concepts. Another possible application of these investigations and results presented, can be in study of volume reflection, where the particles are deflected from a curved channel. This is a phenomena complimentary to bent crystal channeling and has applications in shielding from radiation, both in the contexts of high energy accelerators as well as outer space radiation.

In our final chapter we have tried to find the channeling conditions in a periodically bent channel affected by dislocations. All the earlier investigations on undulators are classical predictions and never considered any effects of defects in the channel. Our formulations can give a better model for realization of the crystalline undulators.

References

1. J. Lindhard, *Phys. Lett.* **12**, 124 (1964).

2. C. Erginsoy, *Phys. Rev. Lett.* **15**, 360 (1965).

3. J. Lindhard, *K. Dan. Vidensk. Selsk. Mat. Fys. Medd.* **34**, No.14 (1965).

4. J. Lindhard, V. Nielsen and M. Scharff, *K. Dan. Vidensk. Selsk. Mat. Fys. Medd.* **36**, 10 (1968).

5. I. M. Torrence, *Interatomic Potentials*, (Acad. Press, New York, 1972).

6. M. Born and J. E. Mayer,*Z. Phys.* **75**, 1 (1932).

7. N. Bohr, *K. Dan. Vidensk. Selsk. Mat. Fys. Medd.* **18**, No.8 (1948).

8. J. Mory and Y. Quere, *Rad. Eff.* **13**, 57 (1972).

9. J. Rosner, W. M. Gibson, J. A. Golovchenko, A. N. Goland and H. E. Wegner, *Phys. Rev. B* **18**, 1066 (1978).

10. A. P. Pathak, *J. Phys. C.* **8**, L 439 (1975).

11. A. P. Pathak, *Rad. Eff.***61**, 1 (1982).

12. J. U. Andersen, E. Bonderup and E. Laegsgaard, *Topics in Current Physics* **38**, 127 (1985).

13. M. J. Alguard, R. L. Swent, R. H. Pantell, B. L. Berman, S. D. Bloom and S. Datz, *Phys. Rev. Lett.* **42**, 1148 (1979).

14. D. S. Gemmell, *Rev. Mod Phys.* **46**, 129 (1974).

15. R.H. Pantell, M.J. Alguard, *J. Appl. Phys.* **50**, 798 (1979).

16. M. A. Kumakhov and R. Wedell *Phys. Stat. Sol. (b)* **84**, 581 (1977).

17. R. Wedell, *Phys. Stat. Sol. (b)* **99**, 12 (1980).

18. Haakon A. Olesen and Yuri Kunashenko, *Phys. Rev.* **A 56**, 527 (1997).

19. R. L. Swent, R. H. Pantell, M. J. Algaurd, B. L. Berman, S. D. Bloom and S. Datz, *Phys. Rev. Lett.* **43**, 1723 (1979).

20. M. Gouanare, D. Silloun, M. Spiighel, N. Chu, M. J. Gaillard, R. G. Kirsch, J. C. Poizat, J. Remillicux, B. L. Berman, P. Catillon, L. Roussel, G. M. Temmer *Phys. Rev.* **B 38**, 4352 (1988).

21. J. U. Andersen, O. Andreasen, J. A. Davies and E. Uggerhoj, *Rad. Eff.* **7**, 25 (1971).

22. J. U. Andersen, E. Laegsgaard and L. C. Feldman, *Rad. Eff.* **12**, 219 (1972).

23. S. T. Picraux, L. R. Dawson and G. C. Osbourn, *Appl. Phys. Lett.* **43**, 930 (1983).

24. S. T. Picraux, L. R. Dawson, G. C. Osbourn, R. M. Biefeld and W. K. Chu *Appl. Phys. Lett.* **43**, 1020 (1983).

25. John H. Barrett, *Nucl. Instr. Methods* **149**, 342 (1978).

26. L. C. Feldman, *Phyisca Scripta* **28**, 303 (1983).

27. A. Carrigan and J. Ellison, *Relativistic Channeling* (Plenm, New York, 1987).

28. S. P. Moller, E. Uggerhoj, H. W. Atherton, M. Clement, N. Doble, K. Elsener, L. Gatignon, P. Grafstrom, M. Hage-Ali and P.Siffert, *Phys. Lett. B* **256**, 91 (1991).

29. A. Schafer and W. Greiner, *J. Phys. G* **17**, L217 (1991).

30. H. Ikezi, Y. R. Lin-Liu and T. Ohkawa, *Phys. Rev. B* **30**, 1567 (1984).

31. V. G. Barishevsky, I. Ya. Dubovskaya and A. O. Grubich, *Phys. Lett. A*, **77**, 81 (1980).

32. A. R. Mkrtchyan, R. A. Gasparyan and R. G. Gabrielyan, *Phys. Lett.* **A 115**, 410 (1986).

33. A. R. Mkrtchyan, R. H. Gasparyan, R. G. Gabrielyan and A. G. Mkrtchyan, *Phys. Lett.* **A 126**, 528 (1988).

34. L. SH. Grigorian,A. R. Mkrtchyan, B. V. Khachatryan, H. F. Khachatryan, H. Prade and W. Wagner *Radiat. Eff. Defects Solids* **152**, 269 (2000).

35. L. SH. Grigorian,A. R. Mkrtchyan, B. V. Khachatryan, H. F. Khachatryan, H. Prade and W. Wagner *Radiat. Eff. Defects Solids* **152**, 225 (2000).

36. L. Sh. Grigoryan, A. R. Mkrtchyan, H. F. Khachatryan, A. H. Mkrtchyan, H. Prade and W. Wagner, *Rad. Eff. and Defects in Solids* **153**, 13 (1999).

37. L. Sh. Grigoryan, A. R. Mkrtchyan, A. H. Mkrtchyan, H. F. Khachatryan, W. Wagner and M. A. Piestrup, *Rad. Eff. and Defects in Solids* **153**, 221 (2000).

38. L. Sh. Grigoryan, A. R. Mkrtchyan, A. H. Mkrtchyan, H. F. Khachatryan, W. Wagner and M. A. Piestrup, *Rad. Eff. and Defects in Solids* **153**, 289 (2000).

39. L. Sh. Grigoryan, A. R. Mkrtchyan, A. H. Mkrtchyan, H. F. Khachatryan, W. Wagner and M. A. Piestrup, *Rad. Eff. and Defects in Solids* **153**, 307 (2000).

40. A. V. Solov'yov, A. Schafer and W Greiner, *Phys. Rev. E* **53**, 1129 (1996).

41. A. V. Korol, A. V. Solov'yov and W Greiner, *J. Phys. G: Nucl. Part. Phys.* **24**, L45 (1998).

42. A. V. Korol, A. V. Solov'yov and W Greiner, *Int. J. Mod. Phys.* **E8**, 49 (1999).

43. A. V. Korol, A. V. Solov'yov and W Greiner, *Int. J. Mod. Phys.* **E9**, 77 (2000).

44. W. Krause, A. V. Korol, A. V. Solov'yov and W Greiner, *J. Phys. G: Nucl. Part. Phys.* **26**, L87 (2000).

45. A. V. Korol, A. V. Solov'yov and W Greiner, *J. Phys. G: Nucl. Part. Phys.* **27**, 95 (2001).

46. A. V. Korol, A. V. Solov'yov and W Greiner, *Int. J. Mod. Phys.* **E13**, 867 (2004).

47. L. N. S. Prakash Goteti and A. P. Pathak *J. Phys.: Condens. Matter* **9**, 1709 (1997).

48. B. Rath and A. P. Pathak *Radiat. Eff.* **63**, 227 (1982).

49. B. Rath *Rad. Eff.* **106**, 279 (1988)

50. V. V. Beloshitsky and F. F. Komarov *Phys. Rep.* **93**, 117 (1978).

51. Y. Quere, *J. Nucl. Mat.* **53**, 262 (1974).

52. D. Polonsky, G. Desarmot, N. Housseau and Y. Quere, *Rad. Eff.* **27**, 81 (1975).

53. G. Desarmot, *Phys. Lett.* **46 A**, 159 (1973).

54. W. F. Tseng, J. Gyulai, T. Koji, S. S. Lau, J. Roth and J. W. Mayer, *Nucl. Instr. Methods* **149**, 615 (1978).

55. E. Bonderup, H. Esbensen, J. U. Andersen and H. E. Schiott, *Rad. Eff.* **12**, 261 (1972).

56. J. Friedel, *Dislocations* (Pergamon, N. Y., 1964).

57. Y. Quere, *Phys. Stat. Sol.* **30**, 713 (1968).

58. A.P. Pathak, *Phys. Rev. B* **13**, 4688 (1976).

59. A.P. Pathak, *Phys. Rev. B* **15**, 3309 (1977).

60. L.N.S. Prakash Goteti, A.P. Pathak, *Phys. Rev. B* **58**, 5243 (1998).

61. L.N.S. Prakash Goteti, A.P. Pathak, *Phys. Rev. B* **59**, 8516 (1999).

62. S. Sathpathy and A. P. Pathak, *Phys. Stat. Sol. (b)* **153**, 455 (1989).

63. H. J. Kreiner, F. Bell, R. Sizmann, D. Harder and W. Huttl, *Phys. Lett.* **33A**, 135 (1970).

64. K. Komaki, and F. Fujimoto, *Phys. Lett. A* **49**, 445 (1974).

65. A. Tamura and Y. H. Ohtsuki, *Phys. Stat. Sol. (b)* **62**, 477 (1974).

66. A. Tamtura and T. Kawamura, *Phys. Stat. Sol. (b)* **73**, 391 (1976).

67. A P Pathak, *Phys. Rev. B* **31** 1633 (1985).

68. A. P.Pathak, L. N. S. Prakash Goteti and S. V. S. Nageswara Rao, *Nucl. Instr. and Meth. B* **193**, 188 (2002).

69. C. Kittel, Introduction to Solid State Physics (7^{th} edition), *Wiley* (1996).

70. Leonard I. Schiff, Quantum Mechanics, *McGraw Hill* (1968).

71. M. K. Abu-Assy, M. Y. El-Ashry and A. A. Mohamed, *Physica Scripta* **72**, 68 (2005).

72. H. Park, R.H. Pantell, R.L. Swent, J.O. Kephart, B.L. Berman, S. Datz, R.W. Fearick, *J. Appl. Phys.* **55**, 358 (1984).

73. G. V. Dedkov *Phys. Stat. Sol. (b)* **184**, 535 (1994).

74. U. Mikkelsen and E. Uggerhhoj, *Nucl. Instr. and Meth. B* **160**, 435 (2000)

75. W. Krause, A.V. Korol, A.V. Solov'yov, W. Greiner, *Nucl. Instr. and Meth. A* **483**,455 (2002)

76. R. O. Avakian, K. Avetian, K. A. Ispirian and E. G. Melikian *Nucl. Instr. and Meth. A* **508**, 496 (2003)

77. R. O. Avakian, K. Avetian, K. A. Ispirian and E. G. Melikian *Nucl. Instr. and Meth. A* **492**, 11 (2002)

78. S. Bellucci *et. al Phys. Rev. Lett.* **90**, 34801 (2003)

79. V. Guidi, A. Antonini, S. Baricordi, F. Logallo, C. Malagu, E. Milan, A. Razoni, M. Stefancich, G. Martinelli and A. Vomiero, *Nucl. Instr. and Meth. B* **234** (2005)40

80. V. Guidi, L. Lanzoni, A. Mazzolari, G. Martinelli and A. Tralli, *Appl. Phys. Lett.* **9**0, 114107 (2007).

81. L. Lanzoni, A. Mazzolari, V. Guidi, A. Tralli and G. Martinelli, *Int. J. Engin. Scie.* **4**6, 917-928 (2008).

82. A. Kostyuk, A.V. Korol, A.V. Solov'yov and W. Greiner, *Nucl. Instr. and Meth. A* **266**, 972-987 (2008).

83. M. Tabrizi, A.V. Korol, A.V. Solov'yov, W. Greiner, *Phys. Rev. Lett.* **98**, 164801 (2007).

84. M. Tabrizi, A.V. Korol, A.V. Solov'yov, W. Greiner, *J. Phys. G* **34**, 1581 (2007).

85. Juby George, A.P. Pathak, S. Cruz and D. Emfietzoglou *Nucl. Instr. and Meth. B* **256**, 148 (2007).

86. Juby George, Anand P. Pathak , L N S Prakash Goteti and G Nagamani, *J. Phys.:Cond. Matter* **19**, 116210 (2007).

87. Juby George and Anand P. Pathak, *Proceedings of SPIE* **6634**, 66340Q (2007).

88. Juby George and Anand P. Pathak, *J. Phys.:Cond. Matter* **21**, 075401 (2009).

89. Juby George and Anand P. Pathak, *Int. J. Mod. Phys. A* (2009) (in press).

90. Juby George, Anand P. Pathak and A. V. Solov'yov, *J. Phys.: Cond. Matter* (2009) (in press).